POLITECNICO DI TORINO

Corso di Laurea Magistrale in Ingegneria Energetica e Nucleare

Tesi di Laurea Magistrale

Reactor Physic and Thermal Hydraulic analyses for the OECD/NEA MPCMIV Benchmark

Relatori
prof. Sandra Dulla
PhD Marco Cherubini

Candidata
Luana Giaccardi

Luglio 2021

Reactor Physic and Thermal Hydraulic analyses for the OECD/NEA MPCMIV Benchmark

Luana Giaccardi

16 July 2021

Contents

List of Figures III

List of Tables VI

Abstract VIII

1 Introduction 1

2 The MPCMIV Benchmark 4
- 2.1 Pellet Cladding Mechanical Interaction . . . 7
- 2.2 Benchmark organization . . . 9
- 2.3 The experimental facility and tests . . . 12

3 Reactor Physics, Modeling and Simulation 18
- 3.1 Serpent Code . . . 20
- 3.2 R2 Reactor Core Model . . . 23
  - 3.2.1 Fuel Assemblies . . . 23
  - 3.2.2 Control Rod . . . 28
  - 3.2.3 No-fuel assemblies . . . 33
  - 3.2.4 R2 Core . . . 42
- 3.3 Single assembly depletion . . . 46
  - 3.3.1 Identification of the dataset parameters . . . 47
  - 3.3.2 Build up of the dataset . . . 51
- 3.4 Full core burn-up . . . 59
  - 3.4.1 Core loading 1105 . . . 59
  - 3.4.2 Comparison of the discharged fuel assemblies . . . 60

4 Thermal Hydraulics, Modeling and Simulation 63
- 4.1 In-Pile Loop 1 and Ramp Test Facility . . . 64
- 4.2 Ramp tests . . . 68
  - 4.2.1 First cold ramp test . . . 68
  - 4.2.2 Second cold ramp test . . . 72
- 4.3 RELAP5 Code . . . 75

4.4 RELAP5 Model 79
4.4.1 RELAP5 Best Estimate Nodalization 80
4.4.2 Main circuit model 83
4.4.3 In-pile tube model 90
4.5 Input calibration 97
4.6 Transient simulation of the first power ramp test 98

5 Conclusions 106

Bibliography 108

List of Figures

2.1 Link between the physical domains of interest of the MPCMIV benchmark. 7
2.2 Etched cross-section at axial position of maximum LHR which shows pronounced fuel cracking caused by the ramp test [2]. 9
2.3 Benchmark Phases [1]. 11
2.4 General view of the R2 Reactor hall with Neutron Beam Experiment Facilities [1]. 12
2.5 R2 Reactor core configuration [1]. 13
2.6 R2 Reactor vessel section [1]. 14
2.7 Simplified flow diagram of the in-pile loop 1 [1]. 15

3.1 Example of the interpolation procedure to derive the isotopic mass inventory of the "new" assemblies. 19
3.2 Fuel element dimensional drawing from the benchmark specifications [1]. 24
3.3 FA Serpent model, xy-plot at z = 0 cm. 26
3.4 FA Serpent model, xz-plot at y = 0 cm with the fuel area cross section. 27
3.5 Control rod element [1]. 28
3.6 Cross Section of the CR Cd poison section modeled with Serpent (a) and CAD drawing from the specifications (b). 30
3.7 Cross Section of the CR fuel section modeled with Serpent (a) and CAD drawing from the specifications (b). 31
3.8 CR Serpent model, xz-plot at y = 0 cm with the Cd poison area cross section A-A, fuel area cross section B-B, lower member area cross section C-C and piston area cross section D-D. 32
3.9 Beryllium Reflector Assembly from the specifications [1]. 33
3.10 Cross Section of the Beryllium Reflector Assembly modeled with Serpent (a) and CAD drawing from the specifications (b). 34
3.11 Cross section of the aluminum assembly modeled with Serpent (a) and CAD drawing from the specifications (b). 34
3.12 Aluminum assembly adapter CAD drawing from the specifications [1] (a) and modeled with Serpent (b). 35

3.13 IS assembly adapter CAD drawing from the specifications [1] (a) and modeled with Serpent (b). 36
3.14 Cross Section of the IS Assembly modeled with Serpent (a) and CAD drawing from the specifications (b). 36
3.15 Iridium assembly adapter. 37
3.16 Cross Section of the Iridium Assembly. 37
3.17 U-tube Adapter of the Downward Section, CAD drawing from the specifications [1] (a) and modeled with Serpent (b). 39
3.18 U-tube Adapter of the Upward Section, CAD drawing from the specifications [1] (a) and modeled with Serpent (b). 39
3.19 U-tube Downward Section Cross Section at Core Level, modeled with Serpent (a) and CAD drawing from the specifications (b). 40
3.20 U-tube Upward Section Cross Section at Core Level, modeled with Serpent (a) and CAD drawing from the specifications (b). 40
3.21 C3 configurations Serpent cross sections at core central height. . . . 41
3.22 R2 Core box and D2O blanket CAD drawing from [1]. 43
3.23 R2 Core Arrangement [1]. 44
3.24 1105 Core loading configuration. 44
3.25 Serpent R2 Core model xy-plot, z=0 cm. 45
3.26 Single assembly RELAP5 model nodalization. 52
3.27 Temperature distribution inside the three assembly types computed with the RELAP5 single assemby model. 55
3.28 Flux-map of Core 1105, Cycle 0505, at BOC [1]. 57
3.29 Isotope mass curves interpolation example. 58
3.30 Power levels selected for the 1105 core loading. 59
3.31 Mass percentage difference between Serpent simulations and reference data for U-235 and total U. 60
3.32 Mass percentage difference between Serpent simulations and reference data for fissile Pu and total Pu. 61
3.33 Mass percentage difference between Serpent simulations and reference data for Np-237 and U-236. 61

4.1 In-pile part of the loop (U-tube). 64
4.2 The main circuit of the in-pile loop. 65
4.3 The Ramp Rig facility [1]. 66
4.4 The Ramp Capsule [1]. 67
4.5 Drawing of the fuel rodlet 2653. 67
4.6 Position of the father rod (I8) in SVEA-96 fuel assembly 22034 in Forsmark-2 Reactor. 68
4.7 The irradiation history from reactor start-up to the scram in the first ramp test [1]. 70

4.8 Details of the first ramp test from the start of rodlet insertion to initiation of the scram [1]. 71
4.9 Details of the second ramp test from the start of rodlet insertion to initiation of the scram [1]. 71
4.10 Measured differential temperature as a function of reactor power. . 72
4.11 In-pile Loop Pressure, Temperature and Mass Flow Rate and R2 Power for the second cold ramp test [1]. 73
4.12 Main steps of nodalization set up: nodalization schematization (left), RDS of the facility (middle) and RELAP5 input deck (right). 82
4.13 Example of piping schematization. 83
4.14 Module 9 (piping between MF and PUMP) nodalization. 84
4.15 Module 6 (piping between OCP and FFF) nodalization. 85
4.16 Module 8 (piping between AC and MF) nodalization. 85
4.17 First part of module 7 (piping between FFF and AC) nodalization. 86
4.18 Second part of module 7 (piping between FFF and AC) nodalization. 87
4.19 Module 10 (piping between PUMP and HTR) nodalization. 87
4.20 First part of module 11 (piping between HTR and ICP) nodalization. 88
4.21 Second part of module 11 (piping between HTR and ICP) nodalization. 88
4.22 Module 12 (Surge-line) nodalization. 89
4.23 Module 13 (Spray-line) nodalization. 89
4.24 U-tube nodalization. 91
4.25 Inlet Connection Pipe CAD drawing from the specifications [1]. . . 92
4.26 Outlet Connection Pipe CAD drawing from the specifications [1]. . 92
4.27 CAD drawing of CV 1 of HPTD with the RR inside. 93
4.28 Ramp Rig CAD drawing from the specifications [1]. 95
4.29 Ramp Capsule CAD drawing from the specifications [1]. 96
4.30 Flow distribution inside the in-pile tube. 97
4.31 Power calibration period configurations. 99
4.32 Pre-ramp and ramp test period configurations. 99
4.33 Coolant temperature at the inlet and outlet of the in-pile loop. . . . 101
4.34 Coolant temperature upstream and downstream the test section. . . 102
4.35 Mass flow rate inside the loop and inside the ramp rig. 103
4.36 Detail of the power ramp test, temperature distribution downstream the test section. 104

List of Tables

2.1 Partecipants in the MPCMIV benchmark. 5
2.2 Targets for cold ramp test [1]. 16

3.1 Fuel meat isotopic compositions and mass densities for the CF and CA elements. 25
3.2 AG3NE Cladding aluminum alloy and 6061 adapters aluminum alloy compositions and mass densities. 26
3.3 1100-0 aluminum alloy and 6065-T5 extruded housing aluminum alloy compositions and mass densities. 29
3.4 Fuel meat isotopic composition for the CAC element. 31
3.5 High pressure tube and gas jacket stainless steel AISI 316L composition and mass density [3]. 38
3.6 Zircaloy 2 composition and mass density [4]. 42
3.7 Simulation setup for the moderator temperature sensitivity analysis. 48
3.8 Isotope inventories mass difference from the moderator temperature sensitivity analysis. 48
3.9 Simulation setup for the power density sensitivity analysis. 49
3.10 Isotope inventories mass difference from the power density sensitivity analysis. 50
3.11 Matrix Combination simulations setup. 51
3.12 Temperature Profile Evaluation approach, average temperatures for each power value and assembly type. 56

Abstract

High-fidelity, multi-physics Modeling and Simulation (M&S) tools are being developed and utilized for a variety of applications in nuclear science and technology, and show great promise in their abilities to reproduce observed phenomena for many applications. These M&S tools enable rigorous modeling of coupled behaviors that needs to be properly validated against experiments. The Multi-physics Pellet Cladding Mechanical Interaction Validation (MPCMIV) benchmark is organised in this context by the Nuclear and INdustrial Engineering (NINE) company in co-ordination with Studsvik, under the guidance of the NEA Expert Group on Multi-physics Experimental Data, Benchmarks and Validation (EGMPEBV). It is an international project that involves the partecipation of universities and organisations from all over the world. The first revision of the input and output specifications of the benchmark was published in April 2018, but a lot of the Boundary and Initial Conditions (BICs) necessary to adress the different exercises in which the benchmark is organised are still missing. The work addressed in this thesis provides with an important contribution to the completion of the specifications due to the complexity of applicable multi-physics tools. The analysis carried out within the present thesis involves two out of the three physical domains of interest of the benchmark: Reactor Physics (RP) and Thermal Hydraulics (TH). The Reactor Physic analysis focuses on the R2 Swedish Research Reactor, aiming at deriving the the unavailable fuel assemblies initial isotopic compositions. The derivation of the initial isotopic compositions is conducted in two steps: a series of infinite lattice depletion calculations for all the assembly types, followed by a full core burn-up calculation of a core cycle. All the models and simulations are carryed out with the Monte Carlo code Serpent 2. In respect to the Thermal Hydraulic area, after the set-up of a suitable model the RELAP5 code is used to simulate the in-pile loop inserted inside the R2 core, which is used to perform power ramp tests. The selected cold ramp test is then analysed by validating the model against experimental data through the demonstration of the achievement of the steady state conditions. After such successful demonstration, the cold ramp test has been simulated.
All the simulations results of the present analyses for both RP and TH areas show good agreement against experimental data, which entails at the end of the work that the models are validated, their preliminary results are satisfying and so they

allows to proceed with a deeper future analysis. Further developments of the work depends on the fact that the MPCMIV benchmark is a challenging complex project and a great opportunity to study different tools and modeling approaches for research porpouses.

Chapter 1

Introduction

An important branch of the Modeling and Simulation (M&S) codes capabilities that has shown an increasing potential in the last years is the high-fidelity, multi-physics context. Differently from single physic analysis, multi-physic simulation can provide more accurate responses when evaluating complex system behavior, capturing feedbacks that are not modeled when code coupling is replaced by boundary conditions. A real important aspect of this improvement is that the increasing fidelity and sophistication of coupled multi-physics M&S tools need to properly validated against experiments of the underpinning models and data. The multi-physic codes validation, represents a big issue for different reasons. First because this may require a more complex array of validation data taking into account the significant range of time, energy and spatial domains of the physical phenomena that are being simulated, in addition the validation of the coupling approaches has to be addressed as well. Secondly, the validation challenge is further complicated by the fact that legacy experimental data for single or coupled physical phenomena may not be adequate to validate high-fidelity M&S tools. Moreover few experimental facilities are available for conducting complex experiments, and that in some instances instrumentation and experimental techniques may not exist to validate some models or approximations. In order to address the specific challenges with the validation of high-fidelity, multi-physics M&S tools, in 2014 it was created the Expert Group on Multi-physics Experimental Data, Benchmarks and Validation (EGMPEBV) of the OECD-NEA. Under the guidance of this group, the Nuclear and INdustrial Engineering (NINE) company in co-ordination with Studsvik has organised from 2017 the Multi-physics Pellet Cladding Mechanical Interaction Validation (MPCMIV) benchmark.
The MPCMIV benchmark is based on ramp test experiments conducted at the Studsvik R2 reactor that require the coupling of Reactor Physic (RP), Thermal Hydraulic (TH), and Fuel Performance (FP) analyses to reach high fidelity simulations. A significant effort of the benchmark team went into the initial phase in

order to compensate for the lack of information related to certain areas. Nevertheless, a large number of Boundary and Initial Conditions (BICs) necessary to face the different benchmark exercises is still missing. The work presented in this thesis describes the multi-physic analysis that has been conducted over the MPCMIV to compute some of those missing BICs, and also to perform some of the benchmark exercises connected with Reactor Physic and Thermal Hydraulic simulations.
The next chapter introduces the MPCMIV benchmark starting with a description of its structure and organization. The benchmark is divided into different phases and it proposes several exercises that can be solved with both traditional and novel M&S tools, in order to allow partecipants of different levels and experiences to challenge their analytical methods. In that chapter it is also described the objective of the benchmark and the important problem of the Pellect Cladding Mechanical Interaction in the nuclear reactors. Then the R2 reactor and the in-pile loop experimental facility are described. These are the computational domains of interest of the analysis and in which the power ramp tests are performed. This introduction is intended to provide the reader with background information necessary to face the next chapters that deal with the actual analysis, and also to appreciate and recognise the international context in which this benchmark collocates itself. In fact, during the thesis activity there was an important collaboration with the North Carolina State University (NCSU) and the opportunity to join some OECD/NEA Benchmark Workshops. The participation to these International meetings was a great opportunity to deeper understand the benchmark goals and to receive important feedback on the Thesis work. Moreover a paper submitted to the NURETH-19 conference is under review.
The third and fourth chapters describe the Modeling and Simulation (M&S) of the thesis project, for the Reactor Physic and Thermal Hydraulic areas respectively. As far as the RP area is concerned, it is first described the objective of the analysis, which is to derive the initial isotopic compositions of the fuel assemblies loaded in the R2 core at the beginning of the core cycles of interest. So the Monte Carlo code Serpent 2 is used to build the high-fidelity models of the different assembly types and then to perform infinite lattice single assembly depletion calculation for all of them. A complete dataset with the isotopic compositions derived from different simulation setups is elaborated in order to compensate for the lack of information regarding the previous core depletion history. Then, the initial isotopic compositions of the assemblies are derived through an interpolation of the obtained depletion curves knowing the U-235 mass content of each assembly. These are loaded in the full core model and the full core burn-up simulation is performed following the exact setup of the core cycle. This simulation gives the final isotopic compositions of the assemblies that will be compared and validated through experimental data.
For the Thermal Hydraulic area the analysis is carried out with the RELAP5 code and it is focused on the modeling of the in-pile loop located inside the R2 reactor core. The in-pile loop is the experimental facility used to perform several ramp tests

for testing the PCI resistance of the nuclear fuel rods. To do that a special test fuel rodlet is rapidly inserted in the loop to simulate a power ramp. In the forth chapter the experimental facility is described in detail, as well as the elaboration of the simulation model, whose development follows the NINE nodalization techniques. Then, the model is validated against the experimental data of the benchmark by demonstrating the achievement of the steady state conditions for the different thermal hydraulic configurations. Once the model is validated, the transient analysis is performed to simulate the selected power ramp test, and also these simulation results are validated against experimental data following the acceptability criteria used by NINE.
Finally, the last chapter considers quantitavely and qualitatively the results obtained, and give some suggestions on how to procede with the future analysis.

Chapter 2

The MPCMIV Benchmark

In recent years, the nuclear industry demand for an advanced reactor modeling tool of multiple physics phenomena has increased significantly. This demand is due to the fact that challenges constituted by the accurate and realistic simulation of some multi-physics phenomena are of great concern in the industrial environment. A relevant example of multi-physics and multi-scale problems in nuclear reactors is the Pellet Cladding Interaction (PCI), which has been identified as one of the most interesting phenomena to be studied from different physical prospectives. In fact, possible PCI fuel failures reduce reactor performance related to power uprates, higher burn-up and fuel rod manufacturing quality and so it is important to have a deep knowledge of its causes and consequences in order to prevent severe events that may be initiated in this way. This can be done by conducting experiments in research reactors, but also supporting the real tests with Modeling and Simulations (M&S) tools and capability, that can further enlarge the know how in understanding the phenomena. These multi-physics high fidelity M&S tools are of great importance, but considering their complexity and innovation it is not also that simple to find validated tools of this kind. For this reason, several organizations all over the world are working nowadays to improve these promising modeling capabilities. Among them, the Nuclear and INdustrial Engineering (NINE) company leads the first of the kind international benchmark devoted to multi-physics: the Multi-physics Pellet Cladding Mechanical Interaction Validation (MPCMIV) benchmark [1].
The MPCMIV benchmark was proposed by NINE under the guidance of the Nuclear Energy Agency (NEA) Expert Group on Multi-physics Experimental Data, Benchmarks and Validation (EGMPEBV). This expert group is part of the Organization for Economic Cooperation and Development (OECD) and it was formed to address the specific challenges with the validation of high-fidelity, multi-physics M&S tools. The benchmark is organised in co-ordination with Studsvik and involves the partecipation of universities and organisations from all over the world (see Table 2.1).

Table 2.1: Partecipants in the MPCMIV benchmark.

Country	**Organization**	**Acronym**
Italy	Nuclear and INdustrial Engineering	NINE
Canada	McMaster University	UMCM
Germany	Global Research for Safety	GRS
France	The French Alternative Energies and Atomic Energy Commission	CEA
France	Institut de Radioprotection et de Sûreté Nucléaire	IRSN
Russia	Nuclear Safety Institute of the Russian Academy of Sciences	IBRAE
Switzerland	Paul Scherrer Institute	PSI
UK	EDF Energy	EDFE-UK-BR
USA	Anatech Corp	ANATECHCA
USA	Brookhaven National Laboratory	BNL
USA	FPoliSolutions LLC	FPOLI
USA	North Carolina State University	NCSU
USA	Radiation Safety Information Computational Center	RSICC
USA	University of Illinois at Urbana-Champaign	UILLINOIS

The international context in which the benchmark collocates itself is very important also to stimulate collaboration among different organizations and nuclear engineering experts from all over the world. Regarding the thesis activity, this resulted in a continuous correspondence with the Noth Carolina State University (NCSU). Every other week online meetings were orginised with professors Kostadin Ivanov and Maria Avramova, and other PhD students from NCSU to discuss about the benchmark activities, methods, tools and simulations. The work presented here is the result also of the important feedbacks of these meetings. Moreover, the fact that the benchmark is organised under the Nuclear Energy Agency allowed the candidate to partecipate to some of the OECD/NEA Benchmark Worshops organised between June and July 2021. During the workshops, experts from the organisations and universities mantioned before (Table 2.1) and many others discussed about reactor physics, thermal-hydraulics, fuel performance, multy-physics and many more topics, giving each other suggestions and opinions about all the benchmarks presented. The candidate had the opportunity to present her own work at the MPCMIV Benchmark Workshop of June 30$^{\text{th}}$, 2021. Moreover, the models

and results obtained have been published in the paper "Reactor Physics and Thermal Hydraulics Analises for the OECD/NEA MPCMIV Benchmark" for the 19th International Topical Meeting on Nuclear Reactor Thermal Hydraulics (NURETH-19) Conference. All these additional activities and collaborations gave a different value to both the quality of the work and the thesis experience at the NINE company, who deserves the merits of having allowed the thesis project realization.
Coming back to the EGMPEBV, the main aim of the group are to provide the member countries of the OECD-NEA with consensus guidelines and recommendations for validating multi-physics M&S tools, to evaluate legacy and new experiments for validation and to demonstrate validation principles for specific industry challenging problems. High-fidelity multi-physics computational tools offer the promise of more sophisticated simulations that provide abilities to model complex, coupled physical phenomena with improved accuracy and enhanced predictive capabilities. However, for this promise to be realized, models, coupling approaches and validation processes need to be established and the limits of validation data need to be understood. Validation of multi-physics M&S tools requires the coupled M&S tools to be validated for each physical phenomenon that has to be simulated as well as the coupling among the physical phenomena. Three task forces were established in the expert group to address these challenges. Task force one primarily focuses on experimental data qualification and development of benchmarks and is closely linked with the activities of task force two, that concentrate principally on the development of validation principles and guidance. Finally, task force three is mainly addressed on demonstrating examples of the validation principles and approaches. The EGMPEBV has selected several industry challenging problems as exercises for which demonstrate validation principles and practices with the first focusing on approaches to validate both traditional and novel multi-physics M&S tools. The MPCMIV benchmark is organised to reach these objectives, and in particular the main scopes are:

- to create methodologies for validation of single and coupled physics phenomena;
- to derive validation requirements;
- to derive an accuracy metric;
- to determine uncertainty methodologies to extrapolate beyond the validation domain.

To reach these objectives, the MPCMIV benchmark initiative is based on experiments conducted at the Studsvik R2 reactor that require coupling between Reactor Physics (RP), Thermal Hydraulics (TH) and Fuel Performance (FP) tools to achieve high-fidelity simulations. These tools are connected among themselves as it is shown in Figure 2.1. At the R2 reactor over 1000 ramp tests were performed,

150 of which were internationally supported specifically for PCI/PCMI problems. The next section descibes this important problem of the nuclear reactors and how it was studied with the power ramp tests conducted at the R2 reactor.

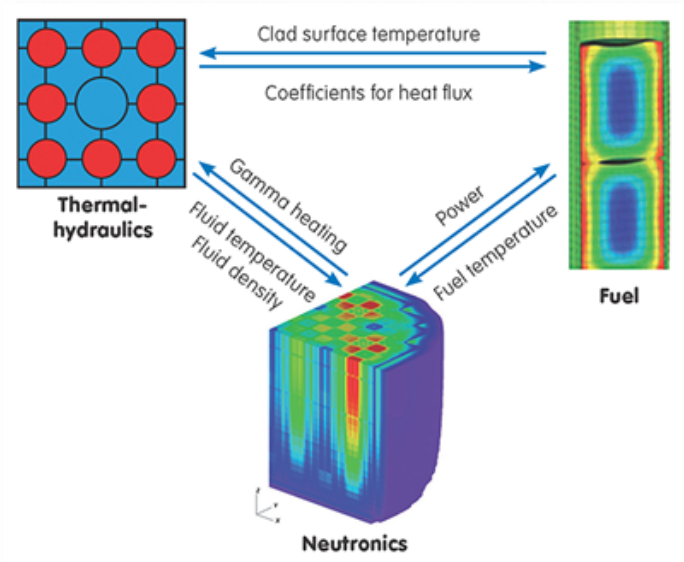

Figure 2.1: Link between the physical domains of interest of the MPCMIV benchmark.

2.1 Pellet Cladding Mechanical Interaction

The Pellet-Cladding Mechanical Interaction (PCMI) is a situation where the pellet and the cladding interact mechanically until break of the cladding, but without the impact of a Stress Corrosion Cracking (SCC) agent such as iodine [5]. The stress is generated from a power increase resulting in an expanding pellet due to thermal expansion and in some cases fission-gas swelling. If these stresses become large enough, PCMI failures may occur. A range of power-increasing transients where PCMI may be important are addressed in the Final Safety Analysis Report (FSAR), and reload licensing analyses (e.g., loss of feedwater heating in a BWR and steamline break in a PWR) of nuclear reactors. If the PCMI stress is low enough or if the cladding ductility is high enough, PCMI failures will not occur. However, in these cases, the cladding temperature may increase to such an extent that the critical heat flux may be exceeded and lead to clad failures due to post-DNB (Departure from Nucleate Boiling) failures (related to rewetting of the heavily oxidized and embrittled fuel cladding). As the burn-up increases, the risk of post-DNB fuel failures decreases while the risk of failure due to PCMI increases.
PCMI has never been reported to cause failures in either commercial BWRs or

PWRs. However, there are some results generated in experimental reactors conducting ramp testing of heavily hydrided fuel claddings which indicate that massive hydride rims formed at the fuel cladding outer surface may cause crack formation at the cladding outer surface and crack propagation towards the inner cladding surface resulting in failures. Other experiments conducted in research reactors consider less severe reactivity transient, that can occur in case of an operator error or a malfunction of the reactor instrumentation, such that a control rod group is withdrawn in an uncontrolled manner. In the limiting case, the most reactive control rod group is withdrawn at maximum rate in the just critical reactor. For this type of transient, affected portions of the core can experience a rather strong reactivity insertion and a fast power increase in just a few seconds. Depending on the characteristics of the transient, the reactivity feedback from the Doppler effect and the void generation will help in limiting the power excursion. For most transients, however, the reactor protection system will be activated as the power exceeds trip set points of the neutron monitoring system. This type of transient is an Anticipated Operating Occurrences (AOO). To establish criteria for use in safety evaluations of such reactivity transients at cold conditions, it has been suggested that PCI/PCMI failure thresholds could be used.
The traditional power ramp tests define a PCI/PCMI failure threshold as a linear heat rate vs. burn-up. Data for such failure thresholds have been collected through series of ramp tests, most of which have been performed at the Studsvik R2 reactor. Power ramp tests are typically carried out at coolant temperatures representative for normal power operation, i.e. typically 286 °C for BWR conditions. However, power ramps can hypothetically also occur in a BWR at low temperature during reactor start-up as discussed above. If the transient occurs at initial coolant and cladding temperatures below 100 °C, the cladding mechanical properties and potential failure mechanisms might conceivably differ from those at normal operating temperatures. To give some experimental confirmation of the fuel behaviour in such a low temperature transient and get some confirmation of enthalpy limits based on PCI/PCMI failure thresholds, a special cold ramp test has been performed to simulate a severe control rod withdrawal error reactivity transient at cold critical start-up in a BWR [6]. This cold ramp test is the one considered in the MPCMIV benchmark (see section 2.3), and it was one of the last irradiation experiments performed before the reactor was permanently shutdown on June 16, 2005.
The rod elongation is measured during the ramp test using an elongation detector, and provides a rapid indication of cladding failure which is indicated by a sudden shortening of the rod length. No plastic deformation, cladding defects, flaws on cladding surface and incipient PCI cracks on cladding inside were detected during the test, so the rod survived without failure. At the same time, gap measurement shows residual fuel deformation and ceramography shows pronounced fuel cracking as shown in Figure 2.2 [2].
The conclusion is that a fuel rod in good condition can be expected to survive

a similar reactivity transient at cold critical start-up conditions in a BWR. The results of the test support the preliminary enthalpy limits as providing adequate protection against PCI/PCMI fuel failures during anticipated transients in a BWR.

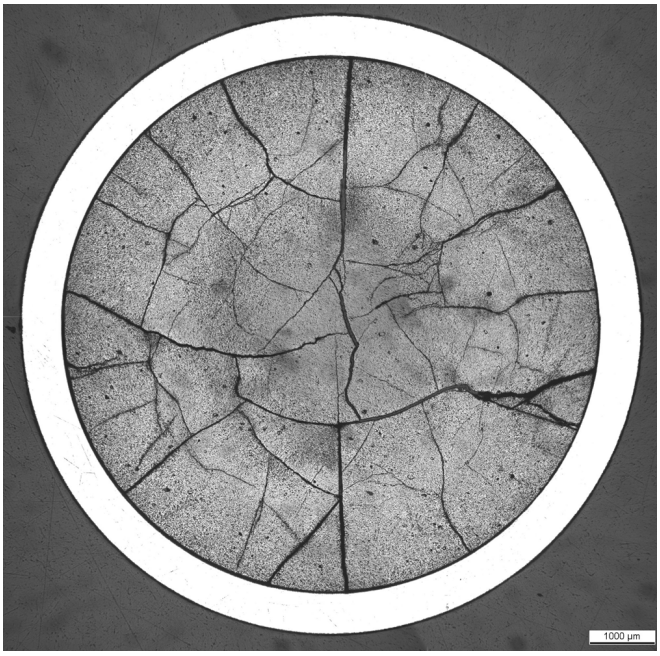

Figure 2.2: Etched cross-section at axial position of maximum LHR which shows pronounced fuel cracking caused by the ramp test [2].

2.2 Benchmark organization

The MPCMIV benchmark is planned to be structured in four main phases (see Figure 2.3):

1. the Model Development Phase;
2. the Pre-Qualification Phase;
3. the Blind Simulation Phase with Uncertainty Evaluation;
4. the Post-Test Phase with Sensitivity Analysis.

For each of these phases the participants are requested to fulfill the established validation requirements.
The "Model Development Phase" has the goal to check and qualify the computational domains developed for each main physical area before performing the simulation phases. The validation requirements to be considered in this phase must

concern not only with the demonstration of the geometrical fidelity between reality and the computational domains, but also the demonstration of steady state achievement for single physics simulations.
The "Pre-Qualification Phase" deals with the first cold ramp test and it consists of two steps:

1. Power Calibration, where an empty rod is placed in the ramp position for performing the power calibration;

2. Ramp Test, where the fuel rodlet is loaded in the ramp position for performing the ramp test.

This phase has the goal to pre-qualify firstly the TH/RP coupled computational domain (step 1) and then the TH/RP/FP coupled computational domain (step 2). This objective will be achieved with the demonstration of steady state achievement for coupled physics simulations, including the coupling and the convergence criteria, and then performing the selected test. Thus, the specifications and the experimental results of the first ramp test are provided to the participants. The validation requirements have to be established to ensure the consistency between the different evaluation models and to quantify the degree of qualification of the computational domains. In addition, the pre-qualification phase includes the accuracy quantification and the quantification of the input uncertainty parameters to be used then in the blind simulation phase for the uncertainty evaluation.
The "Blind Simulation Phase" concerns the modeling and the simulation of the second cold ramp test, prior to the disclosure of the experimental results. During this phase, the simulation results generated by the participants are collected and then compared with the experimental data. In addition, an uncertainty analysis of the results of the blind simulation phase is requested. Therefore, appropriate validation requirements are set to identify how quantitatively the participants select the important uncertainty parameters, the associated range of variations, the probability distribution functions and the propagation of the uncertainty at the level of single-physics and then at multi-physics level.
The "Post-Test Phase" is performed after the disclosure of the measured quantities and it has the goal to provide quantification of the predictive capability of the M&S tools by performing sensitivity analyses. The evaluation of the blind simulation results against the recorded data at the end of phase 3 and consequent re-evaluation of the computational domains will provide the directions for modeling refinements to be pursued during phase 4 of the benchmark.
Considering the challenging nature of the selected experiment, the traditional methods and tools are not able to perform all the steps of the benchmark. For instance, with a classical nodal diffusion simulation, that requires a homogenization step, it is not possible to represent the detail of the fuel rodlet. It is important to note that the detailed modeling of the neutronics of the fuel rodlet is crucial in order to obtain accurate results. Thus, high-fidelity models and methods seem to be

more appropriate for this benchmark. Based on this aspect, the validation exercise is structured into four tiers in order to maximize participation by various groups, namely:

1. Tier-1 is targeted for novel M&S tools that have the capability to model the 3D heterogeneous and high-fidelity multi-physics models for both the reactor core domain and the fuel rod domain;

2. Tier-2 involves the use of a simplified model for novel M&S tools that utilizes boundary conditions for the reactor physics models of the R2 reactor core. The boundary conditions (i.e. neutron and photon sources) are provided with associated uncertainty for the fuel rodlet domain by Monte Carlo simulations of the R2 core;

3. Tier-3 involves the same simplified domain of tier 2 but allows for the use of traditional M&S tools. In this case also the cross-section data for the fuel rodlet domain are provided by the benchmark team.

In addition, a fourth tier (Tier-4) is taken into account to allow participants who have greater experience in the fuel performance area to participate in the benchmark and hence give their contribution from the point of view of the fuel behavior. In this case, it will be used a traditional fuel performance tool with boundary conditions.

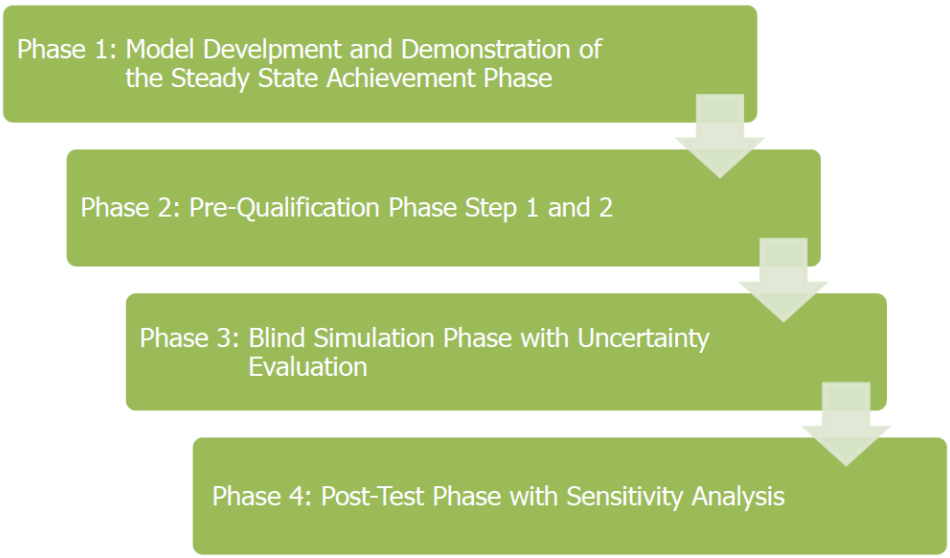

Figure 2.3: Benchmark Phases [1].

2.3 The experimental facility and tests

In this section, a general description of the R2 Research Reactor together with the Ramp Test Irradiation Facility is given. Moreover, an introduction on the description of the selected cold ramp tests is provided hereafter. More detailed data and information are given in the following chapters, in particular sections 3.2 and 4.1 describes in depth in terms of geometrical characterization and materials compositions the core and the in-pile tube, while 4.2 gives the particulars of the two selected cold ramp tests.

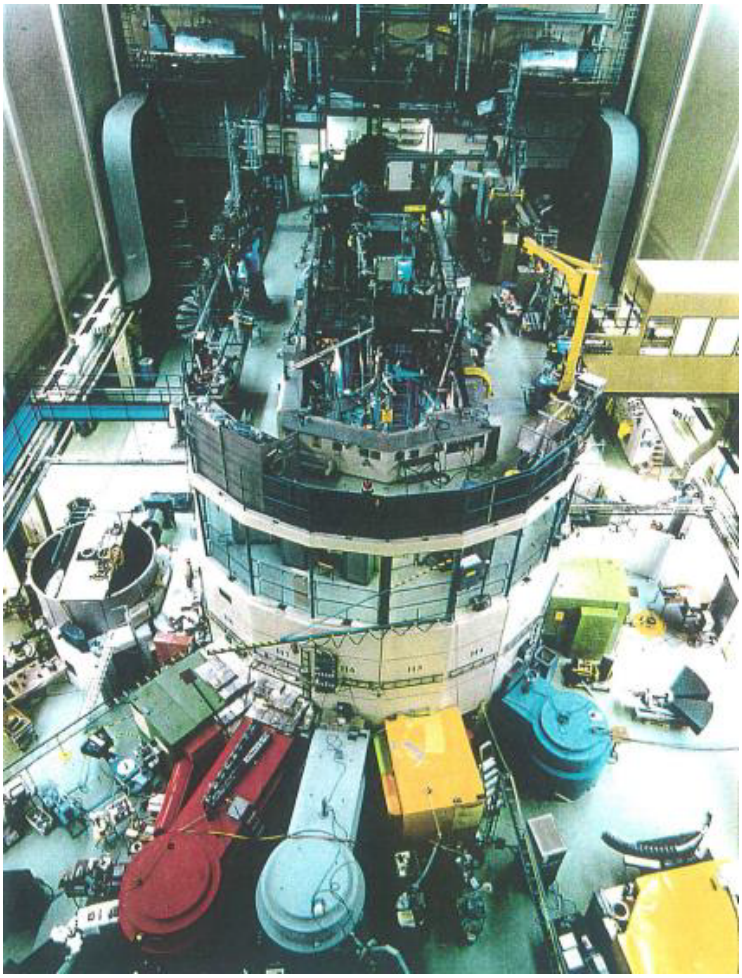

Figure 2.4: General view of the R2 Reactor hall with Neutron Beam Experiment Facilities [1].

The R2 Test Reactor

The R2 reactor is a 50 MW(th) tank-in-pool testing reactor (Figure 2.4), cooled and moderated by light water. The reactor core is contained within an aluminum

vessel located at one end of a large open pool. The vessel consists of three parts, two with a cylindrical shape above and below the core region and a rectangular core box, surrounded by heavy water blankets on three sides of the core (North, South and West sides, see Figure 2.6). The pool, which also serves as storage for spent fuel elements and irradiated experimental equipment, is divided in three sections and is enclosed by heavy concrete walls. All the experiments and the fuel elements can be handled from the top of the pool. The core is equipped with neutron beam experiment facilities which most of them are located in front of the biological shield of the R2 (H1 to H10 in Figure 2.5). The coolant water is circulated through the reactor vessel and flows through pipes and a large decay tank below the reactor hall to heat exchangers cooled with sea water.
The core is arranged in a 10 x 8 lattice (see Figure 2.5) consisting of 46 ($\pm$2) fuel elements, 6 control rods, (max) 16 and normally 10 $\pm$ 2 beryllium reflector assemblies, and the balance of the positions occupied by aluminum fillers, experiments and surveillance irradiation rigs. Apart from the control rods pattern, which is constant, the composition of the core can be varied to suit the experimental program. The fuel elements are of the LEU (Low-Enriched Uranium) type. The fuel is in the form of curved plates of U_3Si_2 with 19.75% enrichment and aluminum cladding. The core reactivity is controlled by five shim-safety rods and one regulating rod placed in the center of the core (see Figure 2.5). They consist of an upper neutron absorbing section of cadmium and a lower fuel section. They are moved vertically by drive mechanisms placed below the reactor vessel.

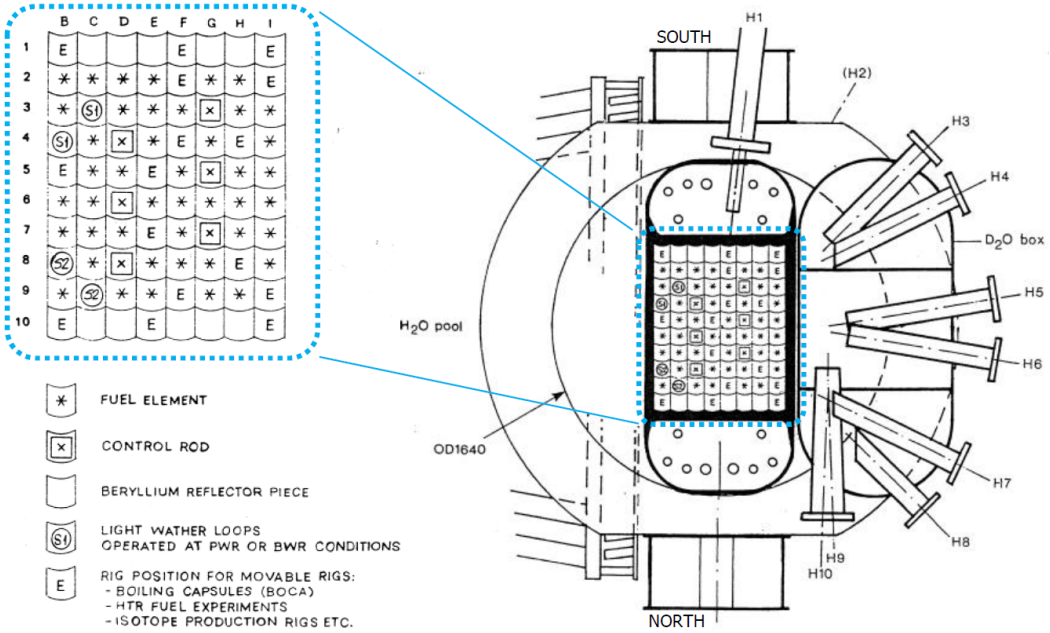

Figure 2.5: R2 Reactor core configuration [1].

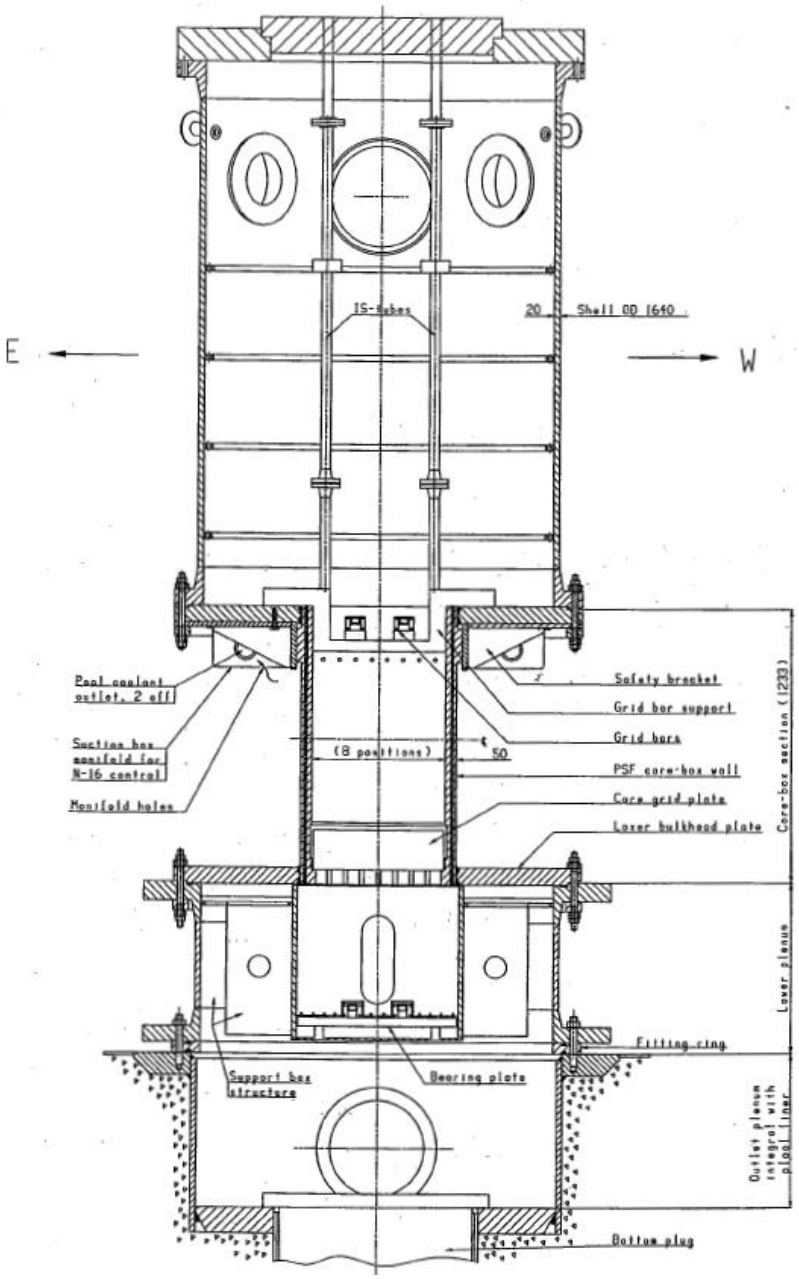

Figure 2.6: R2 Reactor vessel section [1].

In the core there are two in-pile pressurized light water loops (see Figure 2.7) which simulate realistic BWR and PWR temperature and pressure conditions. Each LWR fuel loop is of a U-tube design and utilizes two diagonally adjacent fuel element positions in the R2 reactor. They are thermally insulated from the reactor primary coolant by a gas gap containing CO_2. The loops can be used for the irradiation at constant power of fuel rodlets and structural materials and for power ramp tests

(possible only in loop 1, position C3) of single rodlets. The test rodlet to be ramp tested is installed in the loop in a special ramp capsule, which in turn is inserted in a reloadable ramp rig facility. The ramp rig is surrounded with mini-tube coil which contains ^{3}He gas for controlling the rod power by varying the gas pressure.

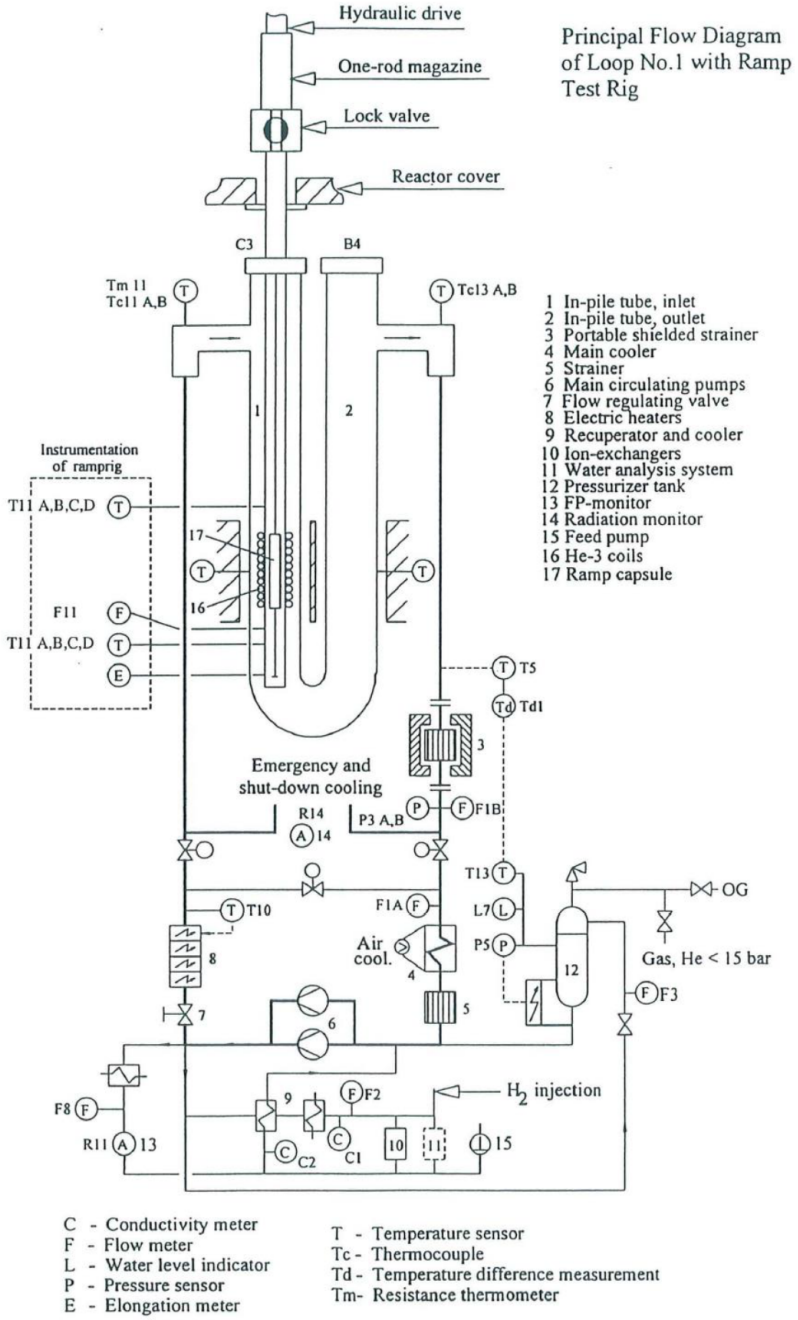

Figure 2.7: Simplified flow diagram of the in-pile loop 1 [1].

Description of the selected cold ramp test

The simulation of a fast reactivity transient at cold critical conditions in a BWR requires some special considerations (see Table 2.2). In particular, a very fast ramp from practically zero rod power to a very high rod power is needed. The ^{3}He absorber system cannot fulfill both these requirements and hence this system cannot be used to simulate the reactivity transient.

Table 2.2: Targets for cold ramp test [1].

Parameter	**Unit**	**Value**
Cold loop conditions	-	20 bar, 50°C
Reactor power	MW	50
Ramp type	-	Fast rod insertion No ^{3}He gas absorber
LHR ramp rate	-	As fast as possible ramp in a few seconds
Conditioning power level	kW/m	0, no conditioning
Ramp terminal level	-	48 kW/m (target in first ramp) as high as possible in second ramp
Holding time	s	15
Ramp termination	-	Manual reactor scram

To satisfy the condition on ramp rate as well as the condition on the power increase, it was proposed to use a method of fast rod insertion. Consequently, the test procedure for the cold ramp is quite different compared to a normal ramp test. The ramp procedure comprises the following steps:

1. Power calibration: the ramp procedure starts with the normal calibration step, where an empty rod (the calibration rod) is placed in the ramp position before reactor start-up. The reactor is then started and the power increased in steps up to 45 MW. Power calibration is performed.

2. The power is then decreased to about 10 MW. The calibration rod is removed and the test rod is loaded in the irradiation position. The rod power at 10 MW is measured. Using this information, the relation between the rod power and reactor power can be determined. The reactor power level required to satisfy the ramp specification is calculated. The test rod is then unloaded from the irradiation position.

3. The reactor power is increased to the appropriate power level.

4. Ramp test: the test rod is loaded into the irradiation position. The time it takes to move the rod from the waiting position to the irradiation position is

about 6 s. The rod moves in the neutron flux during roughly 2 s. Thus, the rod nuclear power increases from practically zero to the maximum value in about 2 s. Due to the low heat conductivity of the fuel, however, the surface heat flux and fuel temperature continues to increase for about 10-15 seconds after the rod has reached the irradiation position.

5. The reactor is shut down by initiating a manual scram 15 s after the rod has reached the irradiation position.

6. The test rod is then unloaded from the ramp position. At this point, the ramp test is finished and the loop can return to normal operation and the reactor can restart.

Chapter 3

Reactor Physics, Modeling and Simulation

One of the exercises of the MPCMIV Benchmark for tier-1 participants consists in performing the burn-up simulations of the three core loadings of interest: 1105, 1106 and 1107. To do that, it is necessary to know the fuel assemblies isotopic compositions at the beginning of each core loading, and then deplete them according to the detailed information of the different core cycles. However, none of the assemblies loaded in the cores of interest are of fresh fuel, and only the initial U-235 mass content per each assembly is known, while there is no information about the other isotopes composition. Considering this lack of information, it is necessary to define a method capable to derive the initial fuel isotopic composition in order to have all the BICs to perform the full core burn-up simulations.
Considering the information available the strategy proposed to calculate the initial isotopic composition of each assembly consists in performing infinite lattice single assembly depletion calculation for each individual assembly type. The reason why more than one single assembly infinite lattice calculation is needed is due to the fact that there are three fuel assembly types throughout all R2 cores: CA elements with a nominal content of 400 g of U-235, CF elements with a nominal content of 490 g of U-235, and CAC fuels of the CRs fuel section with a nominal content of 223 g of U-235. For each of these assembly types the depletion is carried on until the final U-235 mass is below the lowest-mass assembly at the beginning of any core loading of interest.
Once the depletion of each assembly type is completed, it is possible to construct the isotopic inventory for all "new" Fuel Assemblies (FAs). It is important to notice that the term "new" FA does not refer to a fresh fuel element (i.e. zero burn-up), but to one which has not been used in the previous cores among those of interest. Consequently, all of the FAs loaded in core 1105 are "new", likewise 35 out of 53 FAs for core 1106 and 10 out of 52 FAs for core 1107. The isotopic inventory is

obtained by interpolation at the burn-up value matching the specified U-235 mass. Figure 3.1 shows an example of how to do this interpolation: first derive the burn-up value by matching the U-235 mass of each "new" assembly at the beginning of each core cycle, then, using the matched burn-up values, construct a dataset of isotopic concentrations by interpolating from the results of the original three single assembly depletions.

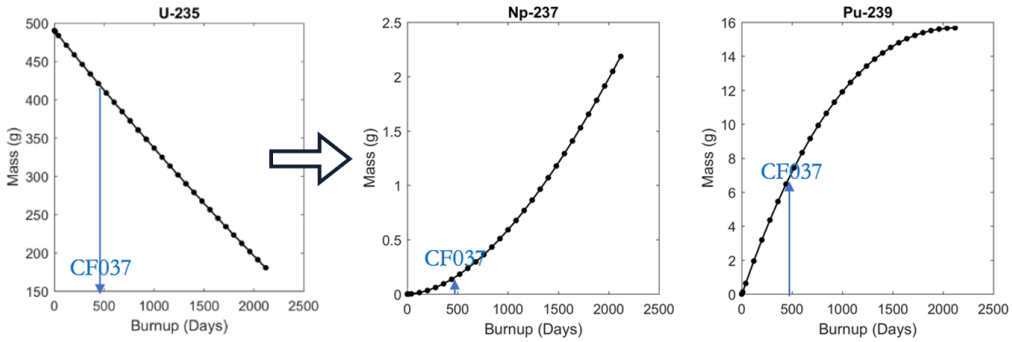

Figure 3.1: Example of the interpolation procedure to derive the isotopic mass inventory of the "new" assemblies.

The last step of the strategy consists in loading these assemblies into the full R2 core model and deplete the entire core according to detailed power/CR history and flux map at Beginning Of Core loading (BOC) of each core loading. At the end of the core 1105, some FAs are shuffled, others are carried over into the next core loading and the remaining ones are discharged from the core. The isotopic composition derived from the core depletion can be compared with some available data from Studsvik that describe the content of some isotopes of the discharged FAs. If the comparison does not give a good match it would be necessary to change some simulation parameters (i.e. fuel temperature, power density, moderator temperature) of the single assembly infinite lattice calculation from which the initial isotopic composition of the single assemblies was derived, in order to find the best approximation. Since there is no exact reference value for the simulation parameters this step is anticipated by defining a priori a dataset of different single assembly types initial isotopic compositions, through which find the one that better approximate the given isotopic composition of the discharged elements at the end of the core loading.
The RP analysis of the benchmark is described in detail in the next sections of this chapter. The code used for the M&S is Serpent 2, of which it is given a brief description on section 3.1, with a particular focusing above all on the features used in the current analysis. The code is used to build the 3D model of the R2 core, which is based on both available data from Studsvik original documents and assumptions that were necessary to compensate for the lack of information. The work done is

described in section 3.2. Once the model is completed it can be used to perfom all the simulations for the single assembly depletions, presented in section 3.3, and for the full core burn-up simulation, described in section 3.4. The latter contains also the analysis of the results with some considerations and suggestions on how to proceed with the activity in the future.

3.1 Serpent Code

Serpent 2 is a multi-purpose three-dimensional continuous-energy Monte Carlo particle transport code [7]. The Code development started out as a simplified reactor physics code at the VTT Technical Research Centre of Finland in 2004, under the working title "Probabilistic Scattering Game", or PSG. This name is used in all publications dated before the pre-release of Serpent 1.0.0 in October 2008. Then the code has been publicly distributed by the OECD/NEA Data Bank and RSICC since 2009 and the capabilities of the next development version, Serpent 2, extended well beyond reactor modeling. The applications of the code can be roughly divided into three categories:

- traditional reactor physics applications, including spatial homogenization, criticality calculations, fuel cycle studies, research reactor modeling, validation of deterministic transport codes, etc.;
- multi-physics simulations, i.e. coupled calculations with thermal hydraulics, CFD and fuel performance codes;
- neutron and photon transport simulations for radiation dose rate calculations, shielding, fusion research and medical physics.

The code version used for this analysis is 2.1.31 released on May 16, 2019 [8], and the continuous-energy interaction data is read from ACE format cross section library based on ENDF/B-VII evaluated data files. The Serpent code has no interactive user interface, all communications between the code and the user is handled through one or several input files and various output files. The input file is divided into separate data blocks, denoted as cards. The file is processed one card at a time and there are no restrictions in what order the cards should be organized. Each input card is delimited by the beginning of the next card.
The input cards used for the M&S of the single assemblies are listed below, with a brief description of their purposes, while the simulation setup and the values given to the cards are described in the next sections of the chapter.

surf: Surface definition. The building of the model starts from the definition of the boundaries that delimit all the geometries and materials of the assembly.

To do that, Serpent provides for various elementary and derived (comprised of two or more elementary surfaces) surface types for geometry construction.

cell: Cell definition. Once all the necessary surfaces are defined, they are used for the geometry description of three-dimensional regions denoted as cells. Each cell is the 3D space of intersection between the regions defined by a set of surfaces, which is filled with the right material. It is very important to define each cell only once, otherwise Serpent will give an overlap error during the the input check, and also to define the all space of the specific domain, called "universe", otherwise a "no cell" error will be produced.

mat: Material definition. Each cell is filled with a specific homogeneous material that has to be defined by the user. Each material consists of a list of nuclides and each nuclide is associated with a cross section library. Nuclide temperatures are fixed when the cross section data is generated and cannot be changed afterwards. It is important to use cross section libraries generated at the right temperature to correctly model the Doppler-broadening of resonance peaks. It is equally or even more important to use the appropriate bound-atom thermal scattering libraries for moderator nuclides.

dep: Irradiation history. The irradiation history in the independent burnup calculation mode consists of one or several burnup intervals, defined by this card. The burn-up step type can be chosen between a list where the only difference among each other is the unit of measurement. The selected one for the single assemblies depletion is "butot", that requires to define the depletion steps as cumulative burnup in MWd/kgU.

include: Read a new input file. This card is usefull to simplify the long input description by dividing the cards into separate files, which are then recursively read from the main file, named "run", using the include-command. The final input of each assembly type consists in five different files: the first define all the surfaces, the second contains the cells definition, other two files define the materials, one the fresh fuel and the other all the materials like the cladding, the adapters ones etc., and finally the "run" file that include all the previous files and the setup of the simulation.

set: Set miscellaneous parameter definition. Serpent has various calculation parameters determined using the "set" command.

powdens: Source rate normalization. The integral reaction rate estimates given by a Monte Carlo simulation are more or less arbitrarily normalized, unless fixed by a given constant. The Serpent code provides for seven options for source rate normalization, the one chosen is "powdens", which is the average power density (kW/g) defined as the total heating power divided by the total initial mass of fissile isotopes.

bc: Boundary conditions. They determine the fate of neutrons escaping outside the defined geometry along x-, y- and z- directions. The Serpent code has three available boundary condition options: 1 - black, 2 - reflective and 3 - periodic. Default is the black boundary, which means that all neutrons streaming into outside cells are killed. Reflective and periodic boundary conditions can be used for setting up infinite lattices. When the neutron encounters a reflective boundary, it is diverted back into the geometry. In the case of a periodic boundary, the neutron is moved to the opposite surface.

pop: Population size and number of cycles. The default calculation mode in Serpent is the k-eigenvalue criticality source method, in which the simulation is run in cycles and the source distribution of each cycle is formed by the fission reaction distribution of the previous cycle. The parameters for criticality source calculation are set using this card, where are given the number of source neutrons per cycle, the number of active cycles run and the number of inactive cycles run, that are used in order to allow the initial fission source distribution to converge before starting to collect the results.

gcu: Group constant generation. The universes in which the group constants are calculated can be set by this card. The homogenization is carried out in the given universes and all higher universes accessed from lattices and filled cells.

inventory: Nuclide list for burnup calculation output. The standard output in the independent calculation mode consists of material compositions, transmutation cross sections, activities and decay heating values. For these simulations all the isotopes, elements, etc. are included in the output by setting the inventory option as "all".

printm: Flag for printing material compositions. This option is used for writing the compositions of depleted materials in a separate output file after each burn-up step.

acelib: File path for xs library directory file. The Serpent code uses a single directory file for determining the cross sections used in the transport simulation, in this case it is "/home/grg/serpent/xsdata/sss_endfb7u.xsdata".

declib: File path for radioactive decay data. In addition to the continuous-energy cross section libraries, burn-up calculation requires radioactive decay data, neutron-induced and spontaneous fission product yields. The ENDF format decay data library file path is set to "/home/grg/serpent/xsdata/sss_endfb7.dec".

nfylib: File path for fission yield data. The ENDF format neutron-induced fission yield library file path is set to "/home/grg/serpent/xsdata/sss_endfb7.nfy".

plot: Geometry plotter. It uses the GD open source graphics library for producing png format output files for visualization. In order to use the plotter, the source code must be compiled with this library included. The orientation of the plot plane is defined as 1 for yz-plot perpendicular to the x-axis, 2 for xz-plot perpendicular to the y-axis and 3 for xy-plot perpendicular to the z-axis. The plotted area is a rectangle defined by the orientation, the position on the perpendicular coordinate axis and the coordinates of the two corners.

For further information on how to use the Serpent code see also the Serpent Wiki [9].

3.2 R2 Reactor Core Model

Following the strategy described at the beginning of this chapter, the first step of the analysis consists in building the models of the three single assembly types in order to perform for each of them the infinite lattice depletion calculation from which derive through results-interpolation the initial isotopic compositions of all the assemblies that consitute the core loadings of interest. Since all the Control Rods (CRs) are formed by a fuel section which is not fresh too, it is necessary to perform the infinite lattice depletion also for them. Then also all the other assemblies and components of the core are modeled, and together with the FAs and CRs are used to construct the core lattice. This lattice is the central part of the core, which is delimited by the core box and heavy water blankets. All of these models are finally put together to build the R2 core model which is used to perform the full core burn-up calculation.
All the RP models are presented in the sections below, with a detailed description of the reference documents and the necessary ipoteses that were made. All the models built are 3D and follow high-fidelity modeling criteria, which means that the objective is to preserve as much as possible the real behaviour of the geometry and materials, by avoiding any kind of simplifications when real information is available. Since the data treated in the benchmark are sensitive information, all the figures taken from original documents from Studsvik and from the specifications contains white labels that cover the quotas and all information that can not be distributed. For the same reason also the geometrical descriptions contain approximated quantities.

3.2.1 Fuel Assemblies

The fuel elements are of the LEU (Low-Enriched Uranium) type and contain 18 curved plates of U_3Si_2 with 19.75% enrichment (see Figure 3.2). This particular fuel elements manifacture tecnique is typically used in the Material Testing Reactors

(MTR), where the fuel elements consist of a variable number (from 14 to 17 tipically) of internal and two external LEU fuel plates of uranium silicide embedded in aluminium powder [10]. The U_3Si_2 with approximately 20% of U-235 is called the fuel "meat". The fuel plates are swaged into grooved side plates and the assembly is open at both ends to aid water cooling requirements during operation. Within this configuratin the water is also allowed to freely circulate through the fuel plates.

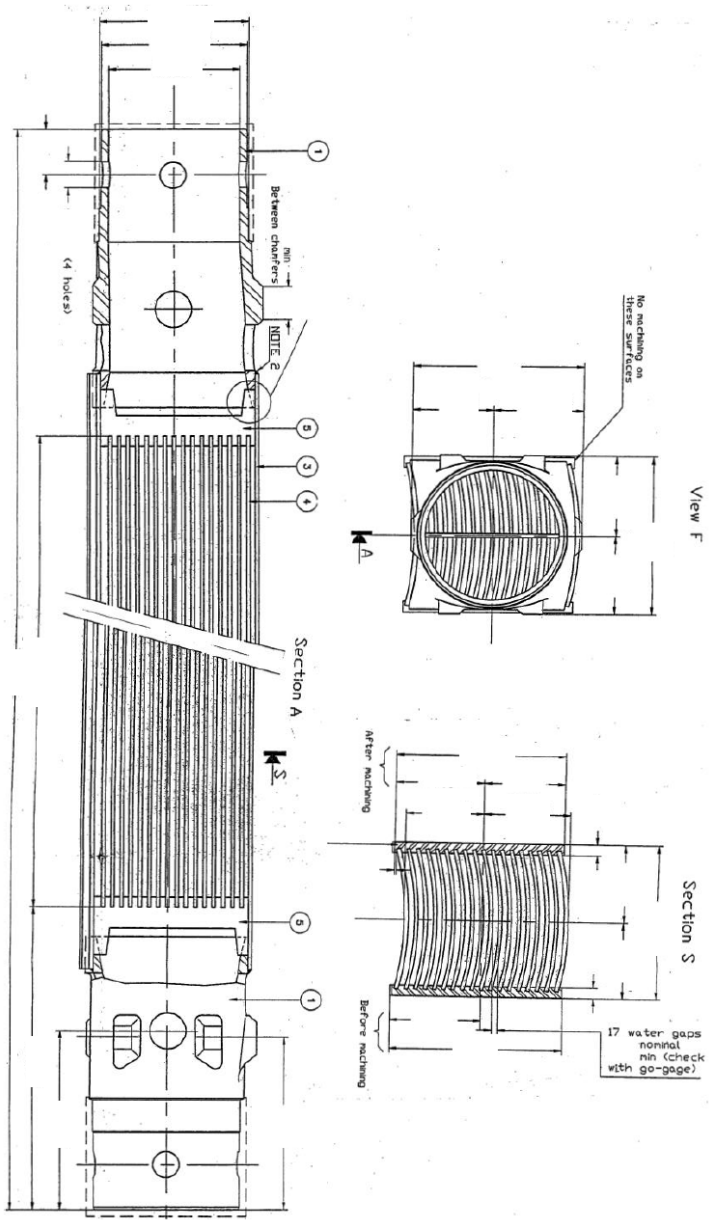

Figure 3.2: Fuel element dimensional drawing from the benchmark specifications [1].

The nominal U-235 loading per fuel element is 490 g for CF elements and 400 g in case of CA elements. The fuel elements are manufactured by CERCA, according to CERCA Specification 45NI007, Rev 1 May 1989. The geometrical characterization of the fuel assemblies is identical for both CA and CF elements and it is well described in the original Studsvik documents [11]. Furthermore, it is of the typical kind used for LEU plate-type research reactor fuels (see [12] for a detailed description).
The 16 inside fuel plates are about 620 mm long and 1.5 mm thick, while the 2 outer plates are about 690 mm long and 2 mm thick. All plates are about 70 mm wide and have a curvature radius of 140 mm. There are 17 flow channels, each of which is near 3 mm wide. The side plates are 690 mm long, 80 mm wide and 5 mm thick. The grooves of the side plates are spaced to allow the same width of flow channel between fuel elements as between plates of the same element. The meat of each plate is about 1 mm thick, 65 mm wide and 600 mm long for both inner and outer plates, consequently the latter have a thicker clad.
The fuel meat composition of the CF fresh fuel element is derived from [13], in which it is given the composition for a fuel element with a sligthly larger enrichment, but with the same U-235 mass content. The composition at the right enrichment is derived from this one by preserving the Al-powder and U-235 mass. The latter divided by the enrichment gives the total U mass and the Si mass is derived preserving the original mass proportionality with respect to the total U mass. Then all these masses are summed together to obtain the total mass which is used to devide each contribution to derive the corresponding weight percentage composition to be given to Serpent. The mass density is simply calculated by dividing the U-235 mass content per each assembly (490 g) for the U-235 weigth percentage, which gives the total fuel meat mass, and then dividing this total meat mass by the total volume of the meat, which is well known from the geometrical description.

Table 3.1: Fuel meat isotopic compositions and mass densities for the CF and CA elements.

Isotope	**CF (wt%)**	**CA (wt%)**
U-238	57.6872	53.2583
U-236	-	0.0947
U-235	14.1972	13.1560
U-234	-	0.1281
Si	5.6682	5.4030
Al	22.4474	27.9600
Density (g/cm^3)	6.5908	5.7944

The CA fuel meat composition instead has been found in an HELIOS input file from Studsvik [14]. Both meat density and composition are exactly taken from there. The final Serpent meat materials values are reported in Table 3.1. Looking at the compositions it is possible to notice that no U-236 mass content is described in the reference for the CF meat composition. This missing initial information will have an impact on the results which is discussed in the final section of this chapter. The cladding is made of AISI 5454 type aluminum alloy, French brand AG3NE and it is metallurgically bonded to the fuel alloy. The cladding composition is taken from [15] and reported in Table 3.2.

Table 3.2: AG3NE Cladding aluminum alloy and 6061 adapters aluminum alloy compositions and mass densities.

Isotope	**AG3NE (wt%)**	**6061 (wt%)**
Al	96.700	97.60
Mg	2.700	1.00
Si	0.090	0.60
Cu	0.005	0.28
Cr	0.105	0.20
Mn	0.400	0.32
Density (g/cm^3)	2.69	2.70

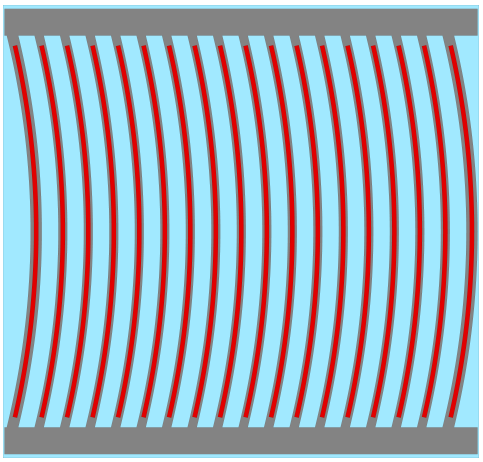

Figure 3.3: FA Serpent model, xy-plot at z = 0 cm.

Figure 3.3 shows an xy-plot of the fuel assembly model at a z coordinate of 0 cm, that is positioned at the center of the FA active length. The geometry of the

side plates modeled with Serpent needed to be a little bit modified with respect to the original one shown in Section S of figure 3.2. In fact, if the dimension along the x-direction of the side plates is modeled as the real case, it exceeds the length that it must occupy in the core model. For this reason, a piece of volume on the left handside of the side plates is cut and put like a stretch on the right handside. In this way, the total volume of material that may impact the simulation results is preserved.
The bottom and top adapters are made of aluminum alloy (6061-T6), AS5G08NE French brand [15], whose composition is reported in Table 3.2, and they are identical. Each adapter has two sets of holes for the coolant flow placed at a different distance from the lower/upper end. The first set has four holes with a diameter of about 10 mm placed at 20 mm from the lower end. The second set has four holes with a diameter of less than 20 mm, 2 of them are placed at 90 mm and 2 of them are placed at 100 mm from the lower/upper end (see Figure 3.2). The end fittings are welded to the side plates and to the outer fuel section. Each fitting contains six integral pads 25 mm from the fuel section to form a gap between adjacent fuel elements for coolant flow. Figure 3.4 shows the final Serpent fuel assembly model.

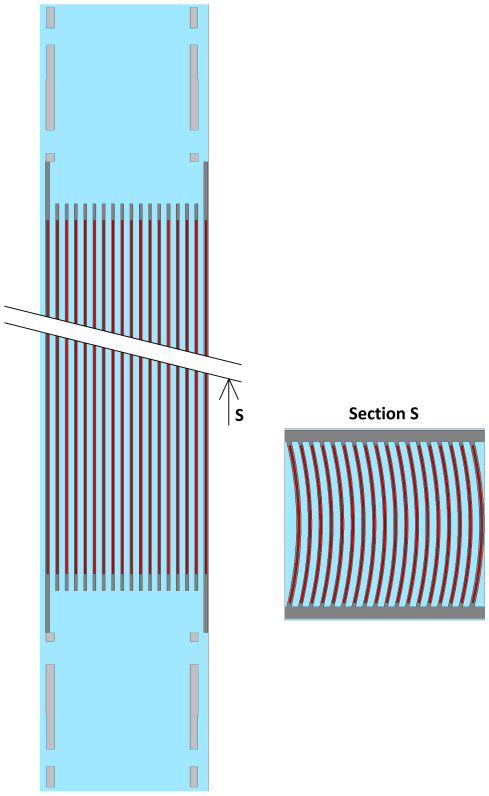

Figure 3.4: FA Serpent model, xz-plot at y = 0 cm with the fuel area cross section.

3.2.2 Control Rod

In each core there are six control rods, five of which are shim-safety rods, and one a regulating rod and safety rod. They are positioned laterally by rod guides and bearings mounted on horizontal bars and plates about 500 mm above and 1300 mm below the core centerline.

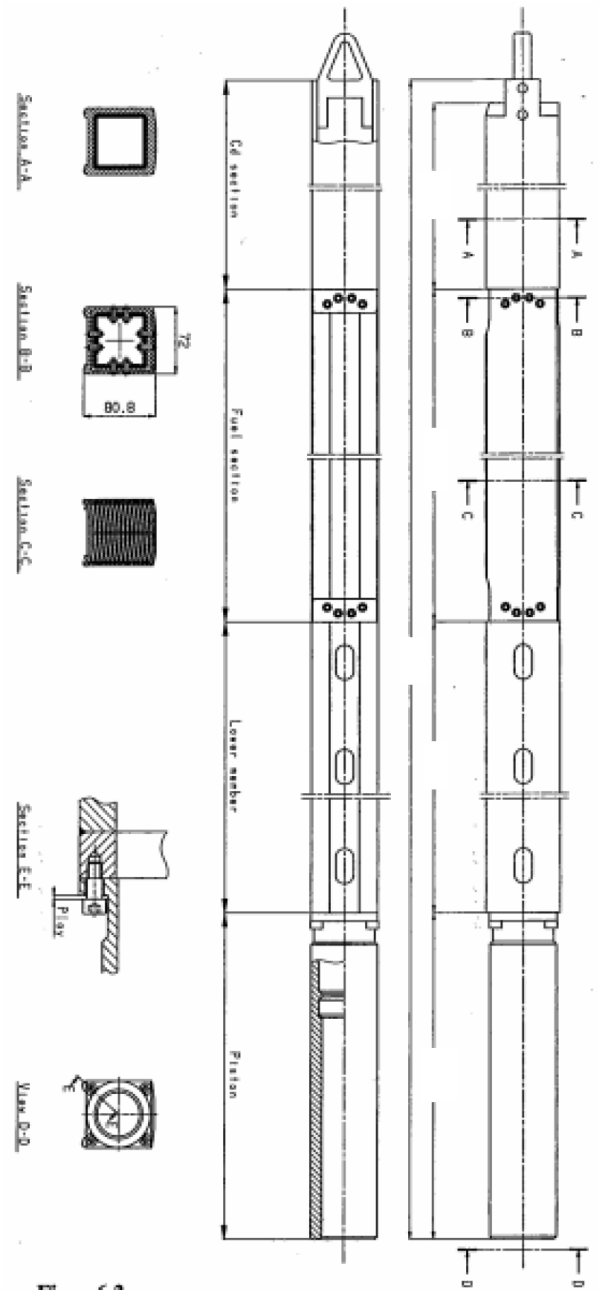

Figure 3.5: Control rod element [1].

The control rods are driven by motors 1780 mm below the lower plug of the reactor. The motors are connected to push rods, and the push rods to adapter pieces which extend through the shock absorbers in the lower plug of the reactor and connect the push rods to the control rods. Leakage from the vessel is prevented by linear seals of V-packing rings between the shock absorber assembly and the drive tube. The main functions of the shim-safety rods (Rods 1 to 5) are to permit coarse control of reactivity during normal start-up, operation and shutdown, and they are used to scram the reactor in case of emergency. Instead the regulating rod (Rod 6) permits manual fine control during start-up and automatic control of transient fluctuations during normal operation. It also acts as scram rod when called upon by safety system [11].
As shown in Figure 3.5 each rod is composed of a cadmium poison section, a fuel section, a lower member section and a piston. The over-all length is about 2920 mm and the outside cross section is 80 mm by 1400 mm to enable the changing of the fuel section of the rod. The regulating rod is identical with the shim rods, except that it has a slightly shorter travel.
The poison section of the control rod, on the upper end of the assembly, is about 970 mm long including 25 mm extensions at both ends. The section consists of an extruded housing of (6065-T5) aluminum and an insert of cadmium sandwiched between (1100-0) aluminum. The compositions of both these Al-alloys are taken from [16] and reported in Table 3.3. The insert is about 815 mm long and 60 mm

Table 3.3: 1100-0 aluminum alloy and 6065-T5 extruded housing aluminum alloy compositions and mass densities.

Isotope	**1100 (wt%)**	**6065 (wt%)**
Al	99.725	95.575
Mg	-	1.000
Si	-	0.600
Cu	0.125	0.275
Cr	-	0.150
Mn	0.050	0.150
Zn	0.100	0.250
Fe	-	0.700
Ti	-	0.100
Bi	-	1.000
Pb	-	0.050
Zr	-	0.150
Density (g/cm^3)	2.71	2.72

square, with a wall thickness of 2 mm; i.e. the cadmium is 1 mm thick and has 0.5 mm of aluminum on each side. The insert is attached to the housing by aluminum rivets. The rod assembly is handled by an eye bolt which is attached to the extension on the upper end of the poison section.
Figure 3.6 shows an xy-plot of the control rod model at a z coordinate of 100 cm, that is positioned in the Cd poison section region, and the reference CAD drawing from the specifications. As it can be seen from Figure 3.6, also in this case the real geometry is a little bit modified in order to allow the control rod to fill exactly a single assembly position in the full core model. Again, the total volume of the material is preserved to make the model consistent.

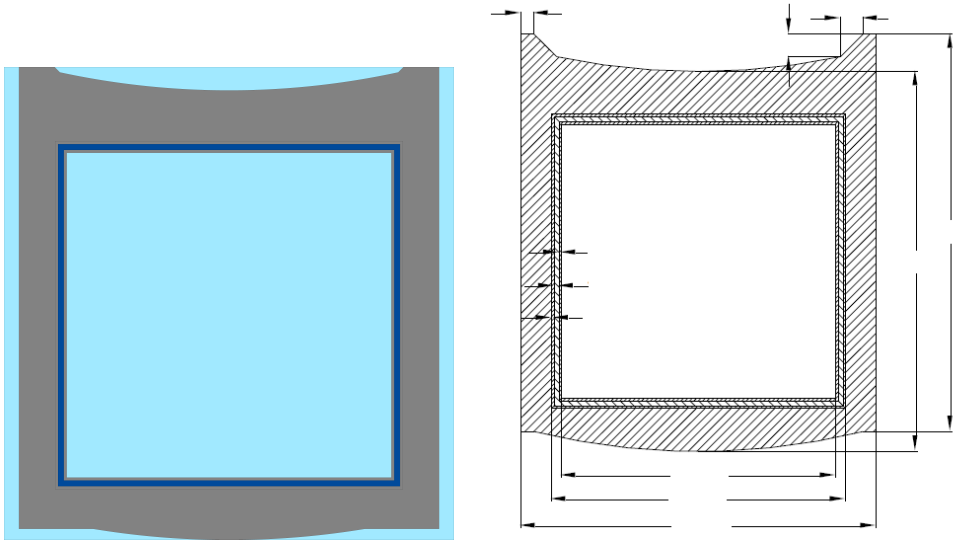

(a) *Serpent xy-plot, z=100 cm* (b) *CAD drawing*

Figure 3.6: Cross Section of the CR Cd poison section modeled with Serpent (a) and CAD drawing from the specifications (b).

The fuel section of the control rod is 685 mm long and contains 15 curved fuel plates swaged to aluminum side plates, whereas the back plate is pin-jointed with OD 2 mm pins at 45 mm axial intervals. The upper and lower ends of the fuel section are riveted to the poison section and the lower member of the rod assembly, respectively. The U-235 enrichment is 19.75% and the U-235 content is 223 g. The fuel plates are 625 mm long, about 1 mm thick, 70 mm wide and have a 140 mm curvature radius. The meat consists of uranium-silicide (U_3Si_2), of which approximated dimensions are 0.5 mm thickness, 60 mm width and 600 mm length. The fuel meat composition reported in Table 3.4 is taken from a CASMO input available in a Studsvik report [17]. The cladding is made in aluminum alloy (AISI 5454), about 0.4 mm thick on the faces (see Table 3.2 for the composition). The

inner surfaces of the front and back plates are machined to the same radius of curvature as the fuel plates, so that all coolant channels within the fuel section are identical. Figure 3.7 shows the Serpent xy-plot at z = 0 cm which is positioned at the center of the CR fuel section.

Table 3.4: Fuel meat isotopic composition for the CAC element.

Isotope	**CAC (wt-%)**
U-238	54.44
U-235	13.42
U-234	0.08
Si	5.51
Al	26.55
Density (g/cm3)	6.09

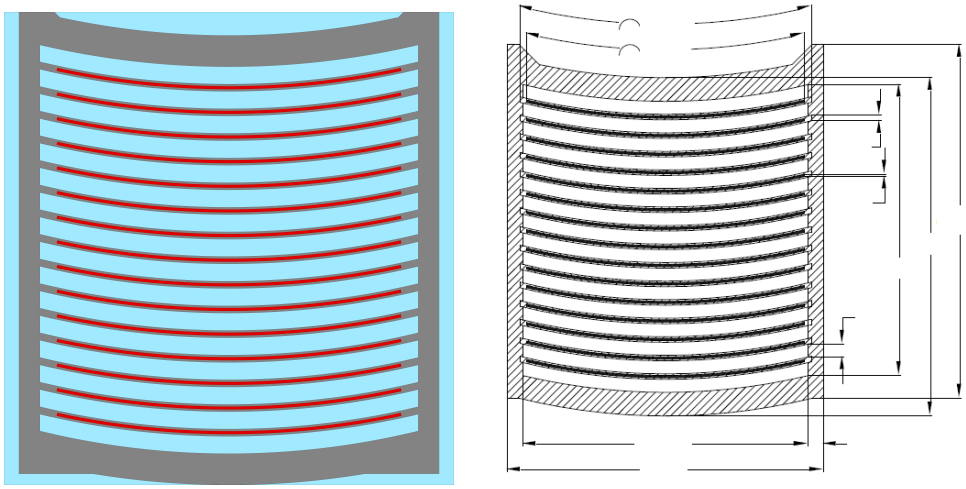

(a) *Serpent xy-plot, z=0 cm* (b) *CAD drawing*

Figure 3.7: Cross Section of the CR fuel section modeled with Serpent (a) and CAD drawing from the specifications (b).

The lower member is made from a (6065-T5) aluminum extrusion and is 950 mm long. The member is hollow and contains 32 slots (about 40 mm by 20 mm) to permit easy discharge of the cooling water from the fuel section. The upper end is riveted to the fuel section and the lower end is bolted to the piston of the rod assembly.
The piston is that part of the shim rod which drops into the shock absorber section

when the rod is inserted. It is at the lower extremity of the shim rod assembly just below the lower member. The external diameter is about 70 mm and the inner one 50 mm, the height is 360 mm and the material is stainless steel.
Figure 3.8 shows the final model of the entire CR through an xz-plot at y-coordinate equal zero, and the xy-plot for the different sections.

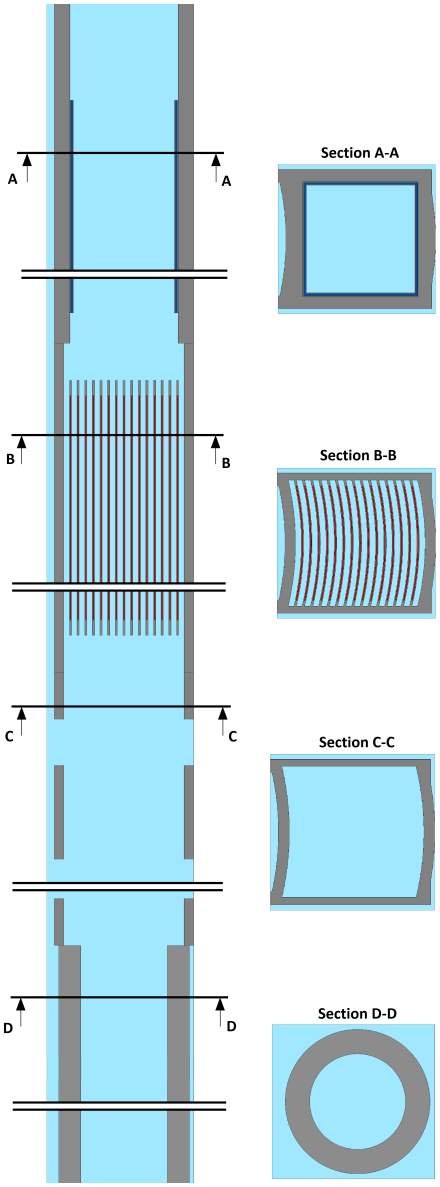

Figure 3.8: CR Serpent model, xz-plot at y = 0 cm with the Cd poison area cross section A-A, fuel area cross section B-B, lower member area cross section C-C and piston area cross section D-D.

3.2.3 No-fuel assemblies

Inside each core, apart from the fuel assemblies and control rods, there are also a variable number of other assemblies that do not contain fuel and are used for different purposes. These assemblies are described in the next paragraphs in terms of geometry and materials, and the final Serpent models are presented. For all of them except the in-pile loops, the geometry is slightly modified to fill a single core position and do not overlap with the neighbouring assemblies in the full core model. This operation is performed preserving the material total volume as described before.

Beryllium reflector assembly

The beryllium pieces are machined to the contour of the fuel elements, and fit in all positions, except in the corner positions which are taken up by aluminum filler elements. A typical beryllium assembly (see Figure 3.9), is approximately 75x80 mm^2 in cross section, and 920 mm long.

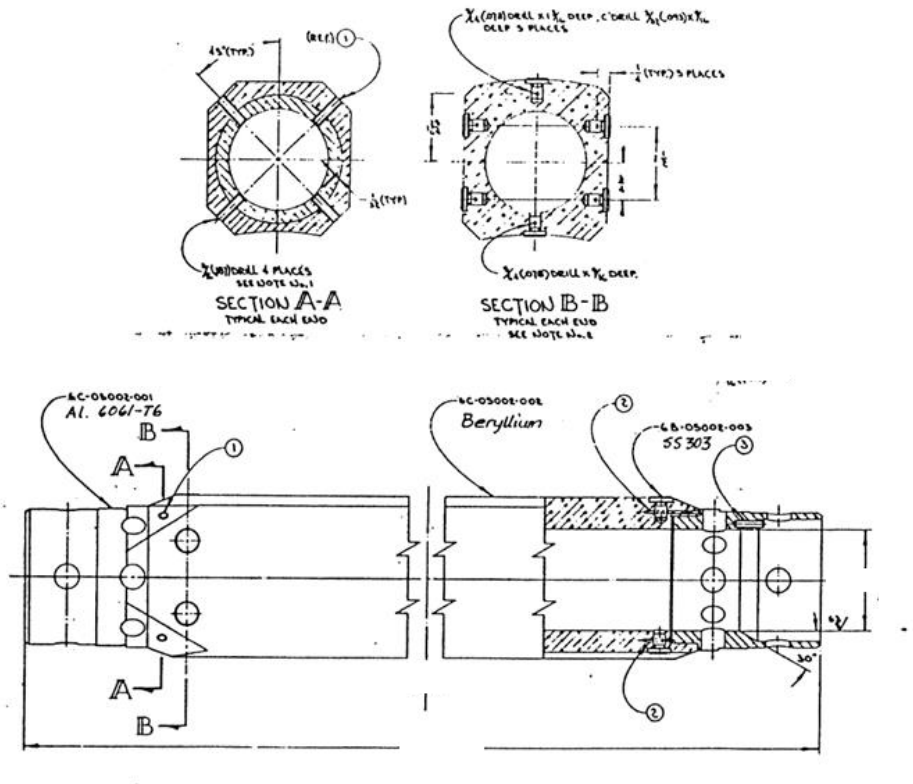

Figure 3.9: Beryllium Reflector Assembly from the specifications [1].

A full-length annulus around the reflector assembly permits water cooling of the beryllium and prevents overheating and distortion. The hollow reflector assembly has perforated aluminum baskets and beryllium plugs 50.8 mm in diameter. The lower end of the reflector assembly is machined, like the fuel element end bowes, to fit into the lower grid plate. The upper end is fitted with an aluminum alloy (6061-T6) adapter which fits into the upper grid (over the control rod rows D and G) and is used to remove/reload the reflector assembly of the ordinary refueling rods/tools. The cross section of the beryllium reflector assembly is shown in Figure 3.10, where the Serpent xy-plot is compared to the CAD drawing of the specifications.

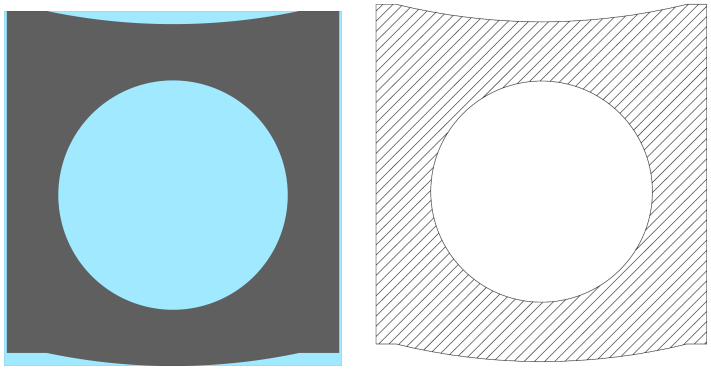

(a) *Serpent xy-plot, z=50 cm* (b) *CAD drawing*

Figure 3.10: Cross Section of the Beryllium Reflector Assembly modeled with Serpent (a) and CAD drawing from the specifications (b).

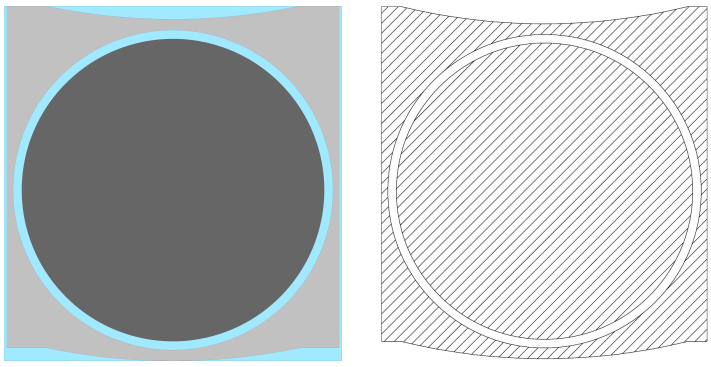

(a) *Serpent xz-plot, y=0 cm* (b) *CAD drawing*

Figure 3.11: Cross section of the aluminum assembly modeled with Serpent (a) and CAD drawing from the specifications (b).

Aluminum assembly

The aluminum assembly is composed by a solid-type adapter (see Figure 3.12) with external dimensions of 75x80 mm^2, inner diameter of 73 mm and a cylindrical aluminum filler of 70 mm in diameter. The total length of the assembly is 860 mm whereas the aluminum filler is 710 mm long. The cross section of this assembly is shown in Figure 3.11, where there are both the Serpent model e the reference CAD drawing on which the model is based.

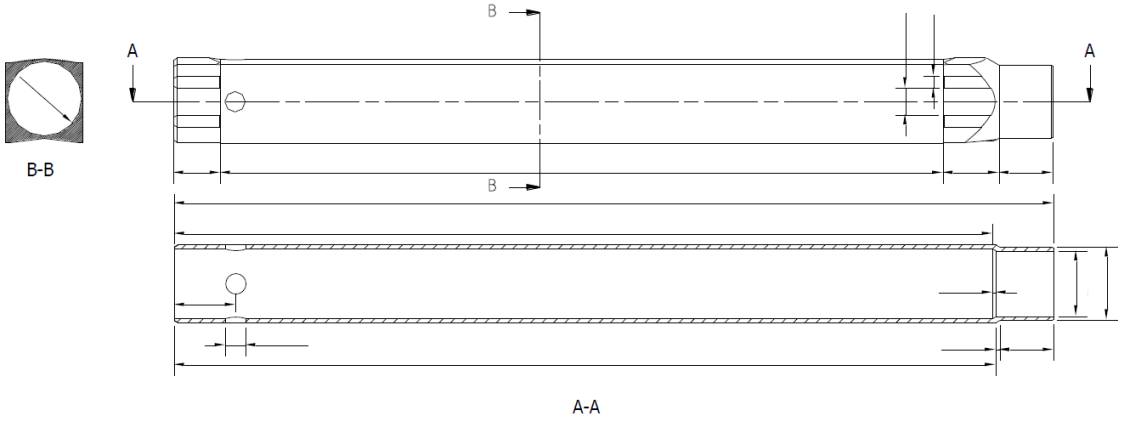

(a) *CAD drawing*

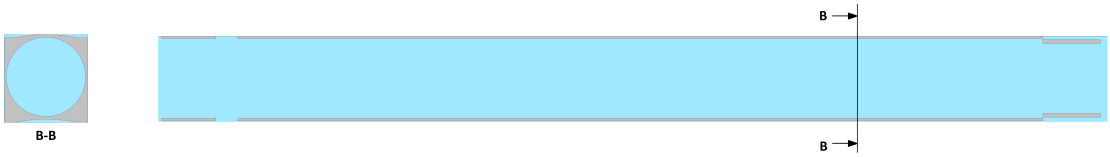

(b) *Serpent xz-plot, y=0 cm*

Figure 3.12: Aluminum assembly adapter CAD drawing from the specifications [1] (a) and modeled with Serpent (b).

IS assembly

The IS assembly is used for most of the isotope production. The IS rig is equipped with two cylindrical containments (first and second walls) of aluminum alloy (6061-T6 see Table 3.2 for the composition), between which the R2 water circulates. In the internal part a maximum of 8 to 10 standard isotope cans are arrayed vertically. The IS assembly is completed with a solidtype adapter with inner diameter of about 50 mm (see Figure 3.13). The cross section of the assembly is shown in Figure 3.14.

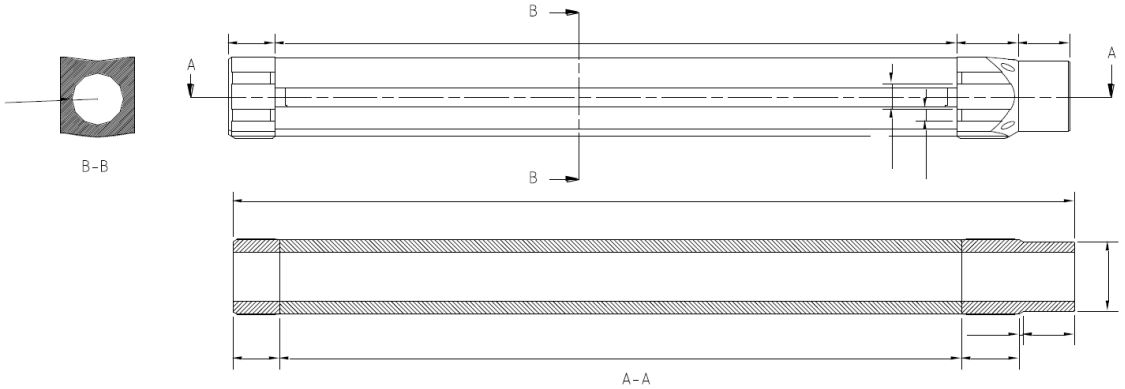

(a) *CAD drawing*

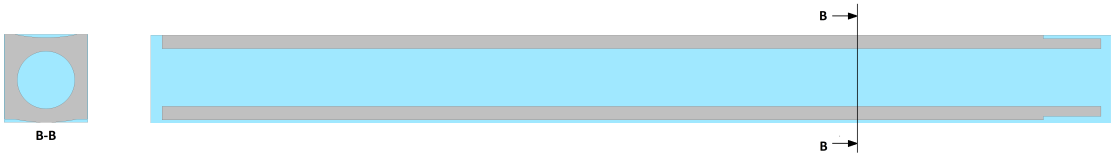

(b) *Serpent xz-plot, y=0 cm*

Figure 3.13: IS assembly adapter CAD drawing from the specifications [1] (a) and modeled with Serpent (b).

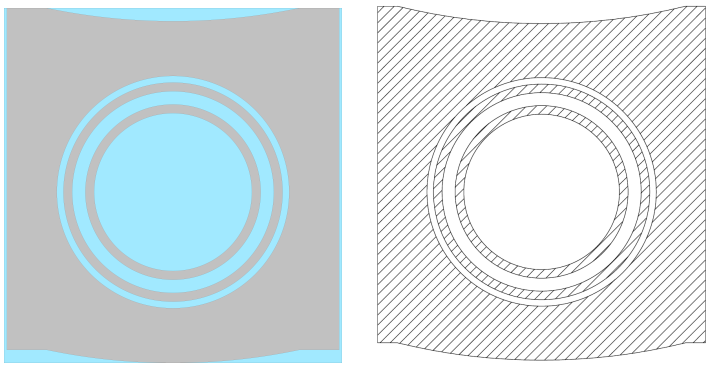

(a) *Serpent xy-plot, z=50 cm*

(b) *CAD drawing*

Figure 3.14: Cross Section of the IS Assembly modeled with Serpent (a) and CAD drawing from the specifications (b).

Iridium assembly

Contrary to the IS assembly, the Iridium assembly is a special experimental irradiation device used for the Iridium irradiation. The adapter is a hollow-type adapter in which water flows inside, with external wall thickness of 1.5 mm. The

internal cylindrical wall has an outer diameter of 50 mm and a thickness of 2 mm (see Figure 3.15). The cross sections of the assembly is shown in Figure 3.16.

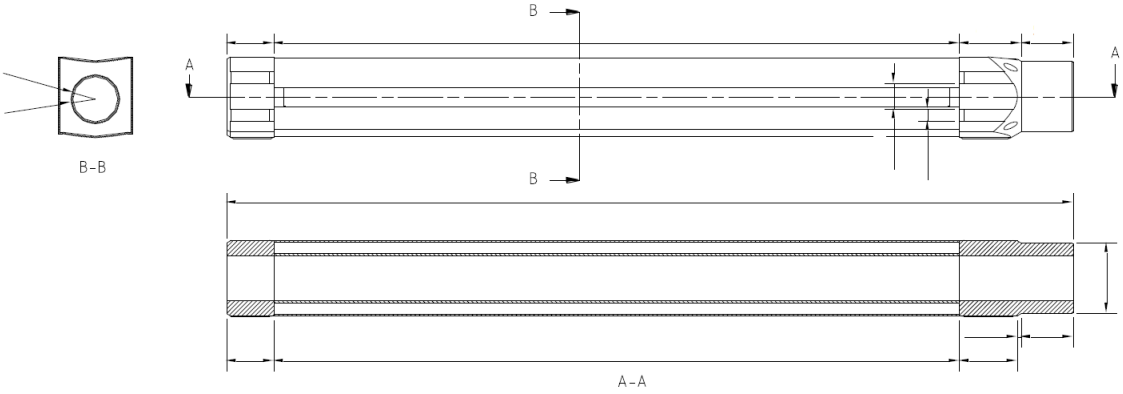

(a) *CAD drawing [1]*

(b) *Serpent xz-plot, y=0 cm*

Figure 3.15: Iridium assembly adapter.

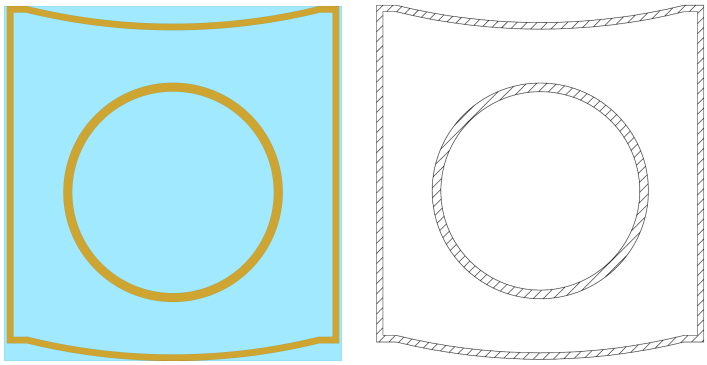

(a) *Serpent xy-plot, z=50 cm*

(b) *CAD drawing [1]*

Figure 3.16: Cross Section of the Iridium Assembly.

Ramp test U-tubes

The last no-fuel assemblies inside the core are the two in-pile loops that are used to simulate PWR and BWR temperature and pressure conditions, in order to

perform several tests. These two loops occupy two diagonally adjacent positions inside the core which are C3-B4 and B8-C9. Both of them consist in a high pressure tube of U-tube shape made with stainless steel AISI 316L (see Table 3.5 for composition), which is inserted inside a gas jacket filled with CO_2. The gas is used to thermally insulate the loop, in which the temperatures can be much larger with respect to the reactor core domain. The inner and outer radius of the high pressure tube are about 23.5 mm and 26.5 mm respectively, while for the gas jacket around 29 mm and 31 mm. Since this loops are much longer with respect to the core heigth (almost 4 m vs. less than 1 m), the lower part of the high pressure tube, which is the U-shaped component that connects the discending and the ascending sides is not modeled, since its influence on the simulation results is completely negligible if we consider that the neutron flux at such distance is practically zero.

Table 3.5: High pressure tube and gas jacket stainless steel AISI 316L composition and mass density [3].

Isotope	**AISI 316L (wt%)**
Fe	65.545
Cr	17.000
Ni	12.000
C	0.030
Mo	2.500
Si	0.750
Mn	2.000
N	0.100
P	0.045
S	0.030
Density (g/cm^3)	7.9

The region where the loops pass through the core is inserted in turn inside an assembly adapter, which has dimensions similar to all the other assemblies (about 860 mm of length 75x80 mm^2 in cross section). Figure 3.17 shows the downward section U-tube adapter and Figure 3.19 its cross section at core level, while the adapter for the upward section is shown in figure 3.18 and its cross section at core level in Figure 3.20 (the violet indicates the CO_2).

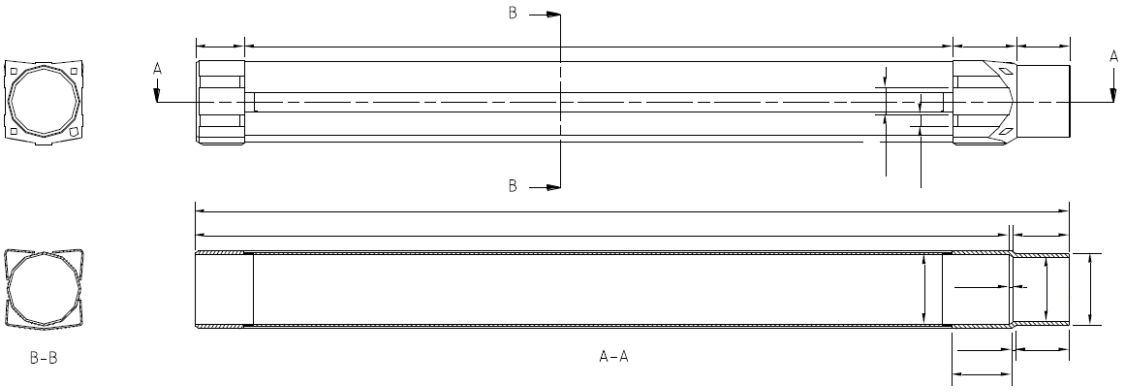

(a) *CAD drawing*

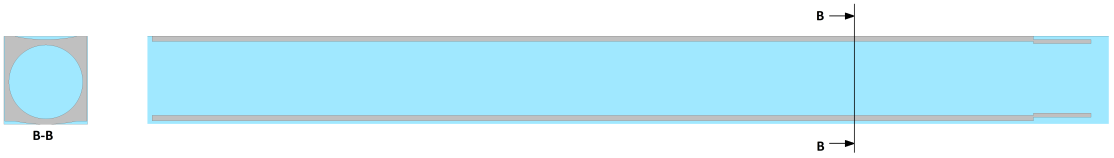

(b) *Serpent xz-plot, y=0 cm*

Figure 3.17: U-tube Adapter of the Downward Section, CAD drawing from the specifications [1] (a) and modeled with Serpent (b).

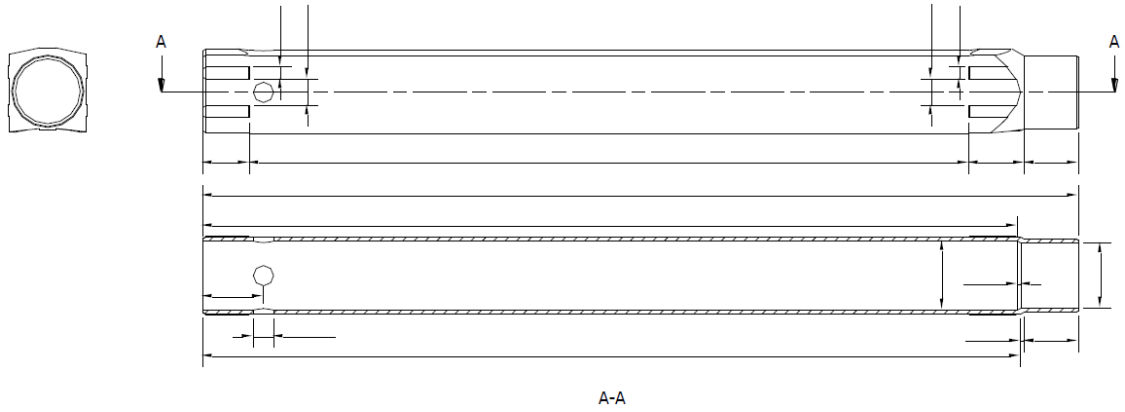

(a) *CAD drawing*

(b) *Serpent xz-plot, y=0 cm*

Figure 3.18: U-tube Adapter of the Upward Section, CAD drawing from the specifications [1] (a) and modeled with Serpent (b).

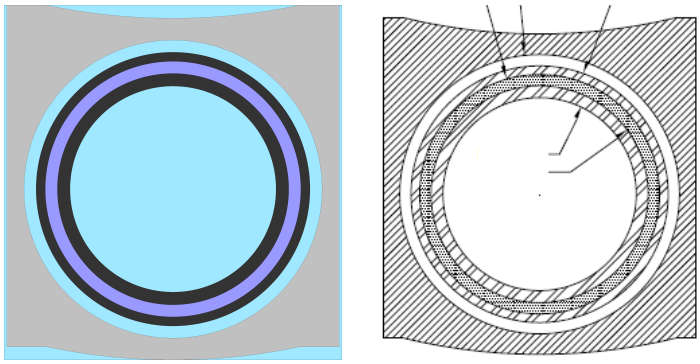

(a) *Serpent xy-plot, z=50 cm* (b) *CAD drawing*

Figure 3.19: U-tube Downward Section Cross Section at Core Level, modeled with Serpent (a) and CAD drawing from the specifications (b).

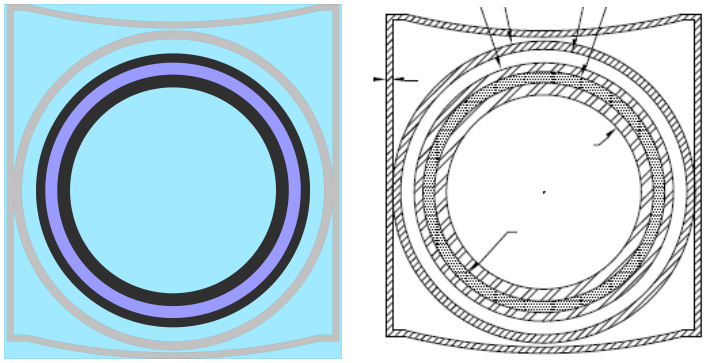

(a) *Serpent xy-plot, z=50 cm* (b) *CAD drawing*

Figure 3.20: U-tube Upward Section Cross Section at Core Level, modeled with Serpent (a) and CAD drawing from the specifications (b).

Furthermore, the high pressure tube in position C3 is used to perform the power ramp tests analysed in the benchmark, which consist in different phases and configurations that follow one another over the course of the core cycle of interest. It has been decided to model all of these different configurations and put the right one during all the phases of the core cycle in order to follow the high-fidelity criteria, even if probably the impact on the results of the full core burn-up simulation may not be that significant since we are talking of very small components. The C3 configurations are:

- Configuration α: the simpler one, in which the ramp rig is inserted inside the high pressure tube. It is a cylindrical component of about 15 mm of outer

radius and 10 mm of inner radius;

- Configuration β: in which the high pressure tube contains the ramp rig with the ramp capsule inserted in it, that protects the empty rod used for the gamma heating measurement. The ramp capsule is about 20 mm OD and 17 mm ID, and it is inserted in the core in correspondence of the fuel active length. The empty rod is about 450 mm long and it is a cylinder of 10 mm of diameter of which the cladding thickness is smaller than 1 mm. It is an exact reproduction of the fuel rodlet, but instead of the fuel some air is put there;
- Configuration γ: in this configuration the ramp rig inside the high pressure tube contains the ramp capsule which hold the fuel rodlet that will be ramp tested. The dimensions are exactly the same as configuration beta, but in this case there is also an He gas gap in the fuel rodlet, smaller than 0.02 mm. The rodlet material is UO_2 with 2.22% enrichment and density equal to 10.6 g/cm^3. The cladding is made in Zry-2 which is described in Table 3.6.

Figure 3.21 shows the cross sections modeled with Serpent of the three different configurations at the z-height corresponding to the core center.

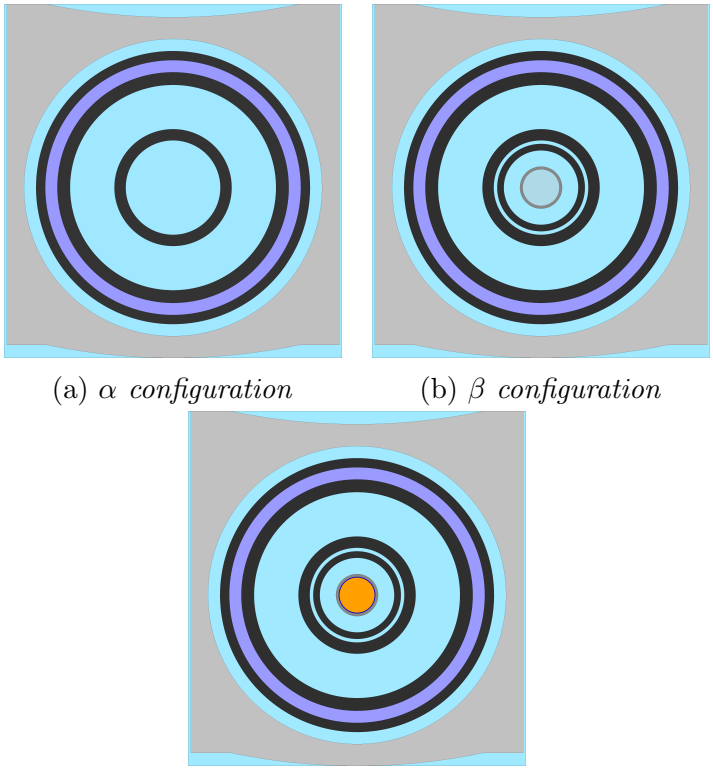

(a) α *configuration* (b) β *configuration*

(c) γ *configuration*

Figure 3.21: C3 configurations Serpent cross sections at core central height.

Table 3.6: Zircaloy 2 composition and mass density [4].

Isotope	**Zry-2 (wt%)**
Zr	98.20
Sn	1.50
Fe	0.15
Cr	0.10
Ni	0.05
Density (g/cm^3)	6.56

3.2.4 R2 Core

Once the models of all the assemblies are completed they can be loaded in each right position in the core box, in order to build the full core model. The Serpent model of the R2 core comprises the core box with all the assemblies inside and the D_2O box aroud it. The D_2O box is geometrically described hereafter, but not in terms of modeling since it was realised by the PhD Simone Di Pasquale from NINE. The R2 core is surrounded on three sides by heavy water blankets and is immersed in light water. On the North and South fronts of the reactor core there are D_2O blanket compartments, the purpose of which is to enlarge the area/volume with high thermal neutron flux. These compartments are integral with the reactor vessel core box and contain axial irradiation channels (ID 40 mm, OD 50 mm) filled with heavy water. The blanket chambers are 85 cm in height and 30 cm width (between the internal surface in N-S direction). In addition, the wall thickness of the chambers is 2.5 cm and the axial centerline is at the same elevation of the core centerline.
On the West side of the core, it is installed a D_2O box which acts as neutron flux trap for the horizontal beams. It consists of a rectangular region with a cross section of about 90x80 cm^2 and two semicircular lateral parts (North and South sides) with an inner radius of 35 cm. The pool height is 70 cm from the bottom of the core box and the wall thickness is 1.5 cm. A sketch of the three heavy water blankets is reported in Figure 3.22.
The core is arranged in a 10 x 8 lattice with an active length of 60 cm. It is surrounded by a rectangular core box with outer dimensions of about 91x72 cm^2 and a height of 80 cm. The walls of the core box have a thickness of 50 mm (East and West sides) and of 45 mm (North and South sides) and are perforated by 190 holes along the perimeter to allow the core box cooling. All the assemblies are arranged inside the core box with a pitch of 80 mm in N-S direction and 75 mm in E-W direction. Instead, the distance of the assemblies from the core box walls is of 3 mm

in E-W direction on both sides and of 8 mm in N-S direction from a corner of the assembly on both sides. All the structures surrounding the core region, including the core box and the D_2O blankets compartments are made of aluminum.

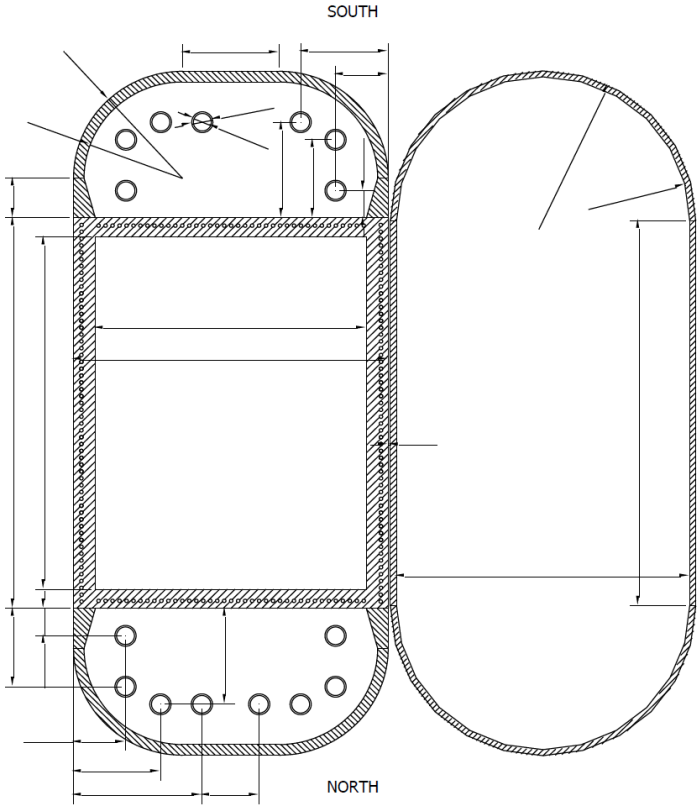

Figure 3.22: R2 Core box and D2O blanket CAD drawing from [1].

The core cosidered to build the model is the 1105, which is the first one between the three of interest for the benchmark. Figure 3.23 shows a general 10x8 lattice layout of the R2 core, while the 1105 core loading configuration is reported in Figure 3.24. The 1105 core loading is composed by the following assemblies:

- 24 CF Fuel Assemblies (CF037 CF041 CF038 CF001 CF029 CF030 CF026 CF031 CF003 CF033 CF040 CF036 CF042 CF028 CF035 CF008 CF032 CF034 CF007 CF020 CF012 CF021 CF006 CF017);
- 23 CA Fuel Assemblies (CA433 CA419 CA458 CA471 CA508 CA407 CA423 CA498 CA505 CA484 CA386 CA501 CA446 CA502 CA490 CA480 CA450 CA422 CA373 CA406 CA397 CA435 CA470);
- 6 Control Rods (CA053C CA057C CA056C CA055C CA050C CA051C);

- 11 Beryllium Reflector Assemblies (BE);
- 6 Aluminium Assemblies (ALH);
- 5 IS Assemblies (K211 K177 K174 K153A M134);
- 1 Iridium Assembly (K180a);
- 2 In-Pile Loops (Loop 1: descending side RAMP, ascending side SL11; Loop 2: descending side SL21, ascending side SL22).

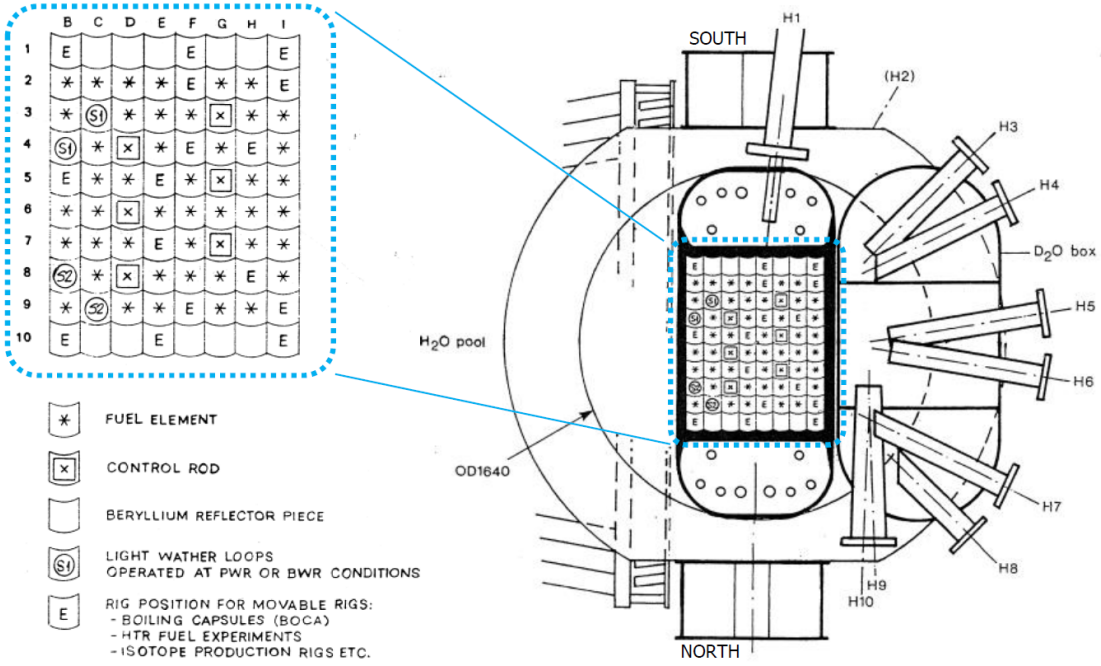

Figure 3.23: R2 Core Arrangement [1].

ALH	BE	BE	BE	BE	BE	K211	ALH
CF037	CF041	CF038	CA433	CF001	CA419	CA458	CA471
CF029	RAMP	CA508	CA407	CF030	CA053C	CF017	CA505
SL11	CF042	CA057C	CF026	K180a	CF031	M134	CF003
CF033	CF040	CF036	K177	CF028	CA056C	CF035	CF008
CF032	CF034	CA055C	CF021	K174	CF006	CA423	CF007
CA498	CF020	CF012	K153A	CA484	CA050C	CA386	CA501
SL21	CA446	CA051C	CA502	CA490	CA480	CA450	CA422
BE	SL22	BE	CA373	CA406	CA397	CA435	CA470
ALH	ALH	ALH	BE	BE	BE	BE	ALH

Figure 3.24: 1105 Core loading configuration.

Finally, Figure 3.25 shows the xy-plot at the z level corresponding to the fuel active length height center of the final 3D R2 core Serpent model. The different light blue shades are used to highligth the difference between light water and heavy water. All the assemblies are put in the right positions as described in 3.24 and they can be seen zoomed in the precedent dedicated sections.

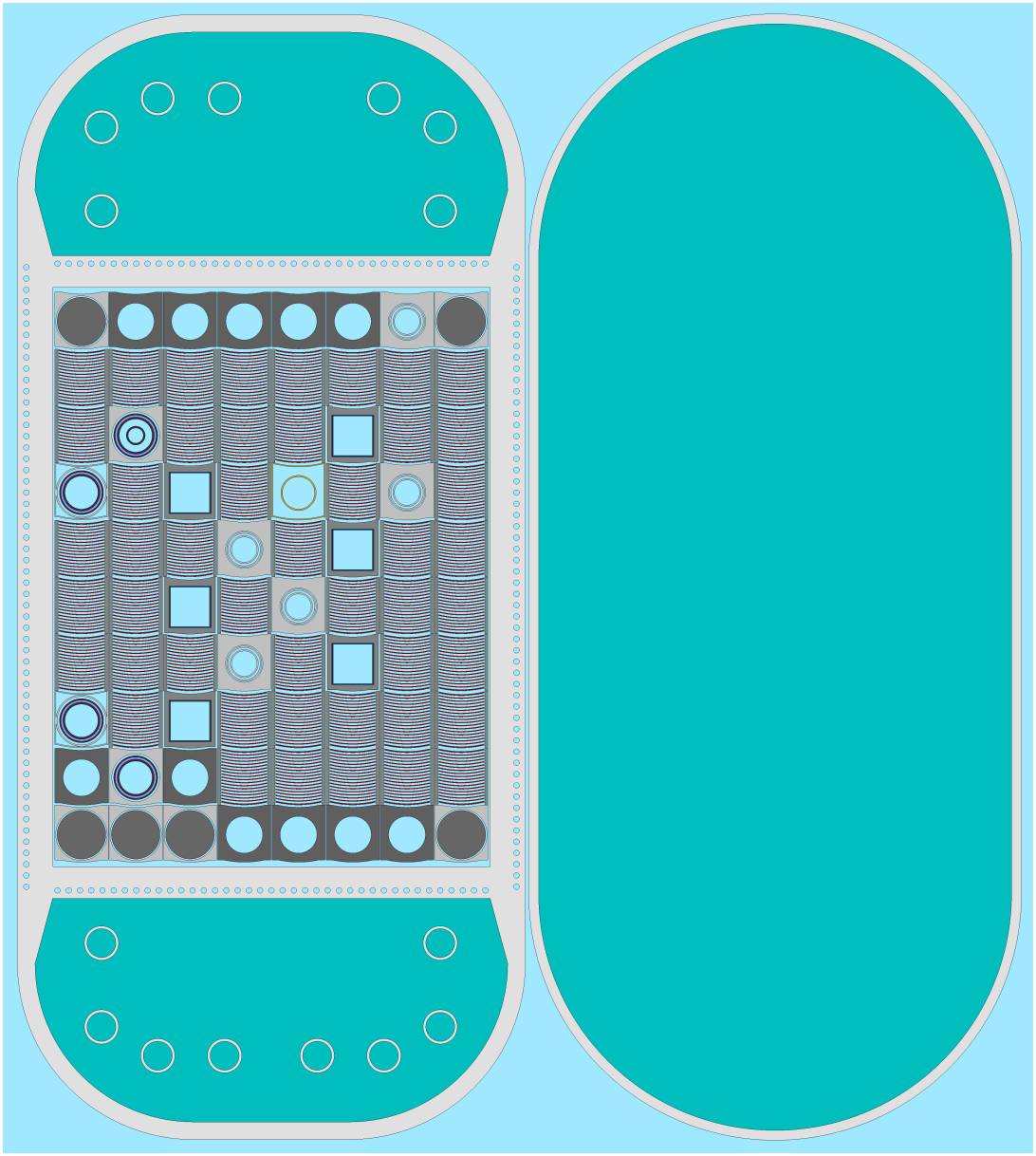

Figure 3.25: Serpent R2 Core model xy-plot, z=0 cm.

3.3 Single assembly depletion

The first set of Serpent simulations is the infinite lattice single assembly depletions necessary to derive the initial fuel isotopic compositions of the assemblies that must be loaded in the full core model. As it has been anticipated at the beginning of this chapter, this step is necessary since the fuel assemblies loaded in the cores of interest are not of fresh fuel, but they have already been used in precedent core cycles during which they have been depleted. This depletion is the incognita of the problem since there are no information about the number of previous cycles of the R2 core, the power and CRs levels, the time of irradiation or not of each assembly and so on. For this reason it is very difficult to simulate exactly the previous history of the fuel assemblies, since it is probably different for all of them and since no one of the numerous simulation parameters is known.
In order to proceed in a systematic way and compensate for this important missing information, it is necessary to consider which data are known and from these ones try to derive the rest. What is known in terms of isotopic compositions is the U-235 mass content of each fuel assembly at the beginning of the core loadings and the isotopic compositions of the discharged fuel assemblies at the end of the core loadings. The first information is used as the starting point, while the second one is used to have an important feedback on the original guess and decide how to improve this guess.
Considering all of this, the proposed strategy consists in performing the infinite lattice depletion calculation for all of the assembly types, following a certain setup of simulation parameters (power level, temperatures), and then derive the initial isotopic compositions at BOC interpolating the curves obtained from this infinite lattice depletion. How the interpolation is done is better explained in the following sections. Then, once that the initial isotopic compositions are derived for all the FAs and CRs, it is possible to load them in the 1105 core model, with all the other assemblies and perform the full core burn-up simulation. At the end of this first core cycle, the isotopic compositions of the discharged fuel elements can be compared with the data from Studsvik. Here it comes the feedback on the original assumptions: if the difference between what is simulated and what is given is low, it means that the original assumptions were very good and they managed to simulate in a simplified way a very complex previous depletion history of the fuel assemblies. However, considering all the incognita of this problem that case would be a quite lucky or rare one and probably there is something that must be changed to improve the quality of the results. This feedback check can be done at the end of each attempt, or can be somehow "anticipated". This "anticipated" means that before to see the results of the full core burn-up calculation, different initial guesses about the infinite lattice depletion are collected in a sort of dataset from which derive the initial isotopic compositions. This dataset is constructed in such a way to cover all the possibilities for the infinite lattice depletion simulation setups, so that among

all of these possibilities there is the best guess. The latter is the chosen option, since it also allows to perform a sensitivity analysis on the simulation parameters in order to see how much they impact the Serpent simulation results.
Hereafter, it is described how the dataset of initial isotopic compositions is built, starting from the selection of the interesting parameters and arriving to the different ways and possibilities to combine them. All of the single assembly depletion calculations adopt boundary conditions of periodic type radially and vacuum axially. The decay period is neglected, since that information is not available and the depletion is carryed on until it get to the lowest assembly U-235 content. Each infinite lattice depletion assumes homogeneous temperatures inside the fuel, the cladding and the moderator. This is a further simplification of the problem, since in Serpent it is not possible to give a continuous distribution of the temperatures, for example using a sinusoidal function, but to do that it would be necessary to define different material cards in which the difference is only the temperature for each specific region. This is of course an important simplification, but it was done in order to manage to arrive to the final results of the full core simulation considering the available time. However, the option to define different materials is still an interesting case to be analysed and a suggested activity for the future.

3.3.1 Identification of the dataset parameters

Considering what can impact the most the results of the depletion calculations, the parameters taken into account during this analysys are the fuel temperature, the moderator temperature and the power density. The fuel temperature is selected a priori, since it has the most important effect on the isotopes cross sections and so it is strictly connected with the depletion of the materials and the isotopes concentrations evolution. For the other two, it is performed a sensitivity analysis which is described in the next paragraphs in order to see their influence on the simulation results, and select only the parameters which have an important effect.

Moderator temperature sensitivity analysis

The sensitivity analysis must consider the realistic range of variation of the moderator temperature, and decide which values to consider in this range to perform the simulations by fixing all the other parameters in order to isolate the effect of this one. The only information about the moderator temperature in give in Table 3.15 of the specifications, where it is indicated the coolant inlet temperature as 34 $\pm$ 2 °C [11] and the temperature variation in the core between inlet and outlet of about 10 °C. In this range, three different moderator temperatures are considered for the sensitivity analysis: 30 °C, 37 °C and 45 °C.
The simulations are porformed for a CF assembly of fresh fuel, and an infinite lattice depletion is considered. The simulation setup for all the other parameters is

fixed and it is described in Table 3.7.

Table 3.7: Simulation setup for the moderator temperature sensitivity analysis.

Parameter	Quantity	Unit
Neutron population	10000	-
Active cycles	500	-
Inactive cycles	50	-
Power density	2.2	kW/gU235
Fuel temperature	90	°C
Cladding temperature	55	°C

	U-235	**U-236**	**Np-237**	**Pu-238**	**Pu-239**	**Pu-240**	**Pu-241**	**Pu-242**
max	0.45%	0.41%	1.08%	1.32%	0.58%	0.98%	1.33%	1.54%
ave	0.39%	0.39%	0.57%	0.56%	0.40%	0.73%	0.90%	1.11%

(a) *Difference between T_1=30 °C and T_2=37 °C.*

	U-235	**U-236**	**Np-237**	**Pu-238**	**Pu-239**	**Pu-240**	**Pu-241**	**Pu-242**
max	0.36%	0.23%	1.12%	1.33%	0.54%	1.31%	1.83%	2.31%
ave	0.20%	0.20%	0.64%	1.00%	0.35%	0.93%	1.17%	1.67%

(b) *Difference between T_1=30 °C and T_2=45 °C.*

	U-235	**U-236**	**Np-237**	**Pu-238**	**Pu-239**	**Pu-240**	**Pu-241**	**Pu-242**
max	0.20%	0.22%	1.14%	0.85%	0.45%	0.57%	0.83%	1.15%
ave	0.19%	0.19%	0.40%	0.52%	0.24%	0.21%	0.33%	0.57%

(c) *Difference between T_1=45 °C and T_2=37 °C.*

Table 3.8: Isotope inventories mass difference from the moderator temperature sensitivity analysis.

Since the objective of the analysis is to derive the fuel assemblies isotopic compositions, the difference in the three simulations is investigated specifically considering the final isotopic composition derived from the three infinite lattice depletions. The considered parameter to be compared is the percentage difference between the computed isotope inventories, calculated as $\frac{|m_{T1}-m_{T2}|}{m_{T2}} \cdot 100$, where m_{Tn} is the mass in grams of each isotope at the T_n moderator temperature. Table 3.8 shows the results of the comparison between the simulations with T_1=30 °C and T_2=37 °C (case a),

T_1=30 °C and T_2=45 °C (case b), and T_1=45 °C and T_2=37 °C (case c). The difference is calculated for all the isotopes at each burn-up step, among all the values the maximum and the average ones are reported in the final results table.
From the results it can be seen that the percentage difference of the isotope mass inventories in the three cases is quite low (about 1% or less). For this reason, the conclusion of the analysis is that the moderator temperature can be fixed for the infinite lattice depletions at an average value of 37 °C. So this one is not considered as an interesting parameter to be taken into account for the dataset construction.

Power density sensitivity analysis

The second parameter considered for the dataset construction is the power density. The power density is connected to the isotopes depletion since low level of power density can little change the isotopes concetration, but if it increases the evolution in time of the isotopes population can change a lot in a non linear way which depends on many factor among which the radioactive dacays that are time dependent and not easy to predict. As described in the section 3.1 the burn-up of the simulations is defined as "butot", that requires to define the depletion steps as cumulative burnup in MWd/kgU. In this way, what changes at each burn-up step between two different power density levels is the irradiation time and not the number of fissions occurred, and it is reasonable to compare the values for the isotope inventories at each step. If the depletion mode is set to a time quantity, like burn-up days, that comparison would be useless, since under the same conditions the results would be the same.

Table 3.9: Simulation setup for the power density sensitivity analysis.

Parameter	Quantity	Unit
Neutron population	10000	-
Active cycles	500	-
Inactive cycles	50	-
Fuel temperature	60	°C
Cladding temperature	40	°C
Moderator temperature	37	°C

Differently from the moderator temperature case, there is no information about the previous power history of the R2 core. The only information is the nominal power of the reactor of 50 MW, but it would be a great assumption to say that the average power of the previous cycles is this one. For this reason different possibilities have to be investigated, and a sensitivity analysis on the power density is performed in order to see if different values produce great differences in the isotopes

evolution. The simulation setup for the sensitivity analysis performed with Serpent is described in Table 3.9.
The power density values considered for the analysis are 1.3 kW/gU235, 1.8 kW/gU235 and 2.2 kW/gU235, which respectively correspond to R2 reactor powers of about 30 MW, 40 MW and 50 MW. The power densities in kW/gU235 are obtained starting from the reactor power values and dividing them for the U-235 mass in grams. This one is of course an assumption for the same reasons explained before (no available information about previous reactor history). The hypotesis made in this case is to consider the beginning of the core as if it is loaded with fresh fuel elements in the same positions as the core loading 1105. So there are 24 CF elements, 23 CA elements and 6 CAC fuels of the control rods. To obtain the total U-235 mass it is sufficient to multiply the number of assemblies for the nominal U-235 content of each of them, that is $24 \cdot 490g + 23 \cdot 400g + 6 \cdot 223g = 22298g$. Table 3.10 shows the results of the difference between the isotope inventories calculated again as $\frac{|m_{P1} - m_{P2}|}{m_{P2}} \cdot 100$, where m_{Pn} is the mass in grams of each isotope at the P_n power density. The case (a) consider P_1=2.2 kW/gU235 and P_2=1.8 kW/gU235, case (b) P_1=2.2 kW/gU235 and P_2=1.3 kW/gU235 and finally case (c) P_1=1.3 kW/gU235 and P_2=1.8 kW/gU235.
The results show that in this case the difference is much higher and important (even 75%). For this reason the power density is one of the parameters that needs to be taken into account for the dataset generation.

	U-235	**U-236**	**Np-237**	**Pu-238**	**Pu-239**	**Pu-240**	**Pu-241**	**Pu-242**
max	0.65%	0.10%	20.49%	35.92%	35.40%	33.78%	33.61%	33.17%
ave	0.13%	0.07%	11.44%	20.83%	7.59%	4.61%	5.09%	5.47%

(a) *Difference between P_1=2.2 kW/gU235 and P_2=1.8 kW/gU235.*

	U-235	**U-236**	**Np-237**	**Pu-238**	**Pu-239**	**Pu-240**	**Pu-241**	**Pu-242**
max	1.32%	0.21%	40.17%	63.46%	62.99%	60.55%	60.62%	59.30%
ave	0.26%	0.15%	22.73%	38.90%	14.42%	8.96%	9.98%	10.80%

(b) *Difference between P_1=2.2 kW/gU235 and P_2=1.3 kW/gU235.*

	U-235	**U-236**	**Np-237**	**Pu-238**	**Pu-239**	**Pu-240**	**Pu-241**	**Pu-242**
max	0.68%	0.11%	33.09%	75.49%	74.56%	67.89%	68.58%	64.23%
ave	0.13%	0.08%	15.84%	33.65%	12.09%	6.91%	7.59%	7.99%

(c) *Difference between P_1=1.3 kW/gU235 and P_2=1.8 kW/gU235.*

Table 3.10: Isotope inventories mass difference from the power density sensitivity analysis.

3.3.2 Build up of the dataset

Considering the results of the sensitivity analyses, the two interesting parameters for the build up of the dataset of the fuel assemblies initial isotopic compositions are the fuel temperature and the power density. The next step, which is described below, is to consider the range of variation of these parameters and inside these to chose different combinations of the two, in order to cover the largest number of cases that may produce different isotope inventories. To do that, two different strategies are proposed in order to find the best solution.

1st Approach – Matrix Combination

The 1st approach is called the Matrix Combination and it consists in selecting 4 different values of the fuel temperature (T_f) and 3 different values for the power density (P) and couple all of them for a total of 12 simulations for each single assembly type. Since there are three different single assembly types throughout all R2 cores these 12 simulations must be performed for each of them, for a total of 12 x 3 = 36 simulations. It is called "Matrix Combination" since the coupling between temperature and power in this case follows a matrix path which combines also the highest power densities with the lowest fuel temperatures, which is less realistic than coupling higher or smaller values for both of them. The reason why this is still done is that there is no certain information about the material properties and the simulation parameters, so a random choice can be useful to have as much different cases as possible in the dataset. The values chosen considering both range of variation of the parameters from original documents [17] and from literature [18] are reported in Table 3.11.

Table 3.11: Matrix Combination simulations setup.

$\mathbf{P_{dens} \backslash T_{fuel}}$	$\mathbf{T_{f1}}$**=40 °C**	$\mathbf{T_{f2}}$**=50 °C**	$\mathbf{T_{f3}}$**=60 °C**	$\mathbf{T_{f4}}$**=70 °C**
$\mathbf{P_1}$**=1.3 kW/gU235**	CF CA CAC	CF CA CAC	CF CA CAC	CF CA CAC
$\mathbf{P_2}$**=1.8 kW/gU235**	CF CA CAC	CF CA CAC	CF CA CAC	CF CA CAC
$\mathbf{P_3}$**=2.2 kW/gU235**	CF CA CAC	CF CA CAC	CF CA CAC	CF CA CAC

2nd Approach – Temperature Profile Evaluation

Differently from the Matrix Combiation approach, the Temperature Profile Evaluation approach considers the real relation between the reactor power and the fuel temperature, and so the values are not randomly coupled in this case, but it is evaluated the heat transfer and the power balance that produces a specific temperature distribution. In this way, starting from the three different power levels a unique value for the fuel, the cladding and the moderator temperature is derived and it is

more realistic with respect to the matrix approach coupling.
To do that a RELAP5 thermal-hydraulic model for each single assembly type (CF, CA, CAC) is developed and it is used to compute the temperature distribution inside the structures starting from a certain power generation. Since the CF and CA elements are geometrically identical only two models are built: one representative of the fuel assemblies and one of the control rods.
The RELAP5 model simulates only the fuel active length section which is 60 cm long and adopts BICs to simulate the rest of the reactor system. The nodalization of the model is shown in Figure 3.26.

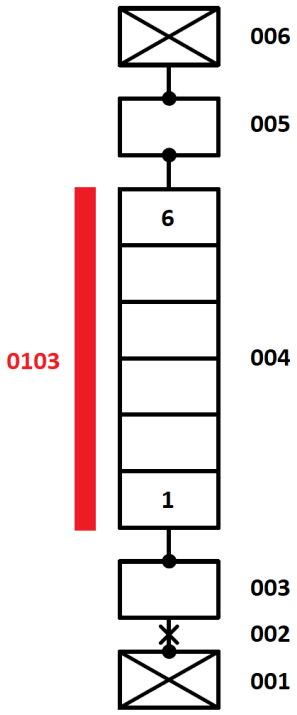

Figure 3.26: Single assembly RELAP5 model nodalization.

As it can be seen from figure 3.26, the model is composed by six hydrodynamic components that simulate the coolant (moderator) and one heat structure that stands for the assembly structure itself. These components are described in detail in the sequent bulleted list starting from the bottom of the nodalization (for the description of the RELAP5 code and an explanation of the meaning of each component/card see section 4.3):

- 001 time dependent volume, this component is used to give the initial conditions of the coolant, which are 305.15 K for the temperature and 311000.0 Pa for the pressure (taken from [1]);
- 002 time dependent junction, it connects the component 001 to 003 and it gives

the initial condition for the average cooling flow rate between the fuel plates. This one is taken from Table 6.5 of [19] and it is different for the control rod model and the fuel assembly model, since the geometry is different. In particular it is equal to 6.2 m/s for the FA model and 4.9 m/s for the CR model;

- 003 branch, it connects the time dependent junction 002 with the pipe 004;
- 004 pipe, this one represents the assembly itself and it simplifies the water between plates complicated geometry as if it was a single pipe. The total length of 60 cm is divided into 6 control volumes of 10 cm each, that preserve the same volume as the real case. In order to take into account the real geometry it is computed the hydraulic diamenter as 4 times the flow area divided by the wetted perimeter. Word 1 of card 0041001 is set to 0000200, which means that the ORNL ANS interphase friction model will be applied. As a consequence of this choise card 0043101 must be defined giving to word 1 the "gap" value, i.e. the width of the flow channels between the fuel plates and to word 2 the "span" value, that is the distance from one end to the other or long length (y direction of Serpent model);
- 005 branch, it connects the pipe 004 to the time dependent volume 006;
- 006 time dependent volume, this one is used to give the outlet pressure condition set to 270000.0 Pa (again from [1]);
- 0103 Heat Structure (HS), it simulates the fuel plates structure with 6 axial heat structures of rectangular geometry divided in 9 radial mesh points. 5 radial intervals are occupied by the fuel meat, while the remaining 3 by the cladding. The properties used to describe these two materials are thermal conductivity and heat capacity. For the cladding they are constant and are respectively 130 W/m K and 2582400 J/m^3 K (taken from [15]). For the fuel meat instead a constant thermal conductivity of 59 W/m K is taken from [20], while the heat capacity depends on the temperature and it is described by the formula (same reference as thermal conductivity) below that gives the result in MJ/m^{3}K

$$Cp(U_3Si_2 - Al) = 0.0122 \cdot V_{\mathrm{F}} \cdot Cp(U_3Si_2) + 0.0027 \cdot (1 - V_{\mathrm{F}} - V_{\mathrm{P}}) \cdot Cp(Al)$$

where V_{P} and V_{F} are respectively volume fractions of porosity and fuel in the meat. The porosity content of the fuel cores produced by a given fabricator remains virtually constant, and it is 4 vol% for CERCA. The fuel meat volume fraction is derived from this one with the formula:

$$V_{\mathrm{P}} = 0.072 \cdot V_{\mathrm{F}} - 0.275 \cdot {V_{\mathrm{F}}}^2 + 1.32 \cdot {V_{\mathrm{F}}}^3$$

$Cp(U_3Si_2)$ is the heat capacity of the uranium silicide without the Al powder and Cp(Al) is the heat capacity of the aluminum, both in J/kg K. They are calculated with the formulas below:

$$Cp(U_3Si_2) = 199 + 0.104 \cdot T(^\circ\mathrm{C})$$
$$Cp(Al) = 892 + 0.46 \cdot T(^\circ\mathrm{C})$$

The HS has an adiabatic condition on the left handside, which represents the center of symmetry of each fuel plate, and a convective type boundary condition on the rigth handside which is connected with the pipe 004. The surface area for the heat exchange is calculated as area of a single plate face times 2, since there are two sides for each plate, times the number of fuel plates (18 for the FAs and 15 for the CR). In this way, the side plates are not modeled and the resulting simplified geometry consists in 18 (or 15) flat plates instead of the real curved plates, with a central layer of fuel surrounded by the cladding on both sides. The important thing is that all the volumes correspond to the real ones, only with a simplified geometry. In addition, also the heat transfer hydraulic diameter (i.e. heated equivalent diameter) is computed as 4 times the flow area divided by the heated perimeter. This number is greater than the volume hydraulic diameter since (heated perimeter) $<$ (wetted perimeter). The last information that has to be given to the HS is the power generation inside the fuel. This is done with a power constant control variable that gives the value in W. Its value is calculated starting from the desired reactor power, like 50 MW, from this derive the power density refered to the U-235 as described before, and then multiply this number by the U-235 mass of that assembly, like 490 g for the CF elements. In addition, the power is distributed axially in a different portion to each control volume following the power profile normalization curve derived with six detectors put in an infinite lattice Serpent simulation for each specific assembly type.

All the BICs are given constant for a simulation time of 1000 s, during which the system manages to reach the steady state conditions. Some simulation results are presented in Figure 3.27, where it is possible to see the plots of the temperature distributions for the three assembly types along the axial direction at different radial positions, i.e. at the center of the fuel, at the interface between the fuel and the cladding, at the interface between the cladding and the coolant and in the coolant. The case considered for the plot is the one with a power value for the assembly correspondent to 50 MW of reactor power.

Finally, the average value of the fuel temperature and the average value of the cladding temperature to be used in the Serpent simulations are obtained in two steps. First, by applying the mean value theorem for integrals over the radial temperature distribution, since radially there is a computed value at each mesh point through which it is possible to interpolate. In this way an average value for each

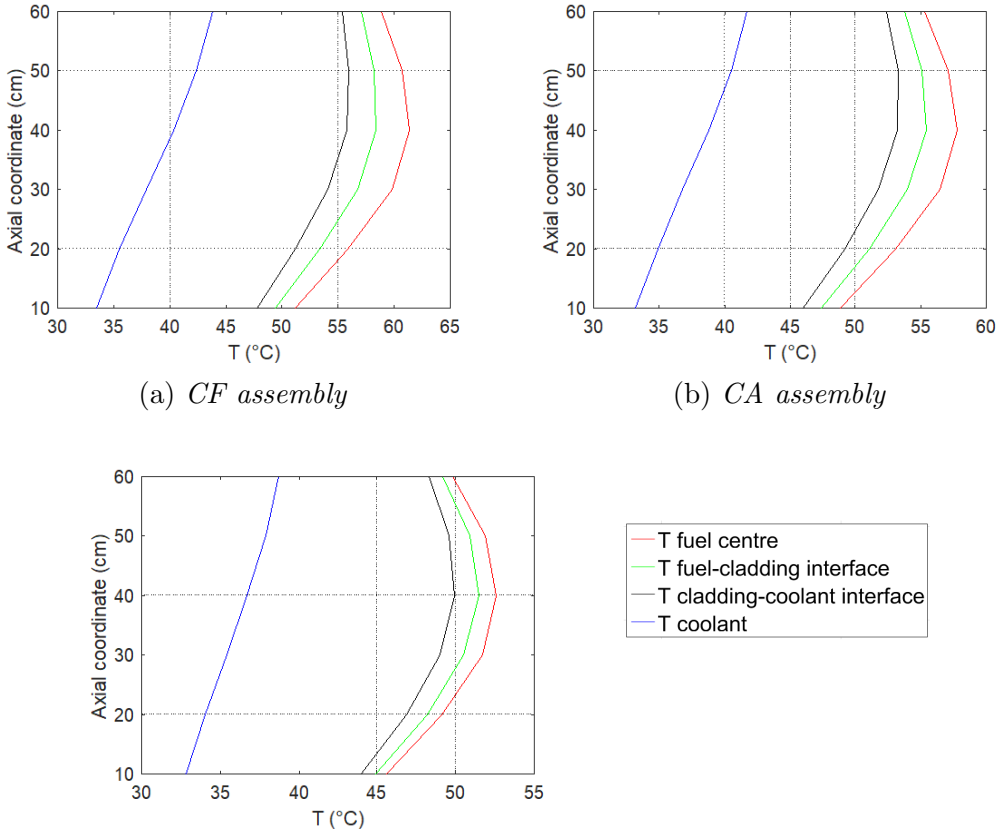

(a) *CF assembly* (b) *CA assembly*

(c) *CAC assembly* (d) *Legend*

Figure 3.27: Temperature distribution inside the three assembly types computed with the RELAP5 single assemby model.

axial position is obtained. Then the arithmetic average value among these has been computed, since axially each value is refered to the centre of the six axial HS, which have the same length. This last step is also applied to compute the average moderator temperature, since in the pipe there are six computed values which refer to the centre of the six control volumes of the same heigth.
Table 3.12 shows the final values to be set in the Serpent simulations. These values are in agreement with both Studsvik documents [17] and NINE previous experience with this kind of MTR (Material Testing Reactors), for the OPAL reactor. As it is clear from the Table, with these values a total of 9 simulations are performed (3 power density levels x 3 single assembly types).
In addition, other 9 Serpent simulations are performed setting the cladding and moderator temperatures at the values computed with the RELAP5 model, but changing the fuel temperature to 90 °C, which is the set value shown in some Studsvik documents [21]. The physical explaination of this larger value of fuel

temperature can be that even if there is not a real gap between the fuel and the cladding, the heat conduction can be reduced by the roughness and the porosity of the materials. The objective of these further simulations is again to enlarge as much as possible the dataset cases to find the best approximation of the fuel assemblies isotopic compositions.

	$\mathbf{T_{fuel}}$(°C)	$\mathbf{T_{cladding}}$(°C)	$\mathbf{T_{moderator}}$(°C)
CF	57.2	54.5	38.9
CA	54.1	51.9	37.6
CAC	49.8	48.6	35.9

(a) *P=50 MW.*

	$\mathbf{T_{fuel}}$(°C)	$\mathbf{T_{cladding}}$(°C)	$\mathbf{T_{moderator}}$(°C)
CF	53.8	51.7	37.5
CA	51.2	49.4	36.5
CAC	47.6	46.6	35.1

(b) *P=40 MW.*

	$\mathbf{T_{fuel}}$(°C)	$\mathbf{T_{cladding}}$(°C)	$\mathbf{T_{moderator}}$(°C)
CF	50.2	48.6	36.1
CA	47.8	46.5	35.4
CAC	44.8	44.1	34.3

(c) *P=30 MW.*

Table 3.12: Temperature Profile Evaluation approach, average temperatures for each power value and assembly type.

The infinite lattice simulations of both approaches are performed with a neutron population of 10000, for 500 active cycles and 50 inactive cycles. Vacuum boundary conditions are given along z-direction, while periodic type boundary conditions are given along x- and y-directions to simulate the infinite lattice. 51 burn-up values are indicated between 0.01 and 145 MWd/kgU. More burn-up steps are given at the beginning of the depletion since that period is crucial for the production of certain isotopes like the Xe.
When the infinite lattice simulations are completed it is possible to pass to the last step of this analysis, i.e. to extract the isotopic compositions of the assemblies to load in the core 1105. First of all, what is there at this point is several curves which describe the isotopes mass evolution as a function of burn-up, and the core-loading map (see Figure 3.28) with the U-235 mass content at BOC for each assembly.

	B	C	D	E	F	G	H	I
1	*ALH*	*BE*	*BE*	*BE*	*BE*	*BE*	*K211*	*ALH*
	3	4.2	4.8	4.1	3.4	2.8	2.2	1.4
	0.82	1.144	1.306	1.204	1.034	0.864	0.71	0.547
	1.078	1.449	1.841	1.991	1.829	1.401	0.938	0.81
2	CF037	CF041	CF038	CA433	CF001	CA419	CA458	CA471
	418.9	440.1	385	158.2	156.7	177.9	195.7	165.3
	1.465	2.147	2.487	2.24	1.88	1.51	1.189	0.874
	0.874	1.083	1.325	1.674	1.505	1.201	0.847	0.734
3	CF029	*RAMP*	CA508	CA407	CF030	CA053C	CF017	CA505
	419.8	12.7	376.8	152.4	317.8	58.1	241.1	209.1
	1.695	2.309	2.794	2.602	2.208	1.447	1.468	1.122
	1.047	1.416	1.433	1.706	1.47	1.62	1.07	0.815
4	*SL11*	CF042	CA057C	CF026	*K180a*	CF031	*M134*	CF003
	9	467	185.4	306.3	12.1	354.5	8.6	201.2
	1.66	2.567	2.49	2.594	2.062	1.929	1.539	1.214
	1.365	1.271	1.727	1.682	2.186	1.352	1.621	0.984
5	CF033	CF040	CF036	*K177*	CF028	CA056C	CF035	CF008
	414.5	389.8	343.9	12.1	300.9	105.3	348.5	203.7
	1.821	2.558	2.62	2.285	2.089	1.642	1.681	1.263
	1.049	1.195	1.498	1.776	1.485	1.524	1.034	0.9
6	CF032	CF034	CA055C	CF021	*K174*	CF006	CA423	CF007
	372.6	352.3	63.7	289.6	8.8	231.2	171.2	211.5
	1.614	2.145	1.84	1.992	1.771	1.668	1.505	1.169
	0.922	1.128	1.889	1.394	1.484	1.219	1.009	0.848
7	CA498	CF020	CF012	*K153A*	CA484	CA050C	CA386	CA501
	212.7	307.2	222	7.8	178.9	43.1	153.4	170.1
	1.135	1.576	1.629	1.584	1.522	1.112	1.228	0.988
	0.831	0.903	1.186	1.275	1.208	1.421	0.95	0.773
8	*SL21*	CA446	CA051C	CA502	CA490	CA480	CA450	CA422
	2.8	147.4	70.2	190.1	179.7	168.2	147.4	146.3
	0.621	0.941	0.971	1.279	1.297	1.17	1.012	0.788
	0.776	0.801	1.168	0.965	0.916	0.886	0.763	0.659
9	*BE*	*SL22*	*BE*	CA373	CA406	CA397	CA435	CA470
	0.6	1.5	2.5	150.3	164.1	148.7	145.5	144.2
	0.304	0.462	0.638	0.905	0.992	0.928	0.774	0.57
	0.658	0.672	0.889	0.782	0.775	0.741	0.629	0.533
10	*ALH*	*ALH*	*ALH*	*BE*	*BE*	*BE*	*BE*	*ALH*
	-0.1	0.1	0.5	1.3	1.7	1.6	1.3	0.8
	0.164	0.247	0.328	0.446	0.505	0.484	0.411	0.321
	0.461	0.507	0.604	0.768	0.864	0.838	0.694	0.537

Non-fuel assembly Assembly name
Gamma power (W/gFe) U235 (g)
Fast flux (*E14) Fast flux (*E14)
Thermal flux (*E14) Thermal flux (*E14)

Figure 3.28: Flux-map of Core 1105, Cycle 0505, at BOC [1].

The mass content of all the other isotopes is derived in two step:

1. take the U-235 mass content at BOC of a certain assembly indicated in Figure 3.28;

2. consider the curve which describes the U-235 mass evolution depending on burn-up, and find which burn-up corresponds to this U-235 mass content;

3. consider the curve which describes the mass evolution depending on burn-up of the other isotopes (e.g. Pu-238), and derive the isotope mass content that corresponds to this burn-up.

The steps 2 and 3 are performed using a matlab function called "comp_extraction.m" that was defined by the PhD Simone Di Pasquale. Since only 51 values on the entire burn-up interval are computed, the function uses a polynomial best fit (in a least-squares sense) of order 20 to fit the values obtained from the infinite lattice depletion, in order to have a better approximation with respect to a simplier linear interpolation. An example of how the interpolation works is shown in Figure 3.29. The results presented with this example derive from the TPE approach simulation, with the temperature values computed from the RELAP5 single assembly model of the CF element at 50 MW of reactor power. The reference assembly for which the interpolation is done is the CF028 that has an initial U-235 mass of 300.9 g. The obtained Pu-238 mass is 0.02 g.

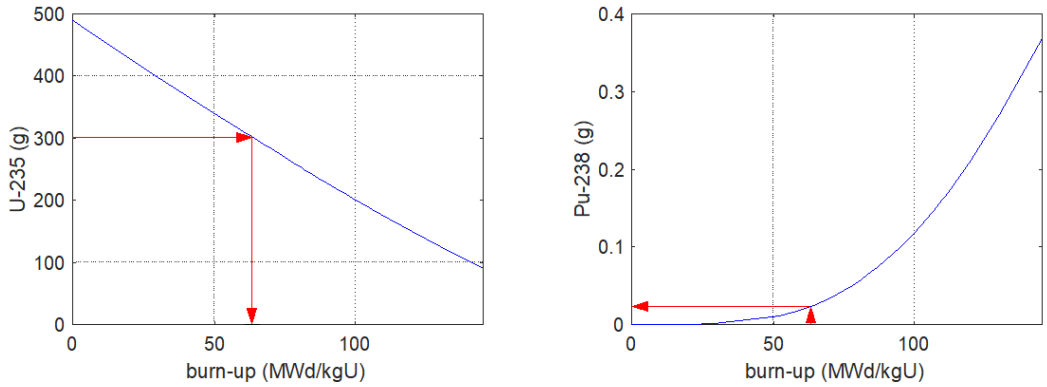

(a) *U-235* (b) *Pu-238*

Figure 3.29: Isotope mass curves interpolation example.

This interpolation is performed for all the isotopes thanks to the matlab function and for all the infinite lattice depletion simulations of the MC and TPE approaches. In this way the dataset of initial isotopic compositions of the fuel assemblies to load in the 1105 core is completed. The dataset is finally composed by 54 different intial isotopic compositions that are used for the full core burn-up simulations of the 1105 core loading. Among these 54 the one that best approximates the final composition of the discharged elements is found. This step is described in the next section.

3.4 Full core burn-up

The core loadings of interest of the benchmark are 1105, 1106 and 1107. For these cores, the entire power and control rods level description is available from the Studsvik documents and so it is possible to simulate them in a quite accurate way. Since there is an entire dataset of the initial isotopic compositions from which perform the full core burn-up simulation, first of all it is necessay to perform the first core loading for all of the 18 infinite lattice depletions and find the one that better matches with the discharged elements compositions given from Studsvik. Then, how to proceed with the other two cores is not a unique choice and the last paragraph of this section will give different solutions about it.

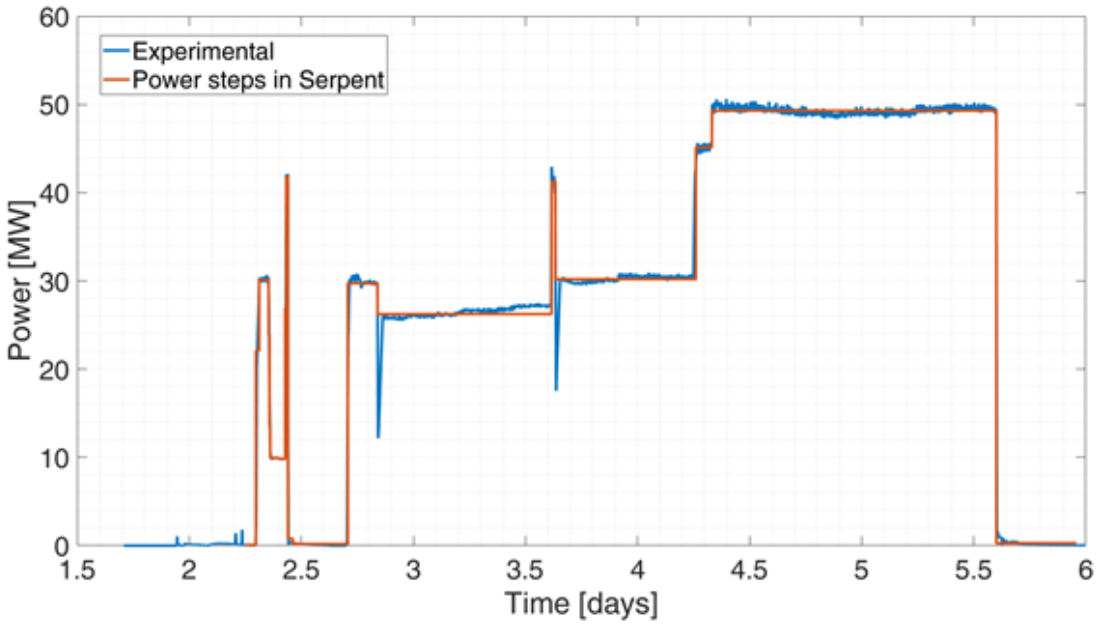

Figure 3.30: Power levels selected for the 1105 core loading.

3.4.1 Core loading 1105

The core loading 1105 map has been presented in the previous section (see Figure 3.28) and it is used to load each assembly in the right position at BOC. Then, once that the core model is completed, it is necessary to choise a proper simulation setup to simulate the core cycle. During the core cycle the R2 power and the CRs level change a lot and the main problem in Serpent is that it is not possible to give a time dependent power distribution. So the entire burn-up cycle is approximated with different steady-state power level. Each power level is evaluated as the average of the measured R2 power in the considered interval. The correspondin fuel, moderator and cladding temperatures are computed with the RELAP5 single

assembly models. Finally, the CR positions is taken from experimental data and also for them it is given an average value for each interval. Figure 3.30 shows the discretized R2 power levels.

3.4.2 Comparison of the discharged fuel assemblies

Once the full core 1105 burn-up simulation is completed, it is possible to compare the composition of the discharged elements with the available data from Studsvik. It is computed the mass difference between the results of the core simulation and the available data, divided by the latter and multiplied by 100.
The results show a good agreement for the U-235 and for the total U (less than 1%, Figure 3.31). This can be expected since the cycle is quite short and as a consequence the depletion is not that consistent. Moreover, the initial mass of U-235 was set to the exact value, so it does not change a lot. A different situation is observed for the U-236 (Figure 3.33 (b)), in this case the difference is about 4% for the CA elements and -15% for the CF elements. The negative value for the CF means that the computed value with the full core burn-up simulation is much smaller with respect to the data given by Studsvik. This is strictly connected to the original assumption that was made on the fresh fuel composition: no U-236 was put in the CF fresh element and as a consequence a too small quantity is measured at the end of the core cycle.
The amount of Pu is larger in the computed cases compared to the Studsvik data (Figure 3.32), and the differences are larger with respect to the previous nuclides. The difference is smaller in the CF elements (about 6%) than the CA elements (about 12%). The reason of this behaviour is not obvious and it requires a further investigation to be properly justified.

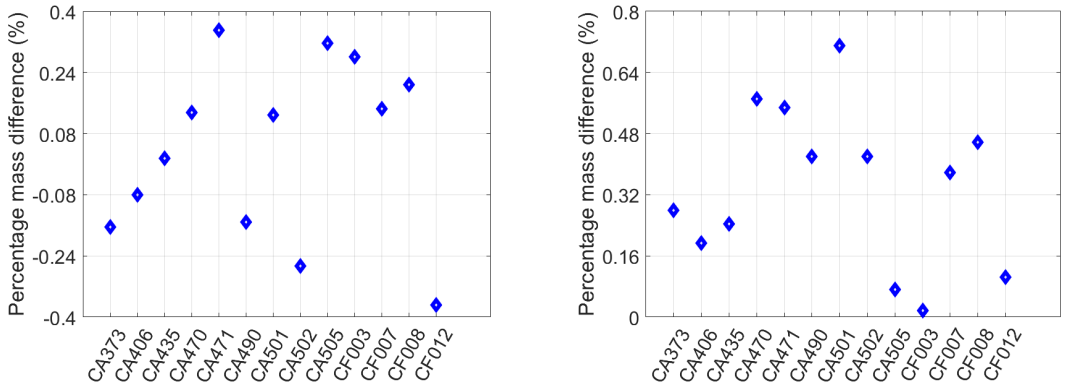

(a) *U-235.* (b) *Total U.*

Figure 3.31: Mass percentage difference between Serpent simulations and reference data for U-235 and total U.

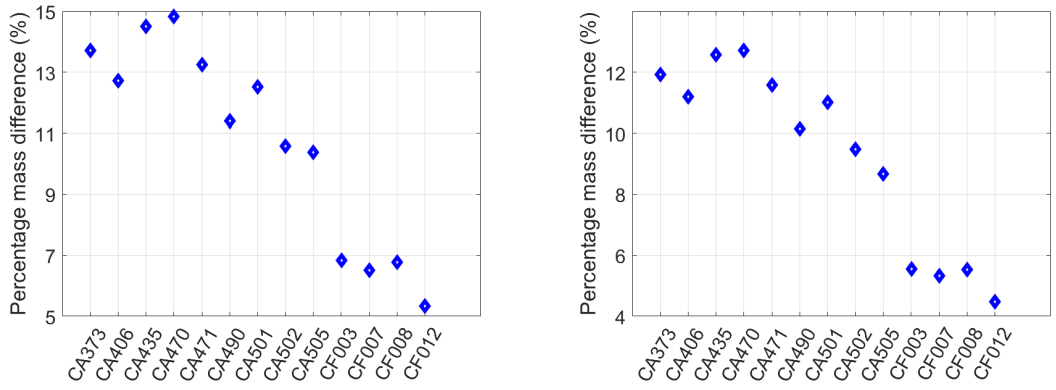

(a) *Fissile Pu.* (b) *Total Pu.*

Figure 3.32: Mass percentage difference between Serpent simulations and reference data for fissile Pu and total Pu.

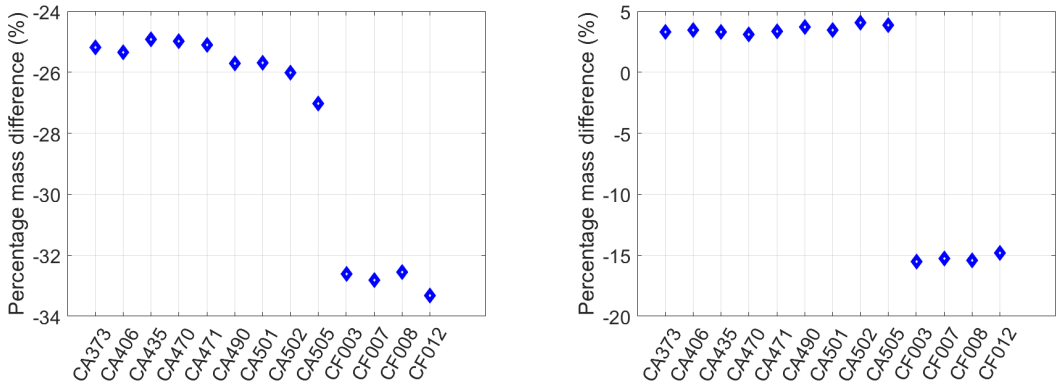

(a) *Np-237.* (b) *U-236.*

Figure 3.33: Mass percentage difference between Serpent simulations and reference data for Np-237 and U-236.

Finally the difference associated to the Np-237 (Figure 3.33 (a)) is very high, about 25% for CA elements and 33% for the CF elements. This probably depends again on the original assumption for the fresh fuel composition. In fact, in natural uranium fueled reactors with long burn-ups, the successive captures in U-235 and U-236 predominate in the production of Np-237 and Pu-238, as described in [22]. The fact that the initial U-236 mass content of the CF elements is set to zero can justify the fact that they are far from the experimental data.
Considering the results, they show on average a quite good agreement with the experimental data, that is a sign that the depletion strategy is a good way to proceed. Nevertheless, a lot of work still need to be done to get to the final solution of the

problem. Suggestions for the future analysis are to try to change the CF fresh fuel composition and to put a contribution of U-236 also in this case. Since the enrichment must be preserved this can be subtructed from the U-238 mass considering the same proportionaly between U-236 and U-238 as the CA elements. Then, all the other infinite lattice depletion must be considered and used to produce other 17 discharged compositions to compare with the experimental results. After some full core burn-up simulation results analyses it will be more clear which is the best way and decisions to make to get the correct solution, i.e. if a best approximation is found by changing the fresh fuel composition or the infinite lattice simulation setup.

Chapter 4

Thermal Hydraulics, Modeling and Simulation

The Thermal Hydraulic analysis focuses on the in-pile loop 1 inserted inside the R2 core, used to perform the selected cold power ramp tests. A detailed description of the in-pile loop and the ramp test facility is given in section 4.1, while section 4.2 describes the way the power ramp tests are performed and how the Linear Heat Rate (LHR) of the fuel rodlet that is ramp tested is obtained.
The objective of the TH analysis is to demonstrate the fidelity of the simulation model with respect to the real system through the achievement of the steady state conditions. Then, once that the model is validated with the experimental data, it is used to simulate the first cold power ramp test which is one of the exercises of the MPCMIV benchmark.
The simulation model is built using the RELAP5 code that is introduced in section 4.3, with the main focus on the features and cards relevant for this analysis. Section 4.4.1 describes how the system is diveded into nodes following the RELAP Best Estimate Nodalization method. The nodes are characterized from the geometrical and thermal point of view, which is as accurate as the detailed information available in the benchmark specifications.
The missing information over the loop is the pressure loss, so all the localized pressure loss coefficients are computed, and then the model is adjusted through the validation with the experimental data. This step is presented in section 4.5. When the model fidelity is demonstrated, it is used to perform the power ramp test which is described in the last section, that contains also the information about the rest of the loop and how to proceed in order to characterize also that part for the future analysis. Lastly, also in this case, since the data and numbers are protected information white labels are used to cover the quotes and graphs axis values, and all the numbers given in the description are approximated quantities.

4.1 In-Pile Loop 1 and Ramp Test Facility

The in-pile loop 1 is a high-pressure water loop system capable of simulating thermal hydraulics conditions representative of BWR and PWR reactors, used to perform several tests to study the material properties. It is composed by two main parts: the in-pile tube (or U-tube) and the main circuit.
The in-pile part of this loop is designed as a U-tube and it occupies the two adjacent R2 core positions C3 and B4. It is formed by a high pressure tube, surrounded by a gas jacket that can withstand the loop pressure in case of a failure of the inner tube. The pressure in this loop goes from 30 bar to 150 bar, since differently from the in-pile loop 2 this one is also capable to simulate PWR conditions, with higher pressures.

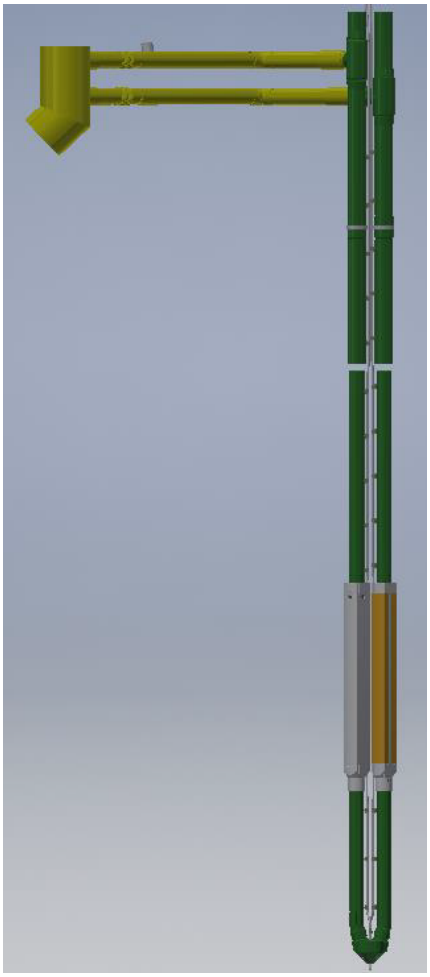

Figure 4.1: In-pile part of the loop (U-tube).

The gap between the high pressure tube and the gas jacket is filled with CO_2 in

order to reduce the heat losses from the U-tube, that can be considered negligible. This is done also because the temperature conditions inside the loop are in general much larger with respect to the coolant of the R2 reactor with a range of variation from 70 °C to 325 °C, so it is good to isolate this component in order to do not influence the R2 core temperature distribution. The in-core inside diameter of the in-pile pressure tube is 47 mm and the useful length in the core is about 670 mm. A general drawing of the in-pile part is provided in Figure 4.1, whereas the detailed drawings are shown later on during the discussion of the nodalization.
The main circuit of the loop (see Figure 4.2) is made of seamless tubes, forged curves and T-shaped joints of stainless steel AISI 316L with an inner diameter of about 38 mm and an outer diameter of about 48 mm. In addition, the loop piping is covered with 50 mm of fiber glass wool for insulation. Following the flow direction and starting from the outlet of the in-pile tube (upward section) the main circuit consists of the fuel fragment filter, the main heat exchanger, the main filter, the pump and the heaters. The surgeline and the spray line of the pressurizer are connected to the main circuit upstream and downstream the pump, respectively. The main heat exchanger is an air-cooled dryer with twelve parallel-connected pipes. Each pipe is 7 meters long with an inner diameter of 12 mm and an outer diameter of 15 mm for a total external cooling area of about 4 m^2.

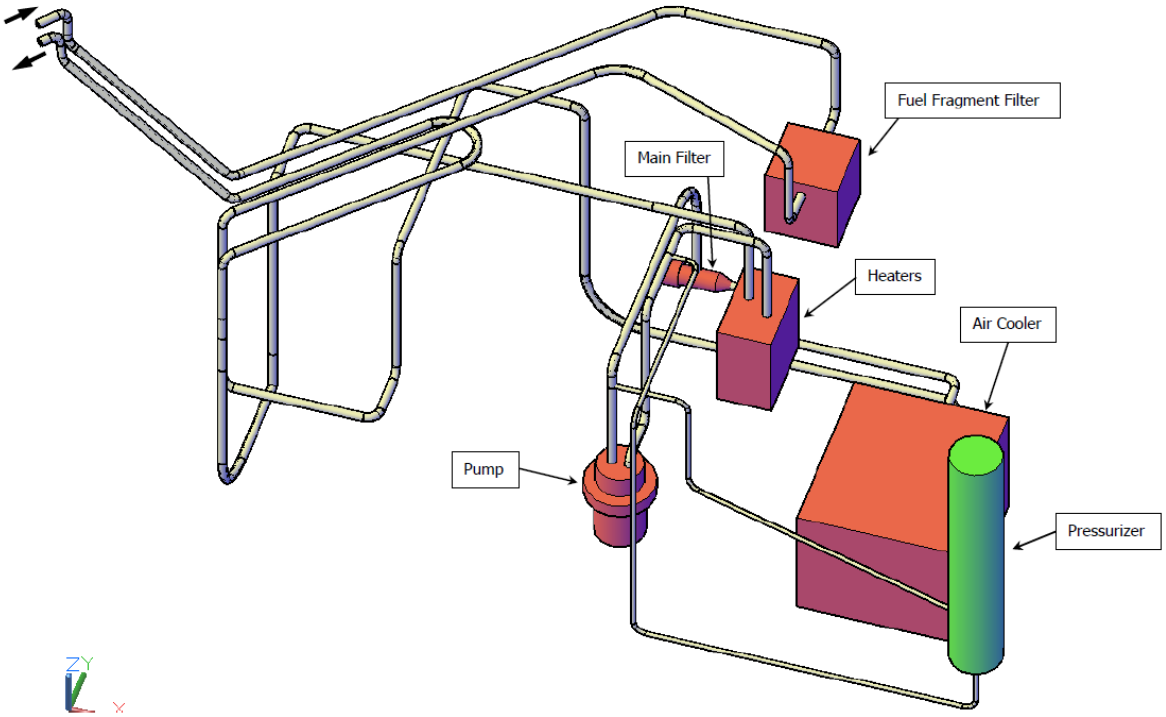

Figure 4.2: The main circuit of the in-pile loop.

The pump is a fully welded Hayward Tyler pump of which rated parameters and homologous curves derived by the benchmark team are provided in the specifications. The heaters consist of four heating rods with high power density made of 3 thermo-coaxial wires wrapped parallel to a copper core and having a cladding of stainless steel on the surface. The rods have an outer diameter of 20 mm, a heated length of 1200 mm and a maximum power of 30 kW at 380 V, corresponding to a maximum output power of 40 W/cm^2.
The ramp rig facility used for performing the ramp tests is placed in the C3 position inside the descending side of the U-tube and it is shown in Figure 4.3. The in-core part of the ramp rig is surrounded by mini-tube coil containing ^{3}He gas used to control the rod power. The mini-tube coil has an outer diameter of 3 mm and a wall thickness of about half a mm. It is wound around the ramp rig forming two separate layers with an average diameter of about 30 mm and 40 mm respectively. Part of the in-pile loop coolant enters inside the ramp rig through 4 holes having a diameter of 12 mm and arranged at 90 degrees around the tube grouped symmetrically two by two on two planes at 20 mm distance, located above the in-core part of the rig. A venturi flow meter and two sets of thermocouples located above and below the in-core part of the ramp rig are used to measure the rod linear heat rate by calorimeter technique. A flow mixer is located below the venturi flow meter before the coolant exit to enhance flow mixing in order to achieve the best possible accuracy in the calorimetric measurement.

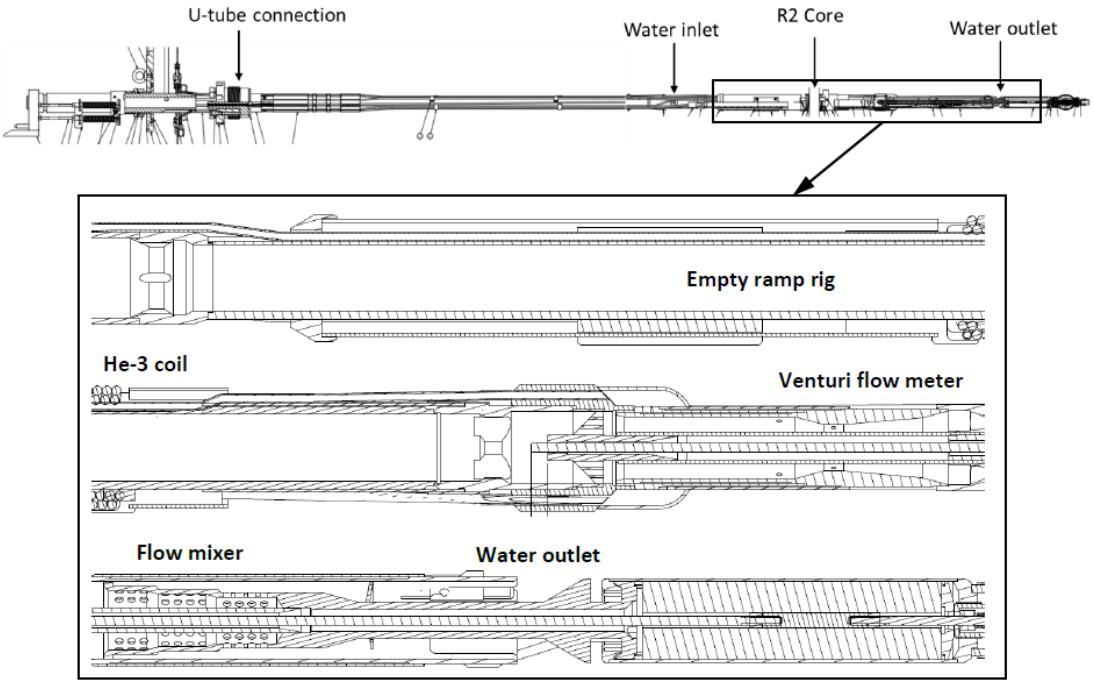

Figure 4.3: The Ramp Rig facility [1].

Each test fuel rod is irradiated individually in a special ramp capsule (see Figure 4.4), that in turn is placed inside the ramp test rig designed to accommodate one capsule at a time. The ramp capsule is open at the bottom end, and it has a series of holes on the upper part to allow the coolant flow. It works as coolant flow guide, rod holder, spacer carrier and as protection shroud during the handling of the test rod. The fuel rodlet is firmly attached to the upper part of the ramp capsule and axially free at the bottom end, where the test rod, when placed in the ramp rig, makes contact with the elongation detector. The rod elongation detector is located at the bottom of the ramp rig clearly below the R2 core. The elongation movements of the test rod are transmitted by a tiny push rod, which is built in at the bottom guide plug of the ramp capsule. The elongation detector is a commercial high-grade differential transformer with μm resolution.

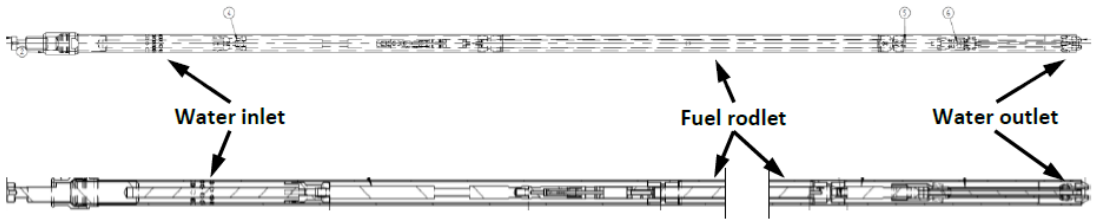

Figure 4.4: The Ramp Capsule [1].

The fuel rodlet is shown in the drawing of Figure 4.5. This rod is inserted inside the ramp capsule to perform the power ramp test, and it originates from a SVEA-96 fuel assembly 22034 taken from the Forsmark-2 reactor. The original assembly occupied position I8 (see Figure 4.6) and it has been irradiated for 3 cycles.

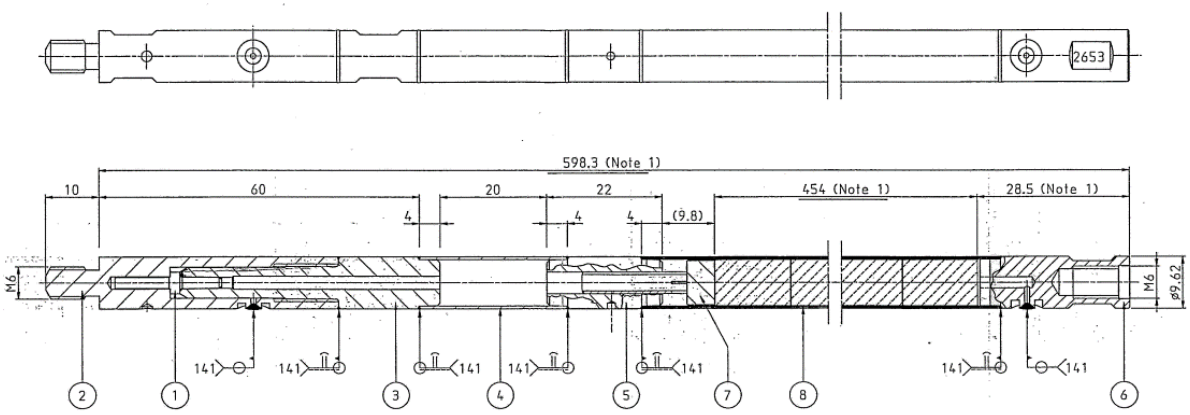

Figure 4.5: Drawing of the fuel rodlet 2653.

The initial father rod enrichment was around 2% (at the level of the rodlet cut) and its average burn-up about 23 MWd/kgU. The fuel rodlet 2653 was taken between 1125 and 1667 mm from the bottom of the fuel stack and has been refabricated using the STUDFAB technique. The local burn-up for the fuel rodlet has been measured as about 26 MWd/kgU.

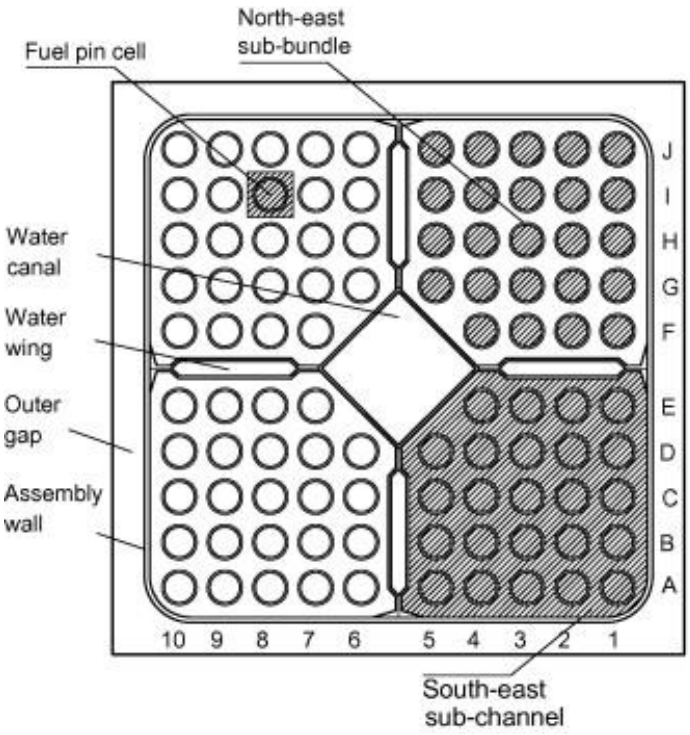

Figure 4.6: Position of the father rod (I8) in SVEA-96 fuel assembly 22034 in Forsmark-2 Reactor.

4.2 Ramp tests

4.2.1 First cold ramp test

The first of the two selected cold ramp tests was performed at the R2 reactor at the beginning of cycle 0505 on May 2nd, 2005. In order to avoid lengthy operation of the loop under cold conditions, it was decided to perform the cold ramp as soon as possible after the reactor start-up. So immediately after pressurization and start-up of the loop, the R2 reactor was started. The ramp schedule during cycle 0505 was very tight and to save time and avoid the effect of Xe-poisoning, it was decided to skip the stepwise power increase usually performed during reactor start-up. For this reason, the values for the temperature correction factor at zero reactor power (T_{PCOR}) were taken from the reactor start-up during the previous cycle 0504. The

average value for T_{PCOR} is -0.13 °C which is also a rather typical value. Figure 4.7 shows the reactor power (PR2NEU), the loop mass flow rate (SL1F1A), the loop temperature (T10D) and pressure (SL1P3A) for all the period of preparation and during the test, which consists in the series of actions summarized in the following list:

- R2 reactor start-up and achievement of criticality;
- quick increase of the reactor power to 30 MW, where control rod 3 was raised 10 cm to yield more power in the ramp rig;
- one hour of irradiation of the calibration rod to measure the gamma correction;
- decrease of the reactor power to about 10 MW;
- exchange of the calibration rod for the test rod;
- irradiation of the test rod for about 40 min. During this irradiation, the average rod power was about 12 kW/m at a reactor power of 10 MW. Since the rod power is directly proportional to the reactor power, it is calculated the reactor power necessary to achieve the target ramp terminal power;
- removal of the test rod from the irradiation position and increase of the reactor power to the computed necessary value.
- start of the ramp test: movement of the test rod from the waiting position to the irradiation position in 6.0 s. This can be clearly seen in Figure 4.8, where the decrease in FLORA (FLOw RAtio equals to rig mass flow rate over loop mass flow rate) indicates the start of the rod insertion. When the rod has arrived, the elongation detector gets in contact with the rod and starts to measure the elongation;
- movement of the rod in the neutron flux for about 2 s before reaching the irradiation position. During this time the nuclear power generated in the rod increases from practically zero to the maximum value. Due to the low heat conductivity of the fuel, however, the fuel temperature and surface heat flux continues to increase for about 10-15 seconds until equilibrium is reached. At equilibrium, the heat produced in the rod is continuously transferred to the rig coolant, where it is measured by calorimeter. During the ramp, the measured LHR starts to increase as the rod moves into the neutron flux and it continues to increase until equilibrium is reached (see Figure 4.8);
- reactor shut down by initiating a manual scram 15 s after the rod had arrived at the irradiation position.

The fall of the control rods shuts down the reactor in a very short time and the measured reactor power (PR2) quickly becomes zero. The correction term in equation 4.5 thus becomes zero immediately after scram, while there is still gamma power left in the ramp rig and coolant that reflects the reactor power before scram. This results in an artificial peak in the measured LHR directly after scram, which can be clearly seen in Figure 4.8. A second later, the gamma power of the reactor has been carried away by the coolant and the LHR then decreases as the stored energy content of the test rod is transferred to the coolant.
The maximum measured LHR value before scram falls far short of the target ramp terminal power. The reactor power to be used during the ramp test was determined based on the calibration irradiation performed at 10 MW and the fact that the rod power is directly proportional to the reactor power. However, the actually measured LHR appears to break the law of proportionality. Therefore, a detailed investigation was launched to find the explanation to this peculiar result.

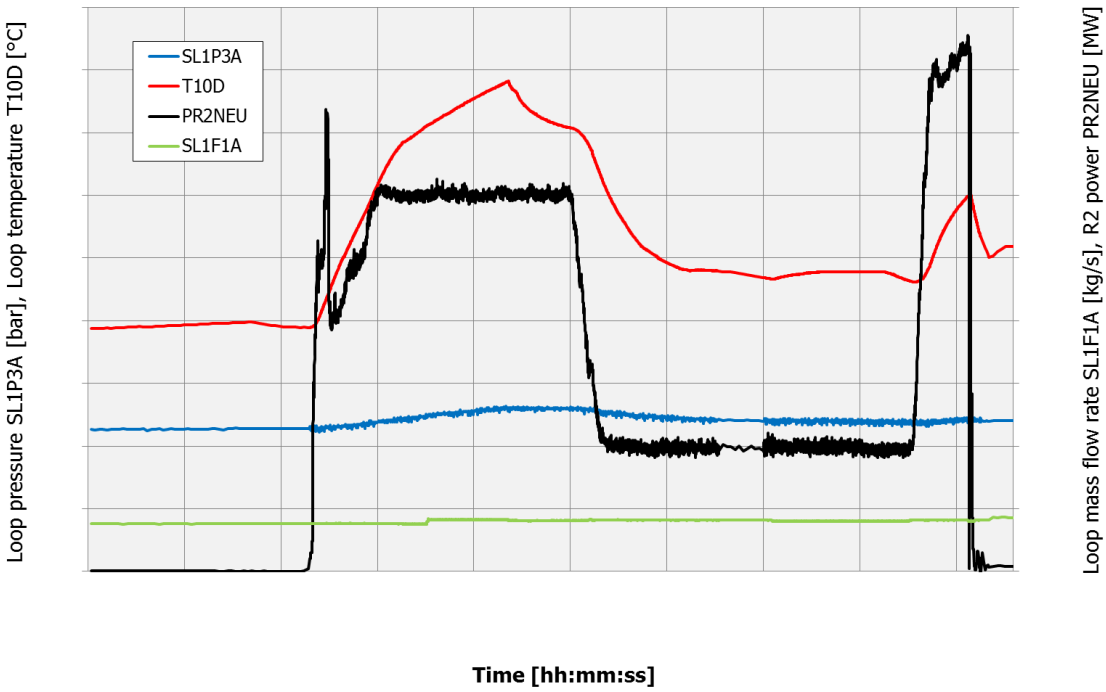

Figure 4.7: The irradiation history from reactor start-up to the scram in the first ramp test [1].

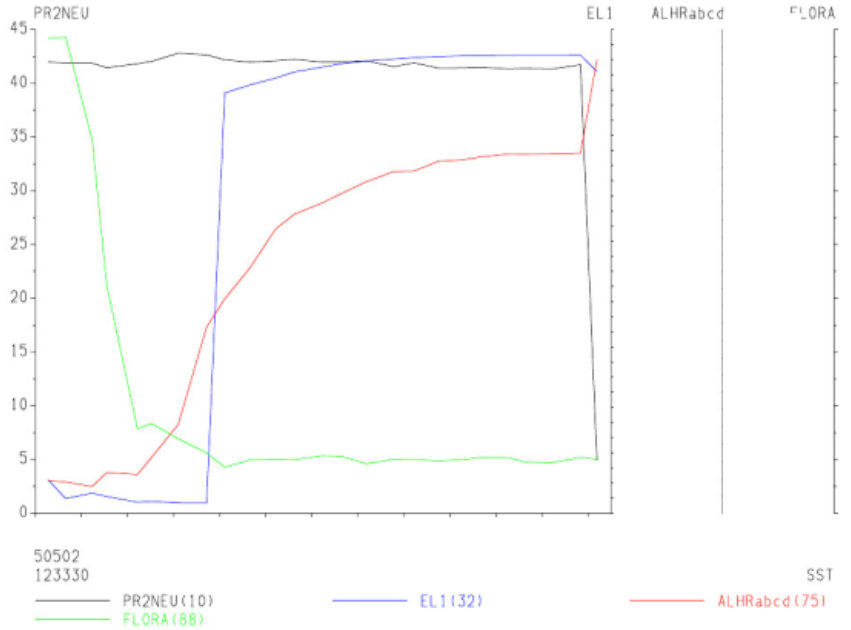

Figure 4.8: Details of the first ramp test from the start of rodlet insertion to initiation of the scram [1].

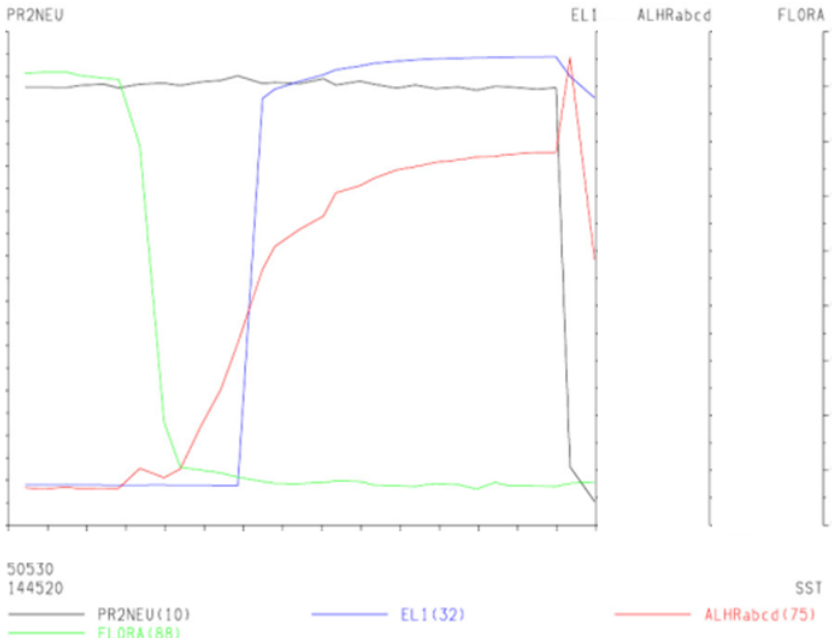

Figure 4.9: Details of the second ramp test from the start of rodlet insertion to initiation of the scram [1].

4.2.2 Second cold ramp test

The second cold ramp test uses the same test rod as before and was performed on May 30th, 2005. After loop and reactor start-up, the reactor power was increased stepwise to eigth power levels between 7 and 45 MW. The power was held steady for about 20 min on each power level, while ramp signals were measured. The measured differential temperature for each thermocouple pair is shown in Figure 4.10 as a function of reactor power up to 25 MW. By extrapolation to zero reactor power, T_{PCOR} is obtained for each thermocouple pair. The average T_{PCOR} value was found to be -0.035 °C. This shows that T_{PCOR} is close to zero at cold loop temperatures, indicating that the heat loss from the ramp rig is very small. A complication now arises because of the manual temperature control of the loop during the cold ramp experiment. In fact, it was not possible for the operator to keep the loop temperature constant. Hence, the loop temperature increases along with the reactor power. Expressed in another way, the T_{PCOR} value becomes dependent on reactor power. To try to avoid the problems associated with a changing loop temperature, it was decided to continue the experiment with T_{PCOR} set equal to zero.

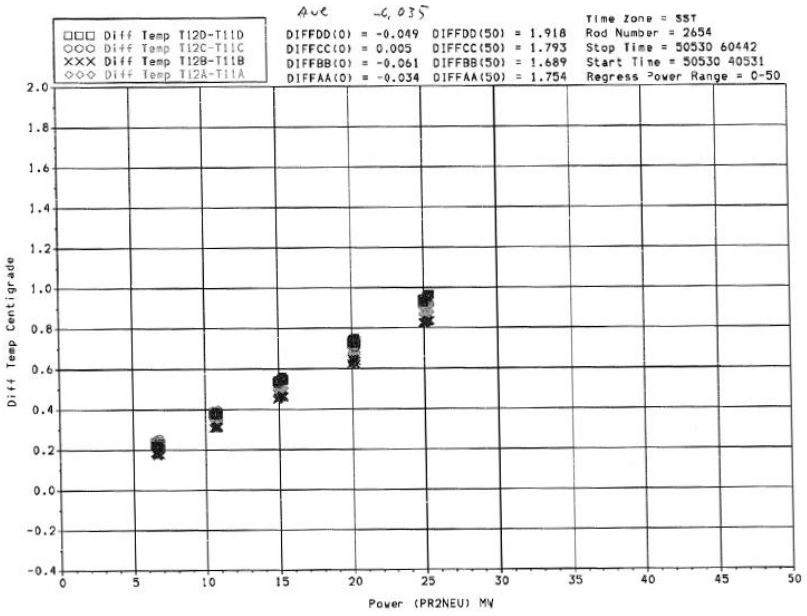

Figure 4.10: Measured differential temperature as a function of reactor power.

The list of actions of the second cold ramp test is quite similar to the previous case:

- lowering of the reactor power to 30 MW and irradiation of the calibration rod for one hour to measure the gamma correction;

- after the calibration, decrease of the reactor power to about 10 MW;
- exchange of the calibration rod for the test rod;
- irradiation of the test rod for about one hour, measurement of the average rod power and average reactor power from which derive the reactor power necessary to reach the target ramp terminal power. With T_{PCOR} set equal to zero it was assumed that rod power is directly proportional to the reactor power. In order to have some margin, the reactor power was increased to a slightly higher value in preparation for the ramp test. In the middle of this work it was decided to change the target ramp terminal level from the precedent one to as high as possible. To accommodate this change in ramp specification, the reactor power was increased to about 50 MW before the ramp was performed;
- ramp test: movement of the test rod from the waiting position to the irradiation position in 6.0 s. The rod moves in the neutron flux for about 2 s before reaching the irradiation position. During the ramp, the calorimetrically measured LHR starts to increase as the rod moves into the neutron flux (see Figure 4.9);
- reactor shut down 15 s after the rod had arrived at the irradiation position.

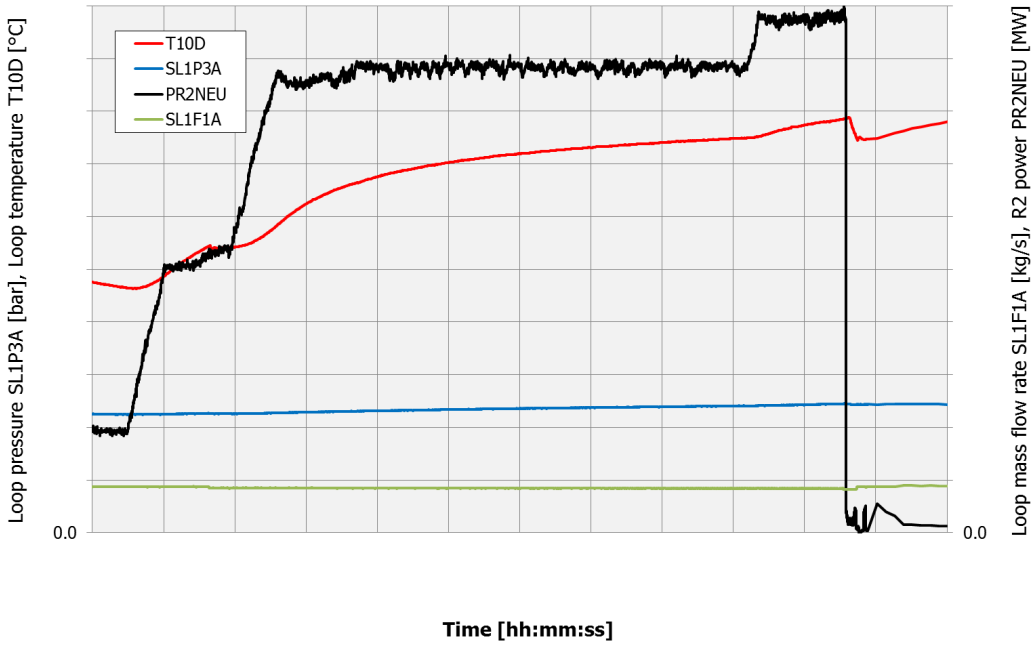

Figure 4.11: In-pile Loop Pressure, Temperature and Mass Flow Rate and R2 Power for the second cold ramp test [1].

After the ramp, the rod was removed from the ramp rig and taken to the hot cell laboratory for post-ramp examinations. Figure 4.11 shows the in-pile loop pressure (SL1P3A), temperature (T10D), mass flow rate (SL1F1A) and R2 power (PR2NEU) for the second cold ramp test.

Rod Power and Calibration Procedure

The test fuel rod power measurement is accomplished entirely by a fast acting calorimetric technique. The temperature increase over the test section is measured by means of four pairs of thermocouples: four thermocouples at the inlet and four thermocouples at the outlet. A venturi flow meter measures the coolant flow and a pressure meter measures the coolant pressure. The total power generated in the test section can be expressed by the equation:

$$Q_{\mathrm{TOT}} = (\Delta T - T_{\mathrm{PCOR}}) \cdot F \cdot Cp(p, T) \tag{4.1}$$

where:

- Q_{TOT} is the total power generated in the test section [kW];
- ΔT is the difference between outlet and inlet temperatures [K];
- T_{PCOR} is the correction for ΔT offset at zero reactor power [K];
- F is the mass flow rate [kg/s];
- $Cp(p, T)$ is the coolant heat capacity as a function of pressure and temperature [kJ/kg K].

The total power ($\mathrm{Q_{TOT}}$) is the sum of the test rod power ($\mathrm{Q_{ROD}}$) and of the gamma heating ($\mathrm{Q_{RS}}$) in the rig structure, the rod end fittings, the ramp capsule and the coolant. The constituents of $\mathrm{Q_{ROD}}$ are fissile power and gamma heating in the fuel ($\mathrm{Q_{FUEL}}$) and gamma heating in the cladding ($\mathrm{Q_{CLAD}}$). The test fuel rod power, which is the wanted quantity, can accordingly be expressed as:

$$Q_{\mathrm{ROD}} = Q_{\mathrm{FUEL}} + Q_{\mathrm{CLAD}} = Q_{\mathrm{TOT}} - Q_{\mathrm{RS}} \tag{4.2}$$

It is not possible to measure $\mathrm{Q_{RS}}$ directly but it is possible to measure the gamma heating in all non-fissile parts, including the cladding. The gamma heating in the non-fissile parts ($\mathrm{Q_{CAL}}$) is determined from measurements using the ramp capsule with a calibration rod with no fuel, especially made to be a copy of the real test rod, referred to as the "empty" rod and is expressed by:

$$Q_{\mathrm{CAL}} = Q_{\mathrm{RS}} + Q_{\mathrm{CLAD}} \tag{4.3}$$

These gamma heating calibration measurements are performed during the stepwise increase of the R2 power at the beginning of each R2 cycle and before each new

experiment. The measurements of ΔT as a function of R2 power give T_{PCOR} (ΔT offset at zero R2 power) by extrapolation to zero power. Together with the mass flow rate readings and heat capacity data, the gamma heating in the non-fissile parts as a function of reactor power (Q_{CAL}) can be determined. Thus, Q_{CAL} includes gamma heating in the clad and Q_{CLAD} takes into account the heating of the empty calibration rod. This power contribution should normally be included in the test rod power. The clad contribution, Q_{CLAD}, is calculated from geometry and gamma heat rate data and deducted from the measured Q_{CAL}. Hence, the gamma contribution is found as:

$$Q_{\mathrm{GAM}} = Q_{\mathrm{CAL}} - Q_{\mathrm{CLAD}}(R2power = 50MW) \tag{4.4}$$

After it has been normalized to full R2 power 50 MW, the test fuel rod power can be expressed by:

$$Q_{\mathrm{ROD}} = Q_{\mathrm{FUEL}} + Q_{\mathrm{CLAD}} = Q_{\mathrm{TOT}} - Q_{\mathrm{GAM}} \cdot PR2/50 \tag{4.5}$$

From this equation, the maximum LHR of the rod is now determined using:

$$LHR(peak) = C_{\mathrm{FAC}} \cdot Q_{\mathrm{ROD}}/L \tag{4.6}$$

where:

- Q_{ROD} is the Test rod power [kW];
- L is the Test rod fuel stack length [m];
- C_{FAC} is the Power peaking factor (max/average power), which is calculated from the profile of fissile material in the rod and the reactor axial power profile;
- LHR is the Linear Heat Rate [kW/m].

4.3 RELAP5 Code

The RELAP5 code is a Light Water Reactor (LWR) transient analysis code, developed at the Idaho National Engineering Laboratory (INEL) for the U.S. Nuclear Regulatory Commission (NRC) [23]. RELAP5/MOD3.3Patch05 has been developed jointly by the NRC and a consortium consisting of several countries and domestic organizations that were members of the International Code Assessment and Applications Program (ICAP) and its successor organization, Code Applications and Maintenance Program (CAMP).
The RELAP5/MOD3.3Patch05 code is based on a non-homogeneous and non-equilibrium model for the two-phase system that is solved by a fast, partially implicit numerical scheme to permit economical calculation of system transients. The

objective of the RELAP5 development effort from the outset was to produce a code that included important first-order effects necessary for accurate prediction of system transients, but that was sufficiently simple and cost effective so that parametric or sensitivity studies were possible.
The RELAP5/MOD3.3Patch05 code manual consists of eight separate volumes and one appendix to Volume II, which are described in the sequent list:

- Volume I describes the modeling theory and associated numerical schemes, the aim is to acquaint the user the NUREG/CR-5535/Rev P5-Vol I xviii with the modeling base and thus aid in effective use of the code;
- Volume II contains more detailed instructions for code application. The Appendix to Volume II contains specific instructions for input data preparation;
- Volume III presents the results of developmental assessment cases run with RELAP5/MOD3.3Patch05 to demonstrate and validate the models used in the code. The assessment matrix contains phenomenological problems, separate-effects tests, and integral systems tests;
- Volume IV contains a detailed discussion of the models and correlations used in RELAP5/MOD3.3Patch05. It presents the user with the underlying assumptions and simplifications used to generate and implement the base equations into the code so that an intelligent assessment of the applicability and accuracy of the resulting calculations can be made. Thus, the user can determine whether RELAP5/MOD3.3Patch05 is capable of modeling his or her particular application, whether the calculated results will be directly comparable to measurement or whether they must be interpreted in an average sense, and whether the results can be used to make quantitative decisions;
- Volume V provides guidelines for users that have evolved over the past several years from applications of the RELAP5 code at the Idaho National Engineering Laboratory, at other national laboratories, and by users throughout the world;
- Volume VI discusses the numerical scheme in RELAP5/MOD3.3Patch05;
- Volume VII is a collection of independent assessment calculations;
- Volume VIII provides information of interest to RELAP5/MOD3.3Patch05 programmers.

The hydrodynamics simulation is based on a one-dimensional model of the transient flow for a steam-water noncondensable mixture. The numerical solution scheme used results in a physical system representation consisting of flow paths, volumes, areas, etc., simulated by constructing a network of Control Volumes (CVs) connected by junctions. The transformation of the physical system to a system of

volumes and junctions is an inexact process, and there is no substitute for experience. The control volumes can be viewed as stream tubes having inlet and outlet junctions. The control volumes are connected in series and have an associated direction, that is positive from the inlet to the outlet. Velocities are located at the junctions and are associated with mass and energy flow between control volumes to represent a flow path. All internal flow paths, such as recirculation flows, must be explicitly modeled in this way since only single liquid and vapor velocities are represented at a junction (i.e., a countercurrent liquid-liquid flow cannot be represented by a single-junction). Which faces of a volume are the inlet or outlet faces depend upon the specifications of the volume orientation. For a positive vertical elevation change, the inlet is at the lowest elevation, whereas for a negative vertical elevation change, the inlet is at the highest elevation of the volume. Instead, for a horizontal volume, whether the inlet is at the left or right depends upon the azimuthal angle (a zero value implies an orientation with the inlet at the left). This orientation of a horizontal volume is not important as far as hydrodynamic calculations are concerned, but it is important if one tries to construct a three-dimensional picture of the flow path.
When systems of volumes or components are connected in a closed loop, the sum of the volume elevations must close when they are summed according to the junction connection codes and sequence, or an unbalanced gravitational force will result. RELAP5 has an input processing feature that finds all loops or closed systems (which are defined by the input) and checks for elevation closure around each loop. The error criterion is 10^{-4} m. If closure is not obtained, the fail flag is set, and no calculation is run.
RELAP5 is equipped with a variety of component models. The ones in which the hydrodynamic model equations are directly applied are:

- Single volumes and junctions: they represent the basic control volumes for mass and energy, on one side, and momentum, on the other;
- Time dependent volumes and junctions: in which prescribed thermodynamic conditions or flow rates are assigned;
- Pipes and annuli: they are systems of volumes and junctions, with different physical behaviour, suitable for the simulation of many 1D sections of a plant.

There are also other particular components in which specific models have been introduced to perform functions needed in plant simulation. The hydrodynamic components that were used for the input writing of the model of the in-pile loop are listed here:

Time Dependent Volume: A TiMe-DePendent VOLume (TMDPVOL) must be used wherever fluid can enter or leave the system being simulated. TMDPVOLs typically are employed in two types of applications: first, TMDPVOLs

may be used to specify pressure boundaries, generally at locations where fluid exits a model, in this case generally the TMDPVOL is coupled to the remainder of the model using a normal type of junction and it actively interacts with the rest of the model. Secondly, TMDPVOLs are used to specify fluid conditions at injection sites. In this application, the TMDPVOL is used simply to provide the proper fluid conditions for an injection flow boundary condition as defined by the TMDPJUN;

Time Dependent Junction: The Time DepenPent JUNction (TMDPJUN) requirements, interpolation, and trip logic are identical to that for time-dependent volumes. The capability of using time-advanced quantities as search arguments can be used to model pressure dependent water injection systems. If the injection flow is a function of the pressure at the injection point, the volume pressure at that point is used as the search argument. A trip is defined to be true when the injection system is actuated. Entry of table data with a negative pressure and zero flows causes the flow to be zero when the trip is false. In order to ensure proper operation for zero flow, both a card with negative pressure and a card with a zero pressure need to be entered. The remaining table entries define the injection flow as a function of positive pressures. The source of injection water is a time-dependent volume;

Pipe: It is a string of volumes, that can be different sizes and orientations, with interior connecting junctions with different options for flow models. It is used for 1D pipes or channels in 2D/3D flow volumes. More than one junction may be connected to the inlet or outlet. If an end has no junctions, that end is considered a closed end. The volumes in a pipe are usually considered one-dimensional components and flow in the volumes is along the x-coordinate. Crossflow junctions can connect to any of the pipe volumes in the y- and z-coordinate directions using a form of the momentum equation that does or does not include momentum flux terms. It is also possible to connect external junctions to the x-coordinate direction faces of any of the pipe volumes using a form of the momentum equation that does or does not include the momentum flux terms. It is also possible to include or not include the momentum flux terms in internal pipe junctions;

Single Junction: It is used to connect two control volumes without imposing a specific flow condition, but simply transferring what came from the inlet connection to the outlet connection;

Branch: The branch component may be thought of as a single-volume component that may have single junctions appended (up to 9). Any number of junctions may be defined as a part of a branch component. Note that other external junctions (e.g., single-junctions, valves, and time-dependent junctions) that are defined separately may also connect to a branch. If an end has no junctions,

that end is considered a closed end. If more than one junction is connected on one end of a branch, each junction should be modeled as an abrupt area change;

Finally, Heat Structures (HS) provided in RELAP5 allows calculation of the heat transferred across solid boundaries of hydrodynamic volumes. Modeling capabilities of heat structures are general and include fuel pins or plates with nuclear or electrical heating, heat transfer across steam generator tubes, and heat transfer from pipe and vessel walls. Heat structures are assumed to be represented by one-dimensional heat conduction in rectangular, cylindrical, or spherical geometry. Surface multipliers are used to convert the unit surface of the one-dimensional calculation to the actual surface of the heat structure. Temperature-dependent thermal conductivities and volumetric heat capacities are provided in tabular or functional form either from built-in or user-supplied data. Finite differences are used to advance the heat conduction solutions. Each mesh interval may contain a different mesh spacing, a different material, or both. The spatial dependence of the internal heat source may vary over each mesh interval as well. The time-dependence of the heat source can be obtained from reactor kinetics, one of several tables of power versus time (chosen option for current analysis), or a control system variable. Finally, boundary conditions include symmetry or insulated conditions, convective boundary conditions, a correlation package, tables of surface temperature versus time, heat transfer rate versus time, and heat transfer coefficient versus time or surface temperature.
The next section presents the nodalization of the system, which is translated into a series of hydrodynamic components and heat structures in which proper BICs are imposed for the RELAP5 null transient simulations to demonstrate the achievement of the steady state conditions and validate the model fidelity through experimental data.

4.4 RELAP5 Model

The RELAP5 Code is used to build the simulation model of the entire in-pile loop, which comprises both the U-tube and the main circuit with all the associated components. At the beginning of the work it was decided to model the entire loop. To do that, in order to follow the RELAP Best Estimate Nodalization tecnique the first effort went to individuate all the important quotes of the system and fix them for the sequent nodalization. After these primary planes were individuated, based on them the system is divided into nodes, which are characterized from the geometrical point of view and in terms of pressure losses. In the middle of the work, considering how many unknowns were there to properly model the main circuit components, it was decided to focus only on the in-pile U-tube and to try to reach the steady state conditions for this one. The simulations performed are presented in the next section, while hereafter the RELAP Best Estimate Nodalization method

is presented and it is described how it was followed to build the simulation model.

4.4.1 RELAP5 Best Estimate Nodalization

The Simulation Model (SM) development and validation process is based on a systematic and comprehensive comparison between experimental and simulation data/results. To do that, it is necessary to implement a strict procedure [24] that strats with the creation of a Database of Facilities and Tests following the SCCRED (Standardized and Consolidated Calculated and Reference/Experimental Database [25]) Methodology. Then, it is possible to develope the Simulation Model (SM), and most important to validate it with the NEMM (NINE Evaluation Model Methodology) Validation Process. This process requires:

- Demonstration of the geometrical fidelity;
- Demonstration of the achievement of the steady state conditions;
- Qualitative and Quantitative Transient Analysis.

During the entire procedure the SM is documented with the Engineering Handbook. Moreover, the SCCRED flowchart assures high quality work that requires coherent and logic flow path, iterative procedure, multiple feedback and review and different levels of analysis.
The first step to develop a SM is the data collection: all the reports, documents, drawings available are collected and analyzed in order to geometrically characterize the selected facility. This step is skipped since it was already performed by the benchmark's organizers to complete the first version of the benchmark specifications. Since the geometry of the facility was very complex and the information were not exhaustive and detailed, they developed a 3D model of the facility, that in this way is well characterized geometrically.
The facility is then analyzed and divided into main components, and each component in turn is divided into modules. The sequent list describes this first division:

- Component 1: In-pile U-tube;
  - Module 1: High Pressure Tube Downward section (HPTD);
  - Module 2: High Pressure Tube Upward section (HPTU);
  - Module 3: High Pressure Tube Lower section (HPTL);
- Component 2: Ramp Rig (RR);
  - Module 4: Inside the flow mixer;
  - Module 5: Outside the flow mixer;
- Component 3: Ramp Capsule (RC);

- Component 4: Main circuit piping;
  - Module 6: Piping between OCP and FFF (p_out_FFF);
  - Module 7: Piping between FFF and AC (p_FFF_AC);
  - Module 8: Piping between AC and MF (p_AC_MF);
  - Module 9: Piping between MF and PUMP (p_MF_PUMP);
  - Module 10: Piping between PUMP and HTR (p_PUMP_HTR);
  - Module 11: Piping between HTR and ICP (p_HTR_in);
- Component 5: Pressurizer and associated lines;
  - Module 12: Surge-line;
  - Module 13: Spray-line;
  - Module 14: Pressurizer (PRZ);
- Component 6: Main circuit components;
  - Module 15: Fuel Fragment Filter (FFF);
  - Module 16: Air Cooler (AC);
  - Module 17: Main Filter (MF);
  - Module 18: Pump (PUMP);
  - Module 19: Heater (HTR);
- Component 7: In-pile tube connection pipes;
  - Module 20: Outlet Connection Pipe (OCP);
  - Module 21: Inlet Connection Pipe (ICP);

Each module is geometrically characterized in the Reference Data Set (RDS). Also the localised pressure loss coefficients due to convergences, divergences and bends that affect the pressure drop and the energy dissipation in the flow are evaluated. The pressure losses evaluation is performed considering the reference standard geometrical configurations available in literature using the "Handbook of Hydraulic Resistance" [26]. This book clearly does not contain all the complicated geometries that are used in the in-pile tube, so several assumptions were needed and they are described in the next sections. Then, also the physical and thermal properties of the materials of the passive structures are evaluated and taken from literature.
The measurement system as well needs to be considered during this phase of the SM development, in particular to take it into account during the nodes subdivision, to put the right value in the closest position to the detector. So a detailed description of the measurement type, location point and elevation in the facility is

also necessary.
When this preliminary phase is complete it is possible to preoceed with the set-up of the nodalization that passes through different steps. First, the nodalization preparation requires the evaluation of the main choices of the SM characteristics. General recommendations from NINE nodalization tecnique consider the ratio between volumes and lengths of two adjacent nodes between 0.5 and 2 (with exceptions). Then, it is also suggested to adopt the "slice technique" approach in order to improve the capability of the SM to simulate phases of transients involving with natural circulation phenomena. This "slice technique" consists in dividing all the hardware in parallel horizontal planes placed at different elevations. Among these, the relevant elevations of the main components (abrupt area change, plates, different components, bends, etc.) are evaluated with respect to the centerline and fixed. The main resulting issue of this operation regards the incopatibility between two or even more relevant elevations, that can be so close that they do not allow the creation of a vertical hydraulic node between them. In this case it is necessary to make a proper choice depending on the case, that can be either to change the elevation of a certain component or to not apply the slice technique for that specific node. Other general reccomendations are to use more than nine mesh points for simulating the heat structures where a larger temperature difference is expected to occur.
The next step is the build-up of the discretization scheme of the various parts of the facility, which is described in detail in the next two paragraphs for both the in-pile tube 4.4.3 and the main circuit 4.4.2.

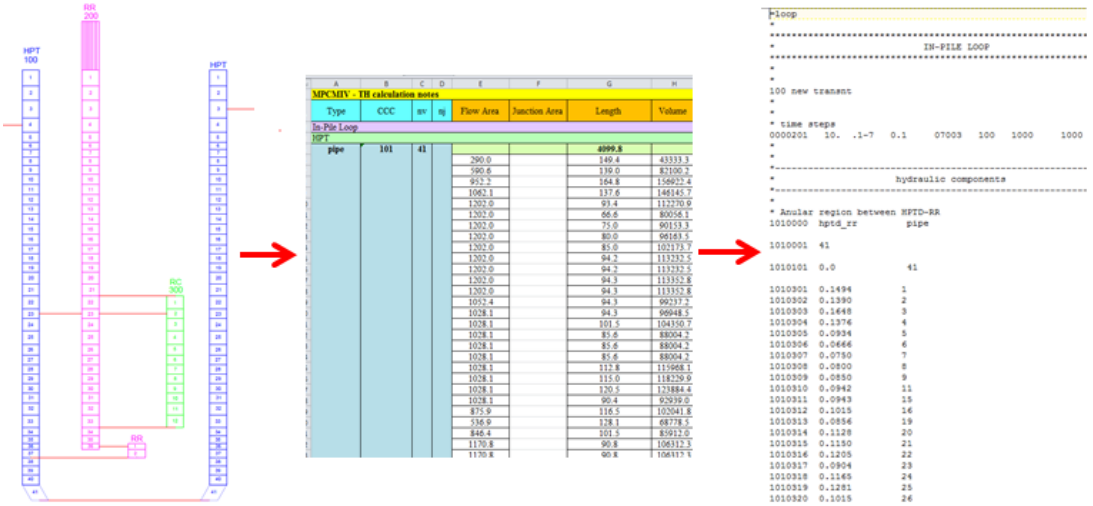

Figure 4.12: Main steps of nodalization set up: nodalization schematization (left), RDS of the facility (middle) and RELAP5 input deck (right).

Finally, the last step to build the RELAP5 simulation model is the input writing

to translate the nodalization schematization into the code language. The code input deck is supported by calculation notes in order to document in a systematic and traceable way how the data in the RDS are converted in the numbers constituting the input. Figure 4.12 shows how the RDS of the facility and the nodalization schematization are used to produce the input deck.
Once that the geometrical fidelity of the model is demonstrated, it is possible to use it to demonstrate the achievement of the steady state conditions and then perform the transient analysis. These simulations are described in 4.5 and 4.6.

4.4.2 Main circuit model

The nodalization of the loop follows the procedure described in the precedent section. So the first step is to identify the parallel horizontal planes, that must be fixed for the nodalization, and to adopt the slice tecnique. To do that, initially a CAD drawing is produced to represent the fluid centerline among all the loop. When the fluid makes a curve in the xy plane, the line continues only along the x direction, it is as if all the loop is roll out in a single parallel direction, while when it changes the elevation along z it is represented in the perpendicular direction. Figure 4.13 shows an example of this process. As it is possible to see from the figure, the pipe is roll out and represented only by a continuing line in the parallel direction, and in fact the last curve in the xy plane is not represented in the figure (b). Instead, all the changes in the elevation are drawn with a perpendicular line with respect to the first one.

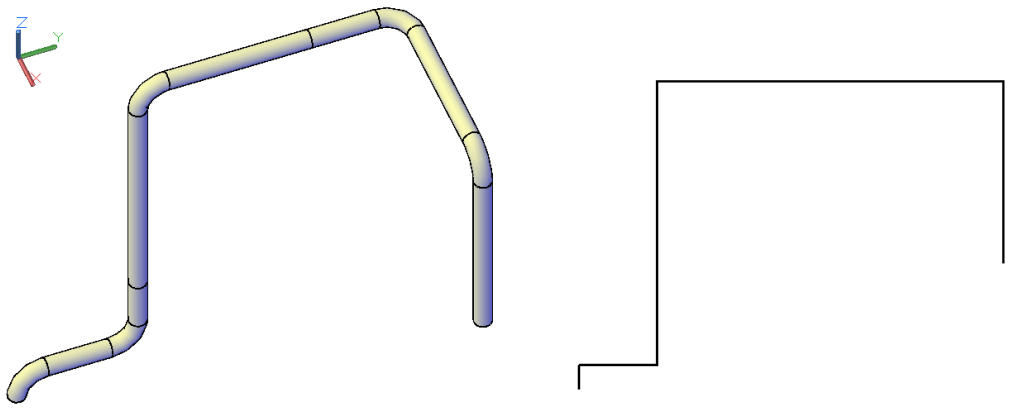

(a) *Section of loop piping.* (b) *Flow centerline.*

Figure 4.13: Example of piping schematization.

Once the all loop is represented in this way, the most important quotas are individuated and parallel lines are drawn in order to see if there are some issues and conflicts between them. Just to give some examples, these important quotas are the curves and change in direction that involves the z-direction, the entrance

and outlet to the main circuit components, the inlet and outlet to the in-pile tube and its components like the holes through which the water flows inside the ramp rig and the ramp capsule, the outlet of these components, etc.; also the changes in the geometry have to be considered like the presence of plates, flow mixer, venturi meter, sudden area change etc. . About 50 parallel planes are individuated and a lot of them are too close to allow the creation of a single node between them. The final solution to these conflicts is that the priority goes to the in-pile tube important planes, that are fixed, then also the main circuit ones are considered and when an issue is occuring the slice tecnique is not respected. This can be done also because the circulation in the loop never turns into natural circulation.
The next step is the final nodalization of the system. This is is done considering first the parallel planes just described and then subdiving the lengths individuated in this way in sub-volumes, respecting the rule of ratio between volumes and lengths of two adjacent nodes between 0.5 and 2. At the end of this process a total number of 521 control volumes are defined for the modules of component 4 (main circuit) and component 5 (pressurizer and associated lines).
In order to easily recognize each component in the RELAP5 input file, they are associated to card numbers that begin in the same way. In particular, the 4nn numbers indicate component 4 (main circuit), while 5nn numbers indicate component 5 (pressurizer and associated lines). All the piping is defined as a pipe component in RELAP5 (see 4.3). The next figures show the final nodalization for each module: Figure 4.15 of module 6 (card component number 401, 68 total CVs); Figure 4.17 of the first part of module 7 (card component number 402, two pipes are needed in this case since each pipe model in RELAP5 con have maximum 99 CVs, 74 total CVs); Figure 4.18 of the second part of module 7 (card component number 403, 74 total CVs); Figure 4.16 of module 8 (card component number 404, 24 total CVs); Figure 4.14 of module 9 (card component number 405, 27 total CVs); Figure 4.19 of module 10 (card component number 406, 25 total CVs); Figure 4.20 of the first part of module 11 (card component number 407, 79 total CVs); Figure 4.21 of the second part of module 11 (card component number 408, 61 total CVs).

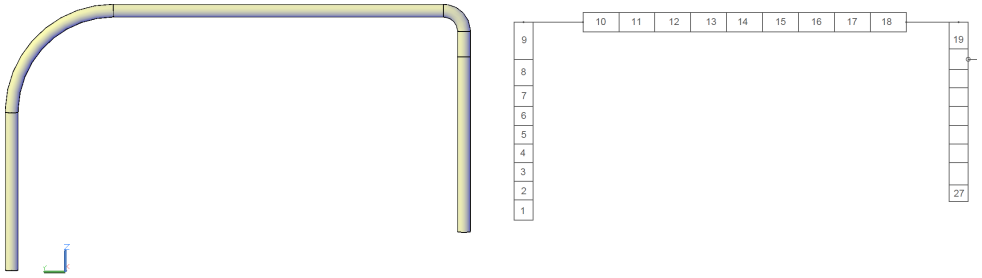

(a) *Section of loop piping.* (b) *Nodalization.*

Figure 4.14: Module 9 (piping between MF and PUMP) nodalization.

Finally, Figure 4.22 of module 12 (card component number 501, 47 total CVs) and Figure 4.23 of module 13 (card component number 502, 42 total CVs).

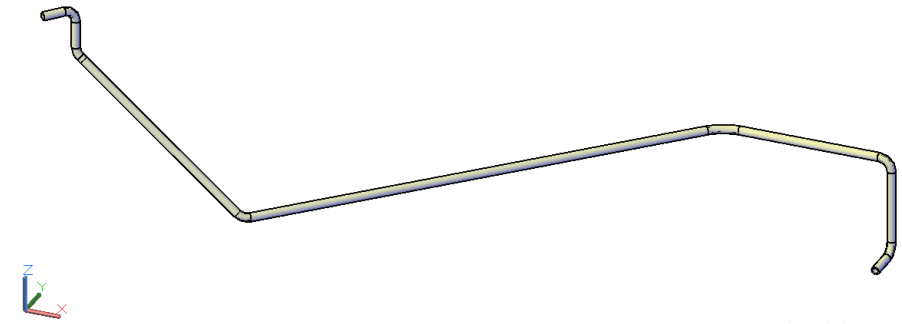

(a) *Section of loop piping.*

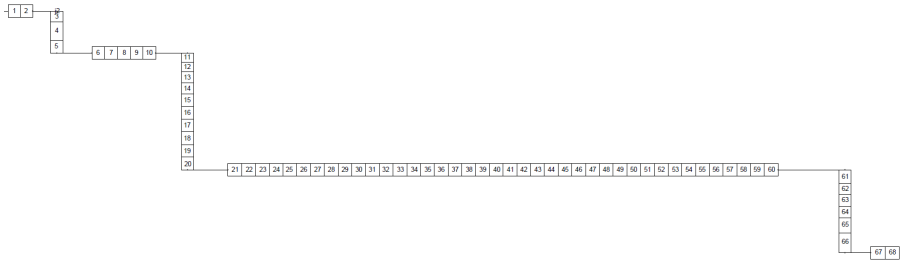

(b) *Nodalization.*

Figure 4.15: Module 6 (piping between OCP and FFF) nodalization.

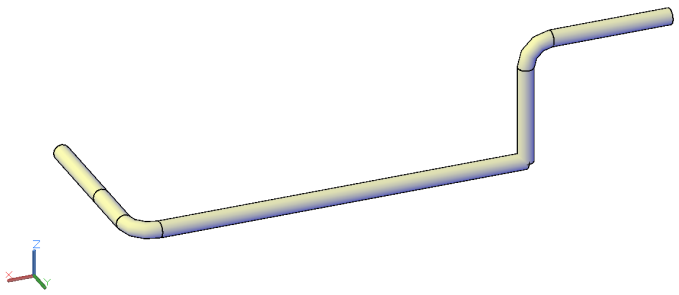

(a) *Section of loop piping.*

(b) *Nodalization.*

Figure 4.16: Module 8 (piping between AC and MF) nodalization.

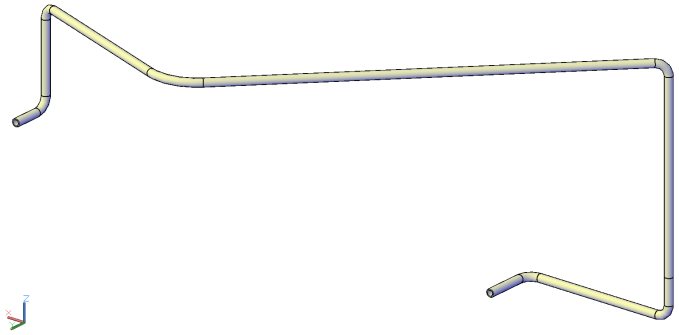

(a) *Section of loop piping.*

(b) *Nodalization.*

Figure 4.17: First part of module 7 (piping between FFF and AC) nodalization.

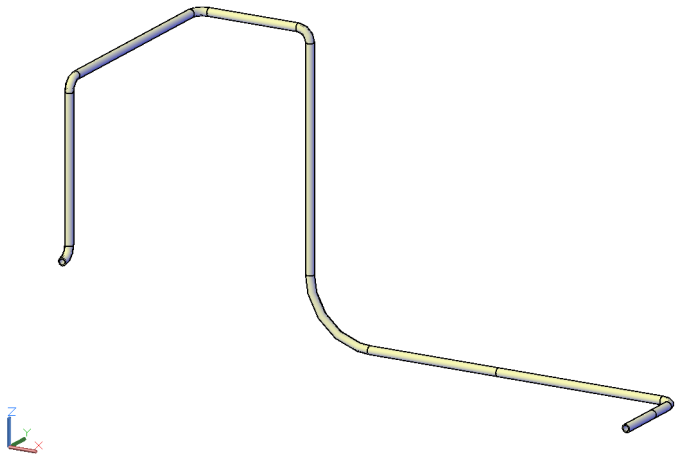

(a) *Section of loop piping.*

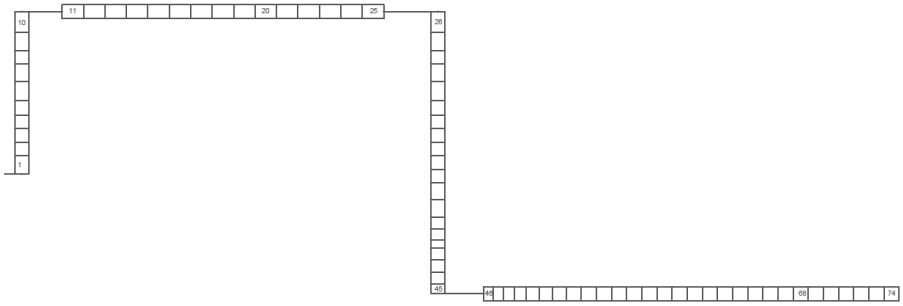

(b) *Nodalization.*

Figure 4.18: Second part of module 7 (piping between FFF and AC) nodalization.

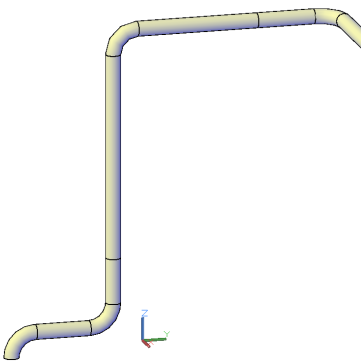

(a) *Section of loop piping.*

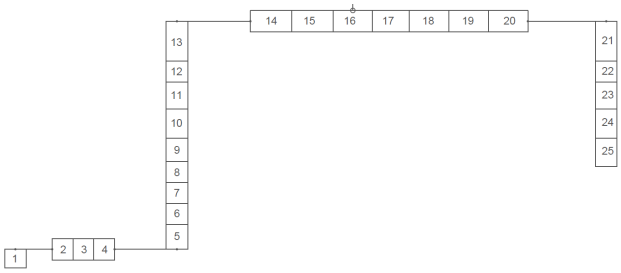

(b) *Nodalization.*

Figure 4.19: Module 10 (piping between PUMP and HTR) nodalization.

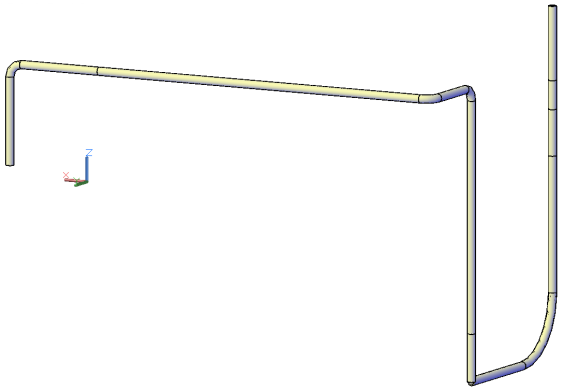

(a) *Section of loop piping.*

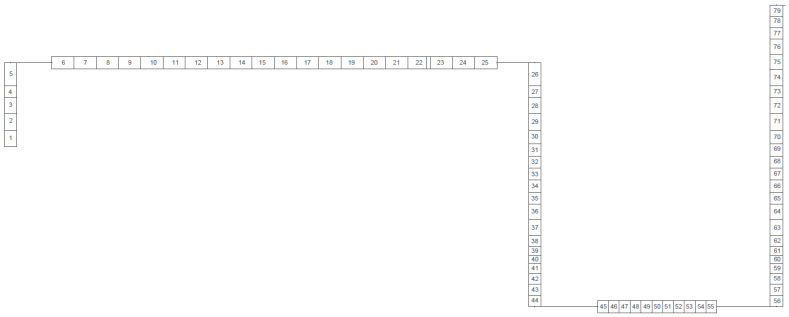

(b) *Nodalization.*

Figure 4.20: First part of module 11 (piping between HTR and ICP) nodalization.

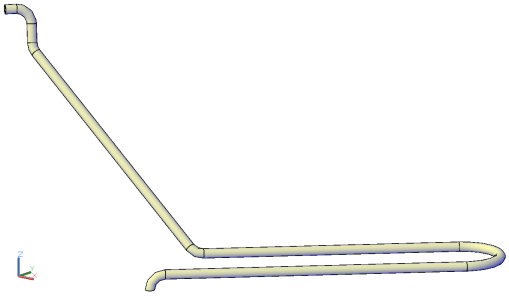

(a) *Section of loop piping.*

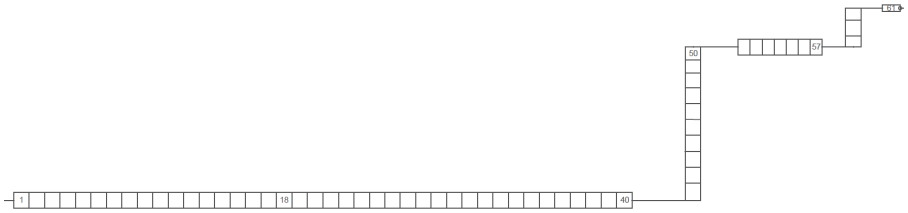

(b) *Nodalization.*

Figure 4.21: Second part of module 11 (piping between HTR and ICP) nodalization.

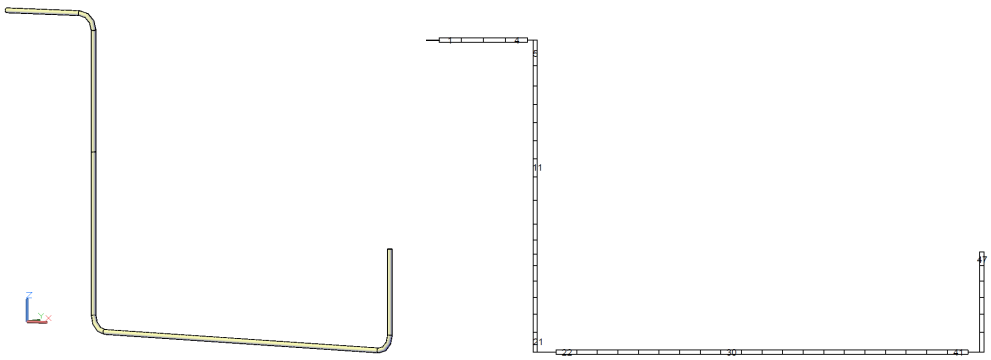

(a) *Section of loop piping.* (b) *Nodalization.*

Figure 4.22: Module 12 (Surge-line) nodalization.

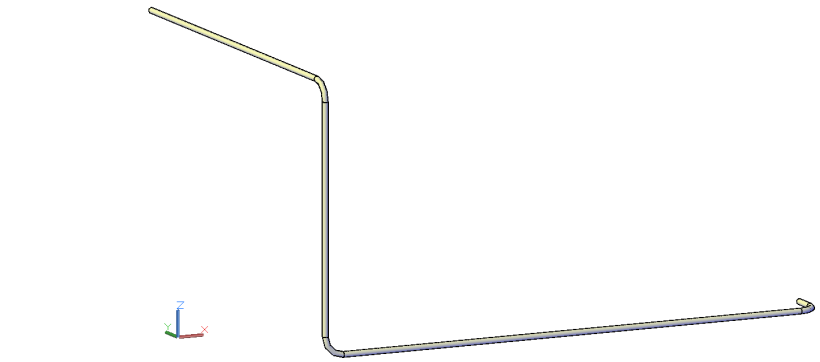

(a) *Section of loop piping.*

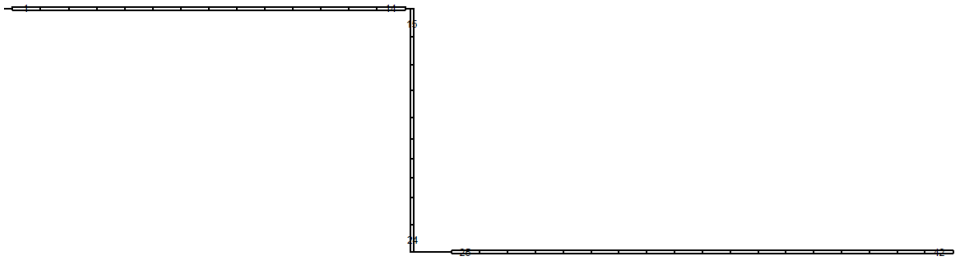

(b) *Nodalization.*

Figure 4.23: Module 13 (Spray-line) nodalization.

Each CV of the pipe components is characterized first in terms of geometry. In this case it is very simple since all the piping has a constant inner diameter and a constant outer diameter. The flow area is computed as:

$$A_{\text{flow}} = ({D_{\text{ext}}}^2 - {D_{\text{int}}}^2) \cdot \frac{\pi}{4}$$

The volume of the CVs is set to zero, so that the code calculates it as flow area

times CV length (which is defined on the base of the nodalization). The hydraulic diameter must be correctly defined as:

$$D_{\mathrm{h}} = 4 \cdot \frac{A_{\mathrm{flow}}}{p_{\mathrm{w}}}$$

where $\mathrm{p_w}$ is the wetted perimeter calculated as:

$$p_{\mathrm{w}} = \pi \cdot (D_{\mathrm{ext}} + D_{\mathrm{int}})$$

The localised pressure losses of these two components are taken from the 6^{th} chapter of [26], where it is described the "Resistance to flow with changes of the stream direction resistance coefficients of curved segments - Elbows, bends, etc.". The diagrams used are the 6.1, 6.2 and 6.7, which describe exactly the geometry of the real system depending on the flow condition. In particular the first diagram describes the bends, the second tubes and channels smoothly curved and the last one elbows with sharp corners.
As far as the components of the main circuit are concerned, they have variation in geometry and flow that cause pressure losses. Since there is an important lack of information about these components, at this point of the analysis it was decided to leave the simulation of this part and to concentrate only on the in-pile U-tube. This nodalization will be used in a future analysis in which also this part will be considered and simulated. Now, the work stops here for the main circuit and it moves to the modeling of the in-pile part. The aim is to try to achieve the steady conditions in the in-pile tube and to demonstrate that it is possible to complete the simulation of the entire ramp test for it. Afterwards, the simulation model will be enlarged considering also the main circuit with more information for both inlet and outlet conditions, that can be used to support the building of the simulation model and to properly characterize the different components.

4.4.3 In-pile tube model

The in-pile tube nodalization follows the procedure described before and the final solution is shown in figure 4.24. Starting from the left there is an horizontal pipe component that represents the Inlet Connection Pipe which is made by 14 CVs. This is the first module of component 7 that is indicated with card numbers starting with 7nn, in particular this one is the 702. Figure 4.25 shows the CAD drawing of this section taken from the specifications, from which it can be seen that its geometry is similar to the main circuit piping. For this reason it is characterized in the same way and also the localised loss coefficients are taken from the same diagrams. The same description is also valid for the Outer Connection pipe which is the number 701 (see Figure 4.26).
The ICP and OCP hydrodynamic models are connected through single junctions to component 1, namely the High Pressure Tube, which is indicated with card

numbers 1nn. The single junction 710 connects the outlet of the ICP to y-inlet face of CV 4 of the descending side of the HPT (component 101), simulating in this way a cross flow connection through which the coolant flow changes its direction from x to y, entering inside the HPTD. The opposite situation is described at the outlet of the ascending side of the high pressure tube by the single junction 170, which connects the y-outlet face of CV 39 of the HPTU (component number 103) to the inlet face of the OCP. The junction numbers are always defined so that the first number refers to the "from" and the second to the "to" component (e.g. 170: 1=from component 1, 7=to component 7).

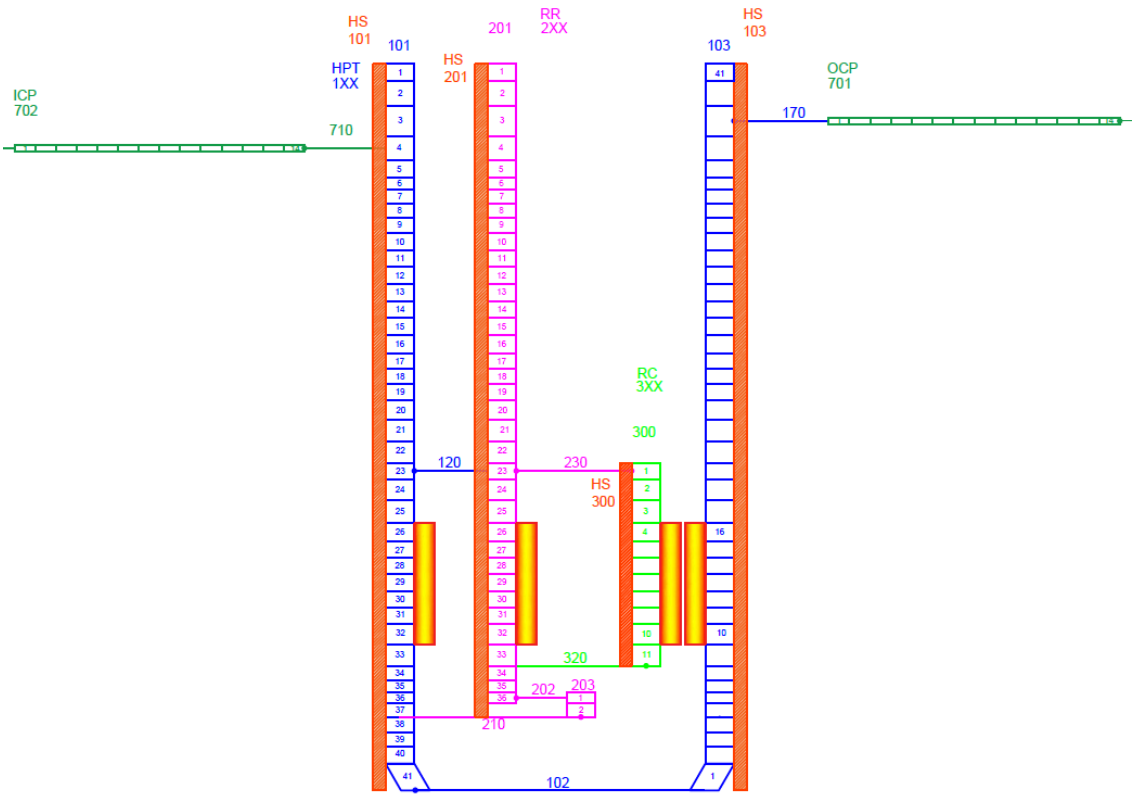

Figure 4.24: U-tube nodalization.

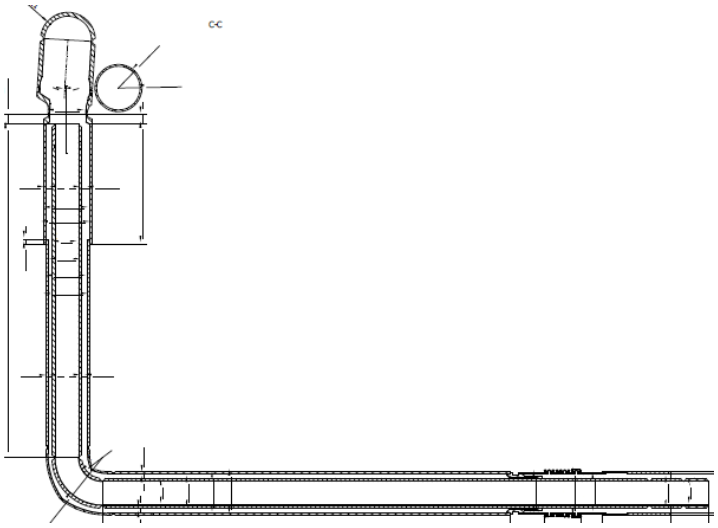

Figure 4.25: Inlet Connection Pipe CAD drawing from the specifications [1].

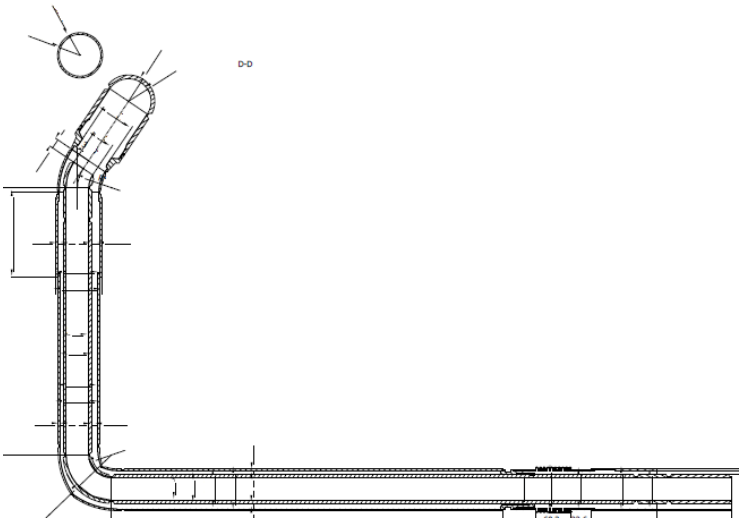

Figure 4.26: Outlet Connection Pipe CAD drawing from the specifications [1].

Components 101 and 103 are two vertical pipes of 41 CVs each that simulate the hydrodynamic volume of the anular region between the high pressure tube and the ramp rig. The geometry of these two is quite complicated and it requires to sub-divide each CV in different sub-sections of the same geometry, characterize each of these sub-sections and then derive the characterization of the CV. Figure 4.27 shows an example of this process.

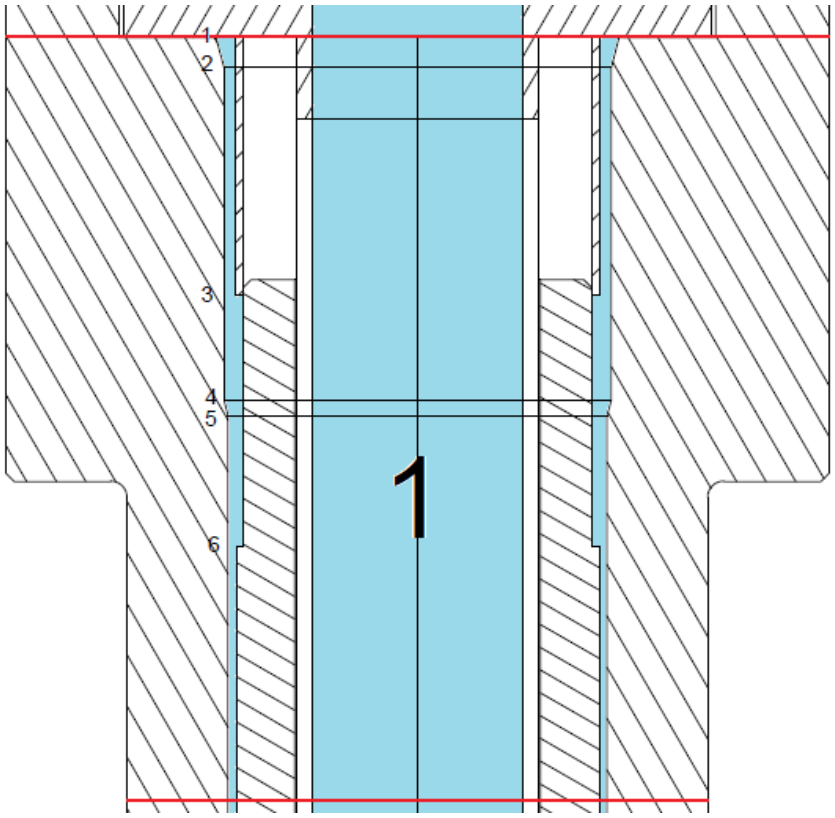

Figure 4.27: CAD drawing of CV 1 of HPTD with the RR inside.

This is a 2D CAD drawing of the first CV of the HPTD with the RR inside. The anular region in light blue is the first CV of pipe 101. Six different sub-division are performed for this CV, in 3D geometry they are: external truncated cone with internal cylinder (geometry 1) for sub-volumes 1 and 4, and annulus pipe (geometry 2) for sections 2, 3, 5 and 6. The corresponding volumes are calculated as (subscript 1 stands for top, 2 for bottom):

$$V_{\text{ext. cone + int. cyl.}} = (\frac{\pi}{12} \cdot ({D_{\text{ext},1}}^2 + {D_{\text{ext},2}}^2 + D_{\text{ext},1} \cdot D_{\text{ext},2}) - \frac{\pi}{4} \cdot {D_{\text{int},1}}^2) \cdot l$$

$$V_{\text{annulus pipe}} = \frac{\pi}{4} \cdot ({D_{\text{ext},1}}^2 - {D_{\text{int},1}}^2) \cdot l$$

There is also a third possibility which is external cylinder with internal truncated cone (geometry 3). In this case the volume is calculated as:

$$V_{\text{ext. cyl. + int. cone}} = (\frac{\pi}{4} \cdot {D_{\text{ext},1}}^2 - \frac{\pi}{12} * ({D_{\text{int},1}}^2 + {D_{\text{int},2}}^2 + D_{\text{int},1} \cdot D_{\text{int},2})) \cdot l$$

The CV volume is defined as the sum of the contibutions of all the sub-sections. The length of the CV is derived from the procedure described before and the flow area is set to zero so that the code calculates it as the ratio between the volume

and the legth of the CV. Considering the complex geometry also the hydraulic diameter must be properly defined. In case of geometry 2 it is used the same formula as before. For geometry 1 and 3 it is calculated an average diameter for the truncated cone side and then this one is summed with the cylinder side diameter and multiplied by π. In this way an equivalent pipe is simulated, that has the same volume of the original one, but with a simplified geometry.
The k-loss coefficients are evaluated again using the reference manual, but in this case the situation is much more complicated. In fact, not all the geometries used in the U-tube are described in [26], for this reason some assumptions are needed in order to manage to reach the steady state conditions. This is better described in section 4.5. Depending on the geometry and flow conditions the reference diagrams used for the first evaluation of the k-losses of the in-pile part are:

- Diagram 3.6: Converging conical nozzle (collector) without wall mounting;
- Diagram 3.7: Converging conical nozzle (collector) wall mounted;
- Diagram 4.1: Sudden expansion;
- Diagram 4.9: Sudden contraction;
- Diagram 4.22: Orifices in a thin wall in the presence of a passing flow;
- Diagram 5.2: Conical diffuser;
- Diagram 5.9: Diffusers of circular cross section with stepped walls;
- Diagram 5.24: Converging nozzles of circular cross section in the system;
- Diagram 6.1: Bends;
- Diagram 7.4: Converging wye;
- Diagram 7.21: Threaded wyes;
- Diagram 8.3: Grid made of thickened laths or perforated thick plate.

Inside the HPTD is inserted the RR which can have different configurations:

- Configuration α: Computational domain of the ramp rig facility, without the ramp capsule inserted in it (empty ramp rig facility);
- Configuration β: Computational domain of the ramp rig facility which is filled with the ramp capsule containing the calibration rod;
- Configuration γ: Computational domain of the ramp rig facility which is filled with the ramp capsule containing the fuel rodlet.

Since the geometry of the last two configurations is exactly the same, only two hydrodynamic configurations are possible. The first hydrodynamic configuration has the empty RR, while the second has the RR with the RC inserted in it.
The RR CAD drawing is shown in Figure 4.28. Even if the details of the geometry are not clear from this drawing, the important thing is to notice that it is en empty pipe for the first part, then there are two main components used for the measurements: the venturi meter and the flow mixer. These two are quite difficult to characterize geometrically and for the pressure losses. The RR is modeled with pipe 201 made by 36 vertical CVs, then another 2 CV's vertical pipe is used to simulate the last part of the rig, where there is the flow mixer. Through this component, the flow passes from the inside to the outside of the rig by a series of holes that enhances the mixing of the flow in order to have the best measurement. This connection is modeled with the single junction 202, that cross connects the y-outlet face of volume 36 of pipe 201 with the y-inlet face of volume 1 of pipe 203. The RR is connected to the HPTD with two single junctions. The single junction 120 simulates the four inlet holes of the rig and it connects the y-outlet face of CV 23 of pipe 101, with the y-inlet face of CV 23 of pipe 201. The junction 210 simulates the outlet of the rig and it connects the x-outlet face of the volume 2 of the pipe 203 with the x-inlet face of volume 38 of the pipe 101.

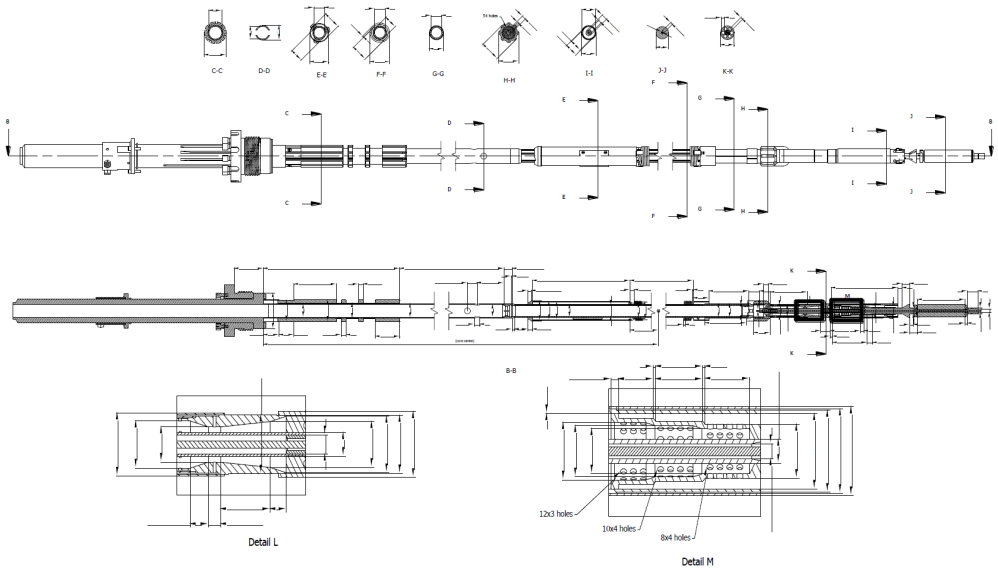

Figure 4.28: Ramp Rig CAD drawing from the specifications [1].

This configuration is sligthly modified when the RC is inserted inside the RR. In this case, the volumes of the CVs from 22 to 33 of pipe 201 will be smaller and some additional pressure losses need to be taken into account. In addition, one more pipe need to be simulated in this case, which is 300 that simulates the water inside the ramp capsule (see figure 4.29). This pipe is vertical and is made by 11

CVs which are connected to pipe 201 with two single junctons. The single junction 230 simulates the inlet holes of the RC and it connects the y-outlet face of CV 23 of pipe 201, with the y-inlet face of CV 1 of pipe 300. The junction 320 simulates the outlet of the ramp capsule and it connects the x-outlet face of the volume 11 of the pipe 300 with the x-inlet face of volume 34 of the pipe 201.

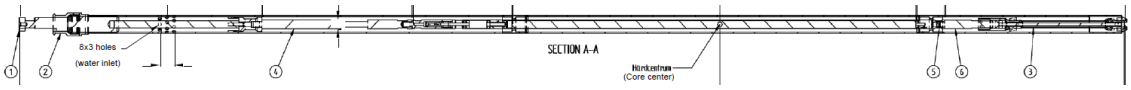

Figure 4.29: Ramp Capsule CAD drawing from the specifications [1].

Pipes 101, 103, 701 and 702 are connected to four heat structures that insulate the system with an abiadatic boundary condition, as it is possible to see from Figure 4.24. The RR and the RC are connected to HSs 1201 and 1300 that use convective boundary conditions to simulate the heat exchange between pipes 101-201 and pipes 201-300, respectively.
In addition to these HS that simulate the pipes of the loop, it is possibe to notice four additional HS made only by 7 axial nodes. These ones are used to simulate the gamma heating inside the core region, that corresponds to this section and CVs. The power given by the gamma contribution is supposed to be calculated from the Serpent core model, measuring its value with a series of detectors. Since the selection of the best core model is out of time for the thesis activity, the power is computed easily considering the available temperature and mass flow rate measurements. First, it is computed the power inside the all loop as:

$$P_{\text{loop}} = m_{\text{flow,loop}} \cdot c_{\text{p,loop}} \cdot (T_{\text{out,loop}} - T_{\text{in,loop}})$$

These temperature measurements derives from the thermo-couples located at the inlet (Tc11) and outlet (Tc13) of the in-pile section shown in Figure 2.7. Then, it is computed the power given in the test section:

$$P_{\text{test sect.}} = m_{\text{flow,test sect.}} \cdot c_{\text{p,test sect.}} \cdot (T_{\text{out,test sect.}} - T_{\text{in,test sect.}})$$

These two values of temperature are the average computed among the four thermo-couples located upstream (T11 - A,B,C,D) and downstream (T12 - A,B,C,D) the test section as shown again in Figure 2.7.
The difference between the first and the second formulas gives the power that must be given in the HPT. The contributions that goes to the HPTD and to the HPTU are computed proportionally to their flow area. As a consequence a 0.38 portion goes to the HPTD and the remaining 0.62 to the HPTU.
A similar procedure is also used to compute the portion of the test section power that goes to the RR and to the RC. In this case, about 1/4 of the power goes to the RR and the others 3/4 to the RC. This of course only in case of β or γ configurations, while for α case all the test section power goes to the RR.
Finally, the power of each HS is uniformly distributed among the 7 axial nodes.

4.5 Input calibration

Once that the model is complete, it is necessary to demonstrate its fidelity with respect to the real system and its capability to reproduce the pressure, temperature and mass flow rate conditions of the in-pile tube. To do that two calibration are needed, since there are two possible hydrodynamic configurations. The first one is the β or γ configuration, where the ramp capsule is inserted inside the ramp rig. The reference experimental conditions against which the model is validated are those at the beginning of the power calibration period, i.e. at the beginning of the test. The BICs that are imposed are the temperature at the inlet, that is given with the time dependent volume 001, the initial mass flow rate of the loop, that is given with the time dependent junction 002, that connects the outlet of the time dependent volume 001 with the inlet of the Inlet Connection Pipe 702, and the pressure at the otlet, imposed with the time dependent volume 004. The inlet of this time dependent volume is connected to theoutlet of the Outlet Connection Pipe with the single junction 003.
The conditions that can be checked are the values of the temperatures in the CVs that correspond to the thermo-couple location and the mass flow rate rate distribution inside the ramp rig, that is measured, and inside the ramp capsule, that is not measured, but of which is available at least an indication as shown in Figure 4.30.

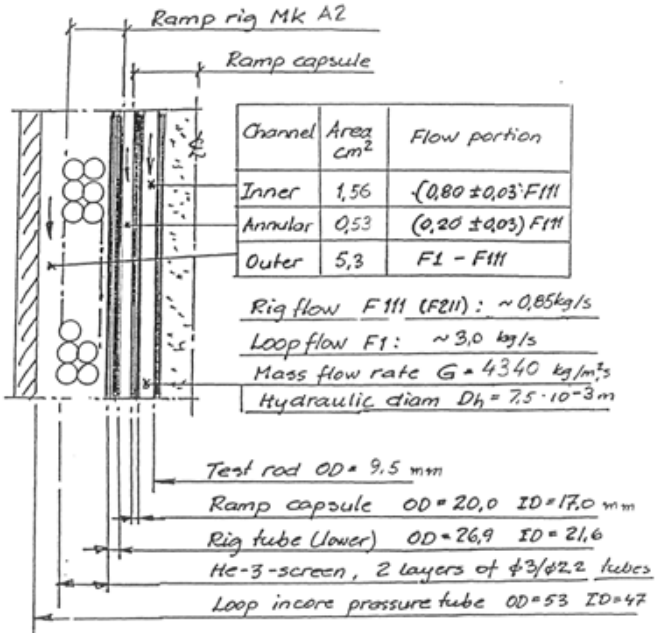

Figure 4.30: Flow distribution inside the in-pile tube.

The largest portion of the test section flow rate passes inside the ramp capsule

(0.8) while the remaining part flows inside the anular region inside the ramp rig and outside the ramp capsule.
A null transient simulation is run to reach the steady state conditions at zero reactor power for this first configuration. Some assumptions are needed in order to properly calibrate the input especially in terms of pressure losses so that the flow distributes in the correct way inside the different components. When too much flow passes inside a component it is necessary to reduce the k-losses of the other regions or increase the flow resistance in that component. The k-losses that are modified are the ones that have the largest impact and at the same time that are the most different from the standard geometry of the Idelchick manual from which they were derived. The convergence of the steady state conditions strongly depends on the initialization of the components conditions. After a first period of oscillation the system manages to converge.
Once that the first hydro-dynamic configuration is validated, the same operation must be performed also for the second one, i.e. the α configuration. Since the only "new" components are pipe 300 and single junctions 320 and 230, only the k-losses associated to these ones can be calibrated, while all the other components are fixed to the value already calibrated. In this way, the steady state conditions are reached also for this configuration.
This preliminary operation is very important since it allows to demonstrate the fidelity of the Simulation Model with respect to the real system. If this step is skipped, considering how many assumptions are needed to model this complicated in-pile tube, it woul be impossible to correctly simulate the ramp test.

4.6 Transient simulation of the first power ramp test

Once the two input files are calibrated it is possible to start the simulation of the first power ramp test. Since during the test there are different phases that were already described in detail (see section 4.2.1), that involves different configurations the entire test is divided into different period:

1. T1 Transient with configuration β simulates both period a and b of the power calibration;

2. T2 Transient with configuration α simulates period a of the pre-ramp 1;

3. T3 Transient with configuration γ simulates period b of the pre-ramp 1;

4. T4 Transient with configuration α simulates period c of the pre-ramp 1;

5. T5 Transient with configuration γ simulates the ramp test;

The next figures show how the ramp test 1 is subdivided into the various phases and the relative configurations.

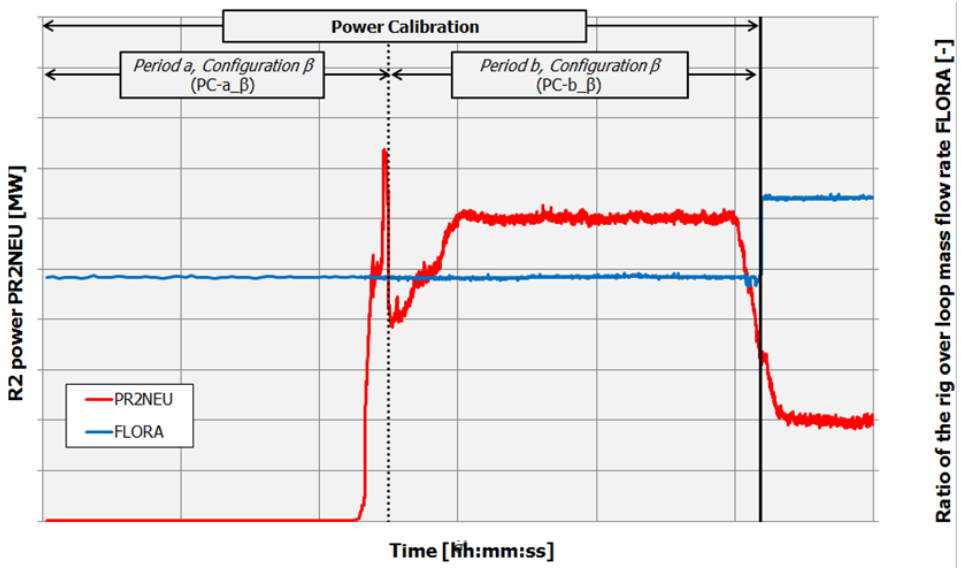

Figure 4.31: Power calibration period configurations.

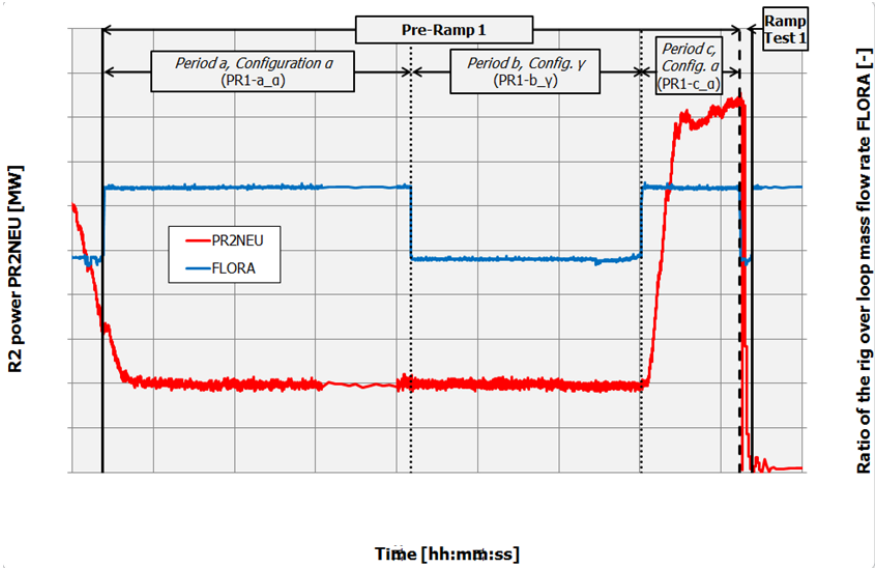

Figure 4.32: Pre-ramp and ramp test period configurations.

Every time the configuration changes it is necessary to perform a restart in RELAP5 by changing the configuration. The components that need to be substituted are rewritten in the restart file. The components that are not used any more

must be deleted, while the new components are simply written in the restart file as new components. It is very important to initialize correctly the temperature and pressure conditions inside the hydrodynamic components and the heat structure, otherwise the simulation may have some problem to converge.
The next figures compare the experimental data with the results of the RELAP5 simulations. The grey region defines the acceptability criteria used by NINE, which is 2% of margin for the mass flow rate and 0.5% for the temperature. So this is not the error due to measurement or uncertainty associated to thermo-couples or flow meter, it is a check on the simulation results in order to see if they are in agreeement with the experimental data following the NINE acceptability criteria.
Figure 4.36 shows a zoom of the ramp test temperature downstream the test section, from which it is possible to see how it increases following a curve while it passes through the neutron flux.
All the results of the RELAP5 simulations are in good agreement with the experimental data and fall inside the accetable region. This means that the model fidelity is demonstrated against validation with experimental data. This is something that was expected, mainly for the temeprature distribution since all the conditions are imposed in this case.

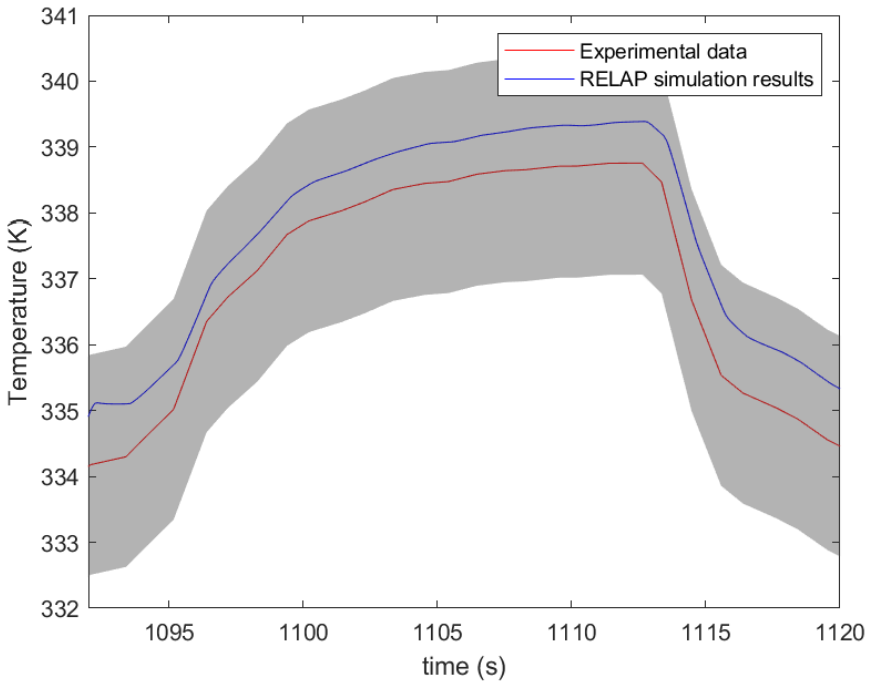

Figure 4.33: Detail of the power ramp test, temperature distribution downstream the test section.

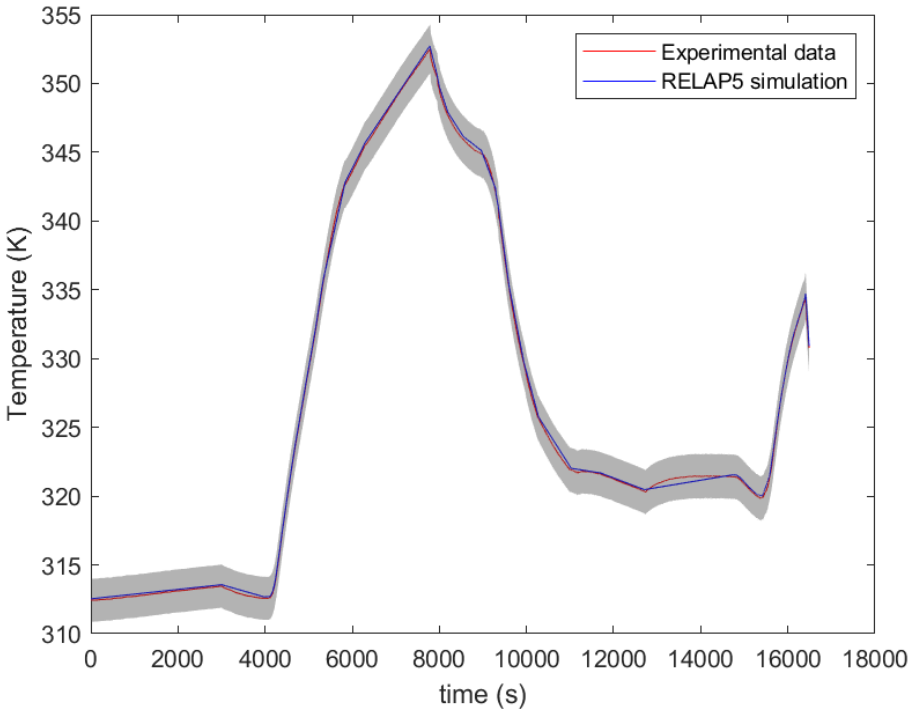

(a) *Inlet.*

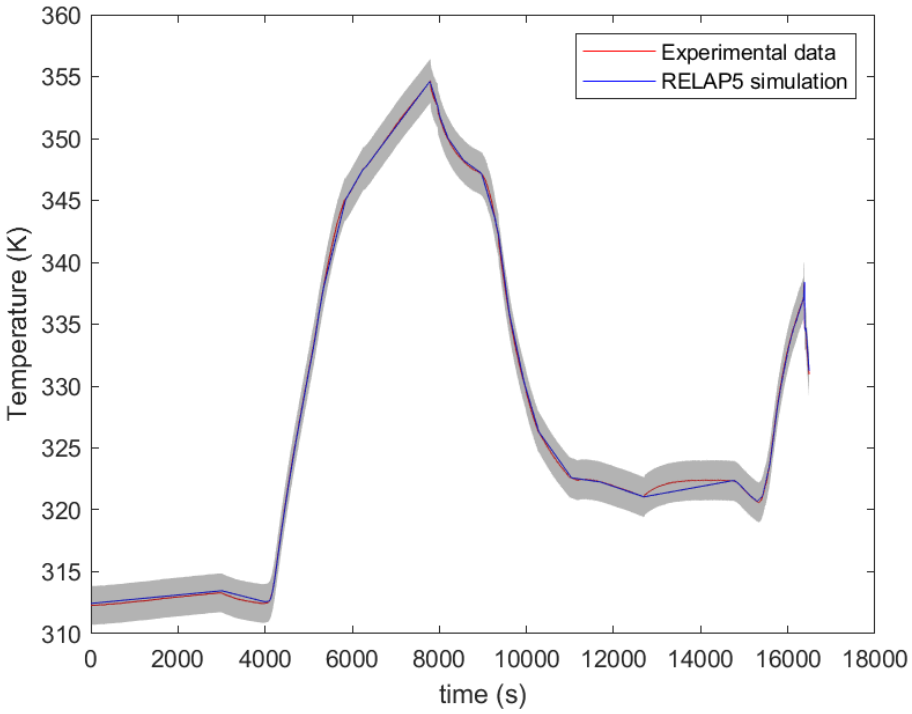

(b) *Outlet.*

Figure 4.34: Coolant temperature at the inlet and outlet of the in-pile loop.

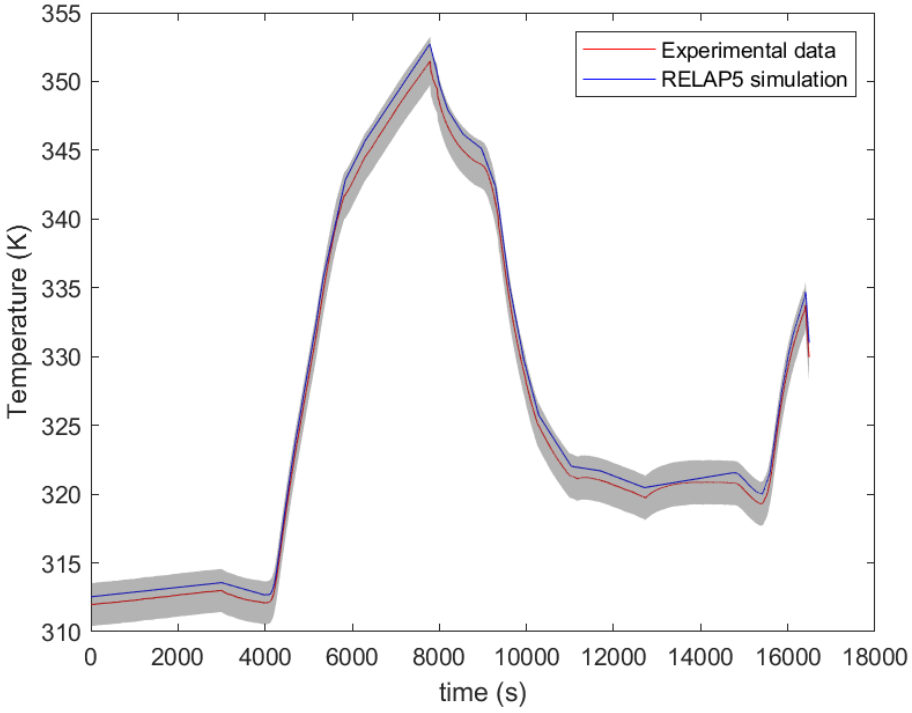

(a) *Inlet.*

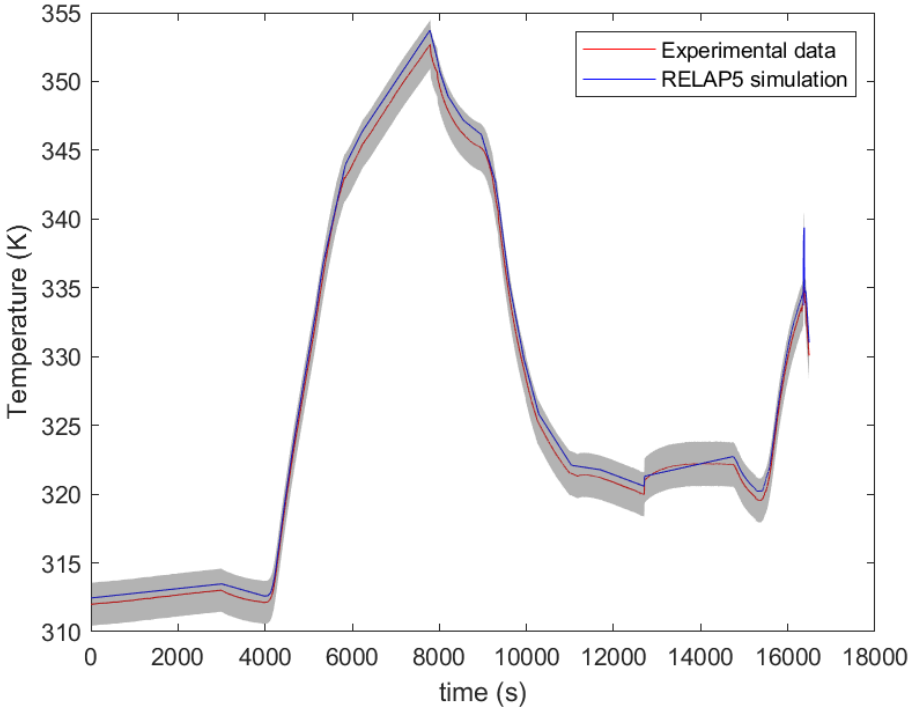

(b) *Outlet.*

Figure 4.35: Coolant temperature upstream and downstream the test section.

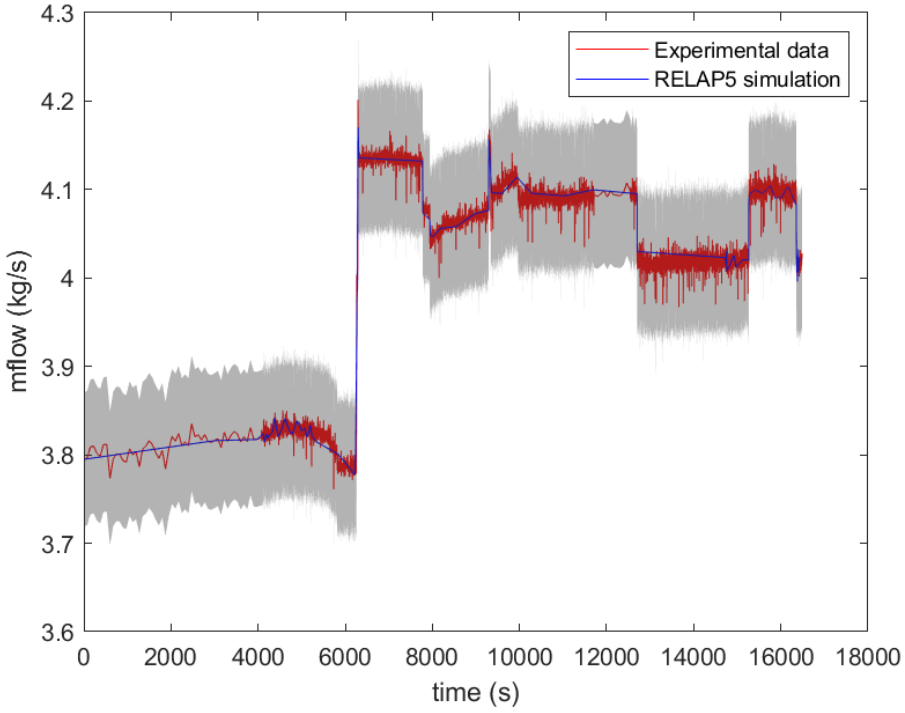

(a) *Loop.*

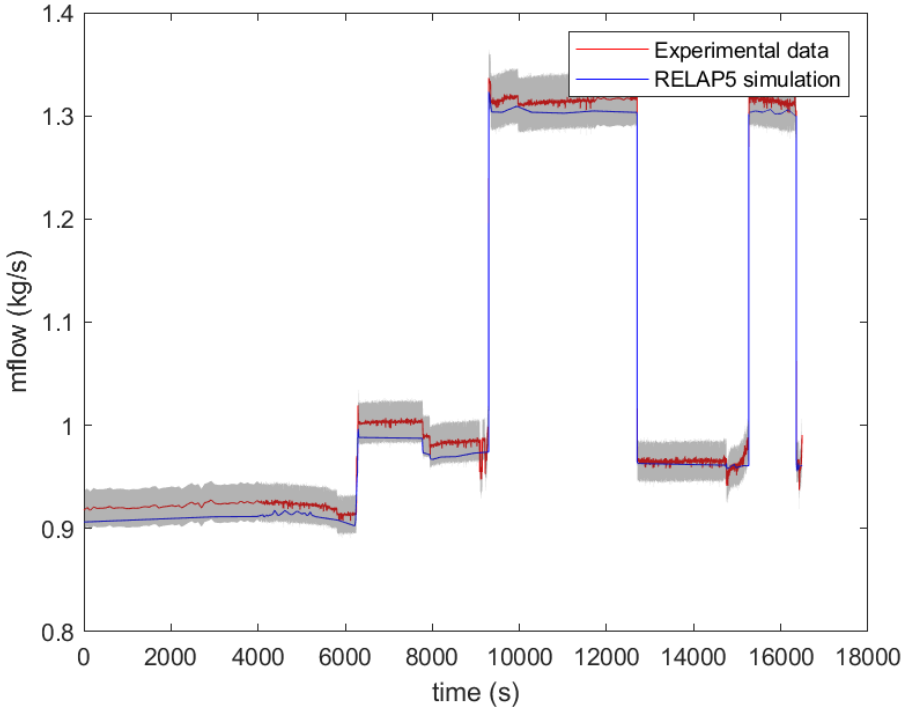

(b) *Ramp Rig.*

Figure 4.36: Mass flow rate inside the loop and inside the ramp rig.

The future analysis will involve the calculation of the gamma heating with the Serpent model of the R2 core. This requires first to indiviuate the best approximation of the core 1105. Once that the core 1105 during which the ramp test is performed is well characterized it is possible to put some photons detectors in the Serpent model in the interesting regions of both coolant and heat structures, in order to study also where the gamma heating becomes negligible. This gamma power distribution will be put in the RELAP5 model and it will be compared with the case described before.
The second ramp test must be also simulated and validated against the available experimental data. This simulation of course can use the same SM, since the experimental facility is exactly the same.
Finally, once that more information about the main loop are available with these simulations, it is possible to move to the entire loop simulation with the objective of characterize the main circuit components. In particular, the in-pile loop computational domain model has to be completed and some simulations must be performed in order to provide proper loop BICs. The main activities to be complted are:

- calculate a proper pump velocity;
- estimate the pressure drops through the main components;
- quantify the heat losses along the loop;
- evaluate the heat exchanged in the air cooler.

Once the modeling phase is completed, some sensitivities have to be performed changing the pump velocity in order to match the measured loop mass flow rate, for the three selected periods, i.e. the power calibration and both cold ramp tests.

Chapter 5

Conclusions

In this work the MPCMIV Benchmark organized by the NINE company has been considered, and the reactor-physic and thermal-hydraulic analyses has been carried out.
The reactor-physic analysis has been focused on the Swedish R2 reactor core region with the main focus to complete the benchmark specifications through the evaluation of some missing boundary and intial conditions necessary to face the benchmark exercises. In particular, a strategy to derive the initial isotopic composition of the fuel assemblies loaded in the core 1105 has been studied and a complete data-set of intial compositions has been built using the results of the infinite lattice depletion. The infinite lattice depletion were performed for each assembly type on different power and temperature conditions to simulate the previous R2 core hystory, which is not available. A total number of 54 simulations has been completed in this way. Then, a full core burn-up simulation of core 1105 has been carried out, this time with the precise information about the power and control rod levels. At the end of the simulation the isotopic composition of the fuel elements discharged from the reactor has been compared with some available data, given in the benchmark specifications that comes from some Studsvik evaluation. The comparision has given a satisfing agreement considering that this was the first evaluation performed, but more simulations are necessary in order to reach the best solution. In particular, some suggestions on how to preoceed in the future has been given, that consist in change the orginal assumptions both in terms of fresh fuel composition and infinite lattice depletion setup. The latter assumes that a different initial composition is taken directly from the dataset that has been built, no adjointive work need to be performed in this case. Once that the best solution for the initial isotopic composition of the fuel assemblies has been found against validation with discharged elements composition, it will be necessary to proceed also with the other two core loadings of interest of the benchmark: 1106 and 1107. For these core loadings the intial isotopic composition of the new fuel assemblies will be already there, since it

is the same of core 1105. Then, starting from core 1106, the full core burn-up simulation will be performed and the discharged elements composition compared with the available data. In this case, another iteration can be performed if the match is not good. One possibility is to keep the core 1105 as before and to change this one only. As an alternative, if the same initial composition want to be kept for all the core loadings, it will be necessary to consider the results of all the comparison and chose the case that better approximate all the core loadings. The latter option is more complicated, since is not trivial to define how to individuate the best initial composition among different core loadings. The future analysis will concentrate on these simulations, that nevertheless require a lot of time to complete all the simulations, but not a lot of work in the sense that all the models and Serpent input files that required the most of the efforts to be completed are already there, and the only thing that has to be done is to start the simulations with different set-ups.
As far as the thermal-hydraulic analysis is concerned, the in-pile loop 1 has been considered and the U-tube model has been built and validated against experimental data. In particular, both steady state and transient analysis has been performed to demonstrate the fidelity of the model and to carry out the simulation of the first cold power ramp test with the RELAP5 code. The results of the simulation show good agreement with the experimantl data, but this is probably due to the fact that the BICs has been imposed and the gamma heating has been computed with an energy balance. The future activity will require to evaluate the gamma power with a reactor physic simulation and check if the model is still validated or something need to be changed. In addition, the model of the main circuit need to be completed and the components to be characterized. So, the thermal-hydraulic analysis has given important results and additional information, but with respect to the reactor-physic analysis it still requires a lot of work to complete the benchmark specifications.
In conclusion, the analyses carried out in this work has shown good agreement with the experimental results for both reactor-physics and thermal-hydraulics. So the models are validated and the preliminary results are satisfying. Furthermore, the models can be used in the future to perform other simulations, with different conditions and set-ups to enhance the quality of the results and conclude the benchmark specifications.

Bibliography

[1] D. D. Luca *et al.*, "Multi-physics pellet cladding mechanical interaction validation input and output specifications," mar 2018.

[2] J. Karlsson, "Special cold ramp test." .pptx, aug 2017.

[3] "2010 asme boiler and pressure vessel code a n i n t e r n a t i o n a l c o d e ii part a ferrous material specifications (beginning to sa-450) materials," jul 2010.

[4] C. L. Whitmarsh, "Review of zircaloy-2 and zircaloy-4 properties relevant to n.s. savannah reactor design."

[5] B. C. Ron Adamson *et al.*, "Pellet-cladding interaction (pci and pcmi)," zirat - 11 special topic report, A.N.T. International, oct 2006.

[6] J. K. Joakim K. *et al.*, "Experimental simulation of a control rod withdrawal error in a cold critical bwr," 2006.

[7] J. Leppänen, *Serpent – a Continuous-energy Monte Carlo Reactor Physics Burnup Calculation Code*. VTT Technical Research Centre of Finland, jun 2015.

[8] M. P. Jaakko Leppänen *et al.*, "The serpent monte carlo code: Status, development and applications in 2013," *Annals of Nuclear Energy*, vol. 82, pp. 142–150, aug 2015.

[9] "Serpent wiki."

[10] H. C. Renato A. Salinas, Ulrich Raff, "Uranium density measurements and homogeneity assessment in quality control of low enriched 235u fuel plates using machine vision," *InstMC Measuremem+Control*, vol. 36, pp. 305–308, dec 2003.

[11] H. Tomani, "Revised hazard summary report, 1993 for the studsvik r2 reactor," Tech. Rep. N(R)-93/002, Studsvik Nuclear AB, jun 1993.

[12] IAEA, "Standardization of specifications and inspection procedures for leu plate-type research reactor fuels," in *IAEA-TECDOC-467*, Report of a consultants meeting organised by the International Atomic Energy Agency, jun 1988.

[13] "Leu-490 fuel.xlsx."

[14] "a.xlsx." HELIOS input file from Studsvik.

[15] G. L. Copeland, R. W. Hobbs, *et al.*, "Performance of low-enriched u3si2-aluminum dispersion fuel elements in the oak ridge reasearch reactor," tech. rep., Argonne National Laboratory, 9700 South Cass Avenue Argonne, Illinois 60439, oct 1987.

[16] "International alloy designations and chemical composition limits for wrought aluminum and wrought aluminum alloys," jan 2015.

[17] H. Odelius, "Casmo/simulate för härdberäkningar på r2," Tech. Rep. N(R)-97/060, Studsvik Nuclear AB, aug 1997.

[18] J. L. Snelgrove *et al.*, "The use of u3si2 dispersed in aluminum in plate-type fuel elements for research and test reactors," anl/rertr/tm-11, Argonne National Laboratory, oct 1987.

[19] N. Addo *et al.*, "Sakerhetsanalys for r2-reaktorn - sar2," Tech. Rep. N(R)-02/050, Studsvik Nuclear AB, jun 2003.

[20] N. R. Commission, "Safety evaluation report related to the evaluation of low-enriched uranium silicide-aluminum dispersion fuel for use in non-power reactors," Tech. Rep. NUREG-1313, Office of Nuclear Reactor Regulation, jul 1988.

[21] J. Eliasson, "Hardberakningar for r2 - modellen i oscar-3," Tech. Rep. N-04/113, Studsvik Nuclear AB, aug 2004.

[22] D. R. Vondy *et al.*, "Production of np237 and pu238 in thermal power reactors." Oak Ridge National Laboratory, oct 1964.

[23] I. S. Laboratories, *RELAP5/MOD3.3 Code Manual Volume I: Code Structure, System Models, and solution methods*. Nuclear Regulatory Commission, Washington, DC 20555, feb 2019.

[24] D. D. Luca, "Development of relap best estimate nodalization for itf: Step by step modelling and application of nemm (lecture th-08)," nov 2018.

[25] A. Petruzzi *et al.*, "Standardized consolidated calculated and reference experimental database (sccred): a supporting tool for v&v and uncertainty evaluation of best-estimate system codes for licensing applications," *Nuclear Science and Engineering*, vol. 182(1), pp. 13–53, 2016.

[26] I. E. Idelchik, *Handbook of Hydraulic resistance*. Begell House, Inc, fourth ed., 2007.